

Hydrogels for Regenerative Medicine: Development and Characterization

Dissertation zur Erlangung des Doktorgrades
der Naturwissenschaften (Dr. rer. nat.)
der Fakultät für Chemie und Pharmazie
der Universität Regensburg



vorgelegt von
Ferdinand Paul Brandl
aus Hirschau

November 2009

Diese Doktorarbeit entstand in der Zeit von Dezember 2004 bis November 2009 am Lehrstuhl für Pharmazeutische Technologie der Universität Regensburg.

Die Arbeit wurde von Prof. Dr. Achim Göpferich angeleitet.

Promotionsgesuch eingereicht am: 17.11.2009

Datum der mündlichen Prüfung: 15.12.2009

Prüfungsausschuss:

- Prof. Dr. Sigurd Elz (Vorsitzender)
- Prof. Dr. Achim Göpferich (Erstgutachter)
- PD Dr. Rainer Müller (Zweitgutachter)
- Prof. Dr. Armin Buschauer (Drittprüfer)

Meinen Eltern
in Liebe und Dankbarkeit.

Contents

Hydrogels for regenerative medicine	1
1 Introduction and goals of the thesis	3
1.1 Principles of regenerative medicine	4
1.2 Biomaterials for regenerative medicine	5
1.3 Goals of the thesis	6
2 Rational design of hydrogels for tissue engineering	11
2.1 Introduction	13
2.2 Environmental factors as morphogenetic guides	14
2.2.1 Integrins as mechanoreceptors	15
2.2.2 Mechanical cues regulate cell behavior	16
2.3 Mechanical properties of materials and their characterization	17
2.3.1 Atomic force microscopy	20
2.3.2 Magnetic resonance elastography	21
2.3.3 Monitoring of cellular traction forces using fluorescence resonance energy transfer	23
2.4 Rational design of hydrogels for tissue engineering	24
2.5 Physical parameters regulate tissue development	28
2.5.1 Impact of mechanical factors on cell function and tissue morphogenesis	28
2.5.2 Influence of degradation profile on tissue formation	30

2.5.3	Cell-responsive hydrogels	32
2.6	Concluding remarks	34
3	Poly(ethylene glycol) based hydrogels for intraocular applications	37
3.1	Introduction	39
3.2	Materials and Methods	41
3.2.1	Materials	41
3.2.2	Synthesis of PEG-amines	41
3.2.3	Synthesis of branched PEG-succinimidyl propionates	42
3.2.4	Preparation and rheological characterization of hydrogels	44
3.2.5	Characterization of hydrogels by NMR	44
3.2.6	Cytotoxicity of cross-linked hydrogels	45
3.2.7	Release of FITC-dextran and fluorescent nanospheres	46
3.3	Results and discussion	47
3.3.1	Preparation and rheological characterization of hydrogels	47
3.3.2	Characterization of hydrogels by NMR	52
3.3.3	Cytotoxicity of cross-linked hydrogels	53
3.3.4	Release of FITC-dextran and fluorescent nanospheres	54
3.4	Conclusion	56
4	Hydrogel-based drug delivery systems	57
4.1	Introduction	59
4.2	Materials and methods	60
4.2.1	Materials	60
4.2.2	Synthesis of polymers	61
4.2.3	Rheological characterization of hydrogels	61
4.2.4	Equilibrium swelling of hydrogels	62
4.2.5	Calculation of hydrogel network mesh size	63
4.2.6	Fluorescence recovery after photobleaching (FRAP)	64
4.2.7	Nuclear magnetic resonance (NMR) spectroscopy	66
4.2.8	Release of FITC-dextran	66
4.3	Results and discussion	67
4.3.1	Physicochemical characterization of hydrogels	67

4.3.2	Estimation of diffusion coefficients	69
4.3.3	Determination of diffusion coefficients by FRAP	70
4.3.4	Determination of diffusion coefficients by NMR	72
4.3.5	Release of FITC-dextran	74
4.4	Conclusion	75
5	Biodegradable hydrogels for time-controlled release	77
5.1	Introduction	79
5.2	Materials and methods	81
5.2.1	Materials	81
5.2.2	Synthesis of PEG-amines	82
5.2.3	Synthesis of non-degradable PEG-succinimidyl carbonates	82
5.2.4	Synthesis of degradable PEG-succinimidyl carbonates	83
5.2.5	Synthesis of alanine-modified PEG-amines	84
5.2.6	Synthesis of 6-aminohexanoic acid-modified PEG-amines	85
5.2.7	Synthesis of lysine-modified PEG-amines	86
5.2.8	Preparation and rheological characterization of hydrogels	86
5.2.9	Equilibrium swelling of hydrogels and determination of network parameters	87
5.2.10	Degradation of hydrogels	88
5.2.11	Mobility of incorporated macromolecules determined by fluorescence recovery after photobleaching (FRAP)	89
5.2.12	Release of FITC-BSA and lysozyme	90
5.2.13	Statistical analysis	90
5.3	Results and discussion	91
5.3.1	Physicochemical characterization of hydrogels	91
5.3.2	Degradation of hydrogels	94
5.3.3	Mobility of incorporated macromolecules	95
5.3.4	Release of FITC-BSA and lysozyme	97
5.4	Conclusion	99
6	Biointeractive hydrogels for adipose tissue engineering	101
6.1	Introduction	103

6.2	Materials and methods	104
6.2.1	Materials	104
6.2.2	Synthesis of amine-reactive polymers	106
6.2.3	Synthesis of collagenase-sensitive polymers	106
6.2.4	Synthesis of non-degradable polymers	108
6.2.5	Rheological characterization of hydrogels	108
6.2.6	Equilibrium swelling of hydrogels	109
6.2.7	Degradation of hydrogels	110
6.2.8	Cell seeding and cell culture	110
6.2.9	Quantitative analysis of intracellular triglyceride accumulation	112
6.2.10	DNA assay	112
6.2.11	Oil red O staining	112
6.2.12	Statistics	113
6.3	Results and discussion	113
6.3.1	Physicochemical characterization of hydrogels	113
6.3.2	Degradation of hydrogels	116
6.3.3	Adipogenic differentiation of 3T3-L1 preadipocytes	119
6.4	Conclusion	123
7	Summary and conclusions	125
	Appendix	157
	Curriculum vitae	165
	List of publications	167
	Acknowledgments	171

Hydrogels for regenerative medicine: Development and characterization

So eine Arbeit wird eigentlich nie fertig, man muß sie für fertig erklären, wenn man nach Zeit und Umständen das Möglichste getan hat.

(Johann Wolfgang von Goethe)

Chapter 1

Introduction and goals of the thesis

1.1 Principles of regenerative medicine

The human body has a remarkable capacity to regenerate aged cells and damaged tissues. After traumatic injuries and severe diseases, however, the regenerative power of adult tissues is often not sufficient to cope with the occurred damage. Occlusion of coronary arteries, for example, will result in necrosis of myocardial tissue and scar formation. Depending on the size of the affected area, this may lead to heart failure or cardiac arrest. Consequently, irreparably damaged tissues or organs have to be replaced with artificial devices, autologous grafts, or donor organs [1–3]. However, despite many advances in this field, medical devices (such as artificial hearts, for example) often cannot replace the lost organ completely. The necessity of alternative strategies is further illustrated by the ever growing mismatch between supply and demand of organs and tissues for transplantation. In the Eurotransplant region, for example, 7,293 people received transplants in 2008, while 15,864 people were awaiting them [4]. The present situation will even intensify in the future, since the average age of the Western population is increasing, and with it the incidence of age-related diseases such as osteoporosis, diabetes, and cardiovascular diseases.

Regenerative medicine promises to overcome this dilemma. This interdisciplinary field emerged more than two decades ago to work toward the common goal of the repair or replacement of cells, tissues, and organs [1–3]. The original approach was to isolate living cells from patients or other human donors, to expand them *in vitro* using polymeric scaffolds, and then to re-implant the tissue-like constructs into the patient [1]. But despite many advances, none of these cell-laden scaffolds have resulted in complete restoration of normal tissue function [2, 3]. The complexity of growing functional tissues *in vitro* has obviously been underestimated and the replacement of whole organs is still a distant milestone in which current studies are laying the necessary groundwork.

The currently investigated strategies are perhaps less complex, but certainly not less ambitious. In the case of tissues with inherent regenerative capacities, tissue regeneration can be promoted by inserting an appropriate biomaterial to prevent undesirable, rapidly proliferating cells from entering the site of defect. In another approach, research tries to stimulate the body’s own repair mechanisms by mimicking the regulatory function of growth factors. This will require the development of “smart”

biomaterials that allow delivering growth factors in a spatio-temporally controlled manner [5–7]. Recently, nanostructured biomaterials have also been proposed that target to the injury site and self-assemble into higher order scaffold structures. These would provide an appropriate microenvironment to recruit and activate endogenous stem cells to form differentiated tissues and organ structures [3].

1.2 Biomaterials for regenerative medicine

Biomaterials play a central role in regenerative medicine and tissue engineering as carrier systems for drug molecules or cells. Commonly used biomaterials include biodegradable poly(glycolic acid) (PGA), poly(lactic acid) (PLA), and poly(lactide-*co*-glycolide) (PLGA). However, these polymers are rather hydrophobic and are typically processed under relatively harsh conditions, which makes the incorporation of fragile biomolecules or living cells a challenge. Most of the fabricated scaffolds were designed to withstand mechanical loads and to degrade within an appropriate period of time, while additional functionalities (such as the ability to trigger specific cellular responses) have often been neglected. During the past decade, however, there has been a substantial paradigm shift in the design criteria of modern biomaterials [8]. Current developments integrate principles from cell and molecular biology to mimic certain aspects of the natural extracellular matrix (ECM).

Therefore, hydrogels have been proposed as potential alternatives for a variety of drug delivery and tissue engineering applications [7, 9–13]. These hydrophilic polymer networks absorb large amounts of water and demonstrate excellent biocompatibility due to their physicochemical similarity to the native ECM. Furthermore, gel formation usually proceeds at ambient temperature without requiring organic solvents. Hydrogels can be classified into natural, synthetic, and composite gels according to their origin and composition. Furthermore, one can distinguish between ‘reversible’ or ‘physical’ gels and ‘permanent’ or ‘chemical’ gels. In physical gels, networks are held together by molecular entanglements and/or secondary forces including ionic interactions, hydrogen bonds, and hydrophobic interactions. In contrast, chemical gels are characterized by covalent cross-links between the individual polymer chains.

In terms of industrial production processes, hydrogels derived from synthetic polymers are especially appealing, as their chemical and physical properties are easily controlled and reproduced. Synthetic materials include poly(vinyl alcohol) (PVA), derivatives of poly(acrylic acid) (PAA), poly(ethylene glycol) (PEG), and synthetic polypeptides. Of these substances, polymers derived from PEG are among the most commonly applied hydrogel-forming materials. The widespread use of these polymers primarily results from their excellent biocompatibility and high solubility in water and organic solvents [14]. The versatility of the PEG macromer chemistry further allows for the design of ‘biomimetic’ hydrogels that mimic the complexity of the natural ECM [10, 11, 13]. These hydrogels can be equipped with molecular cues that guide the adhesion and/or recruitment of cells (e.g. endogenous stem cells), degradation sites for cellular proteases to allow for cell-triggered remodeling, and binding sites for soluble signaling molecules (such as growth factors or cytokines). Altogether, PEG is deemed to be an ideal starting material for the development of sophisticated hydrogel systems for drug delivery and regenerative medicine applications.

1.3 Goals of the thesis

This thesis is focused on the development and characterization of PEG-based hydrogels for controlling drug delivery and promoting tissue regeneration. To achieve these goals, cross-linking methods had to be identified that are sufficiently gentle to be performed in the presence of cells or *in vivo*. This would facilitate injection and provide an effective way to encapsulate drug molecules or living cells (Figure 1.1). Based on the established chemistry, different polymers were synthesized as building blocks for the preparation of hydrogels. As a consequence of this combinatorial approach, a variety of hydrogels could be prepared from comparatively few macromers. The developed hydrogels may serve as inert space-filling agents, as carrier systems for the controlled release of drug molecules, or as three-dimensional scaffolds in cell-based approaches. Similar to the native ECM, synthetic biomaterials must provide an “instructive” microenvironment that directs cell proliferation and differentiation [8, 15–17]. For

these reasons, an exact knowledge of the chemical, physical, and topographical factors guiding tissue morphogenesis *in vitro* and *in vivo* will be crucial.

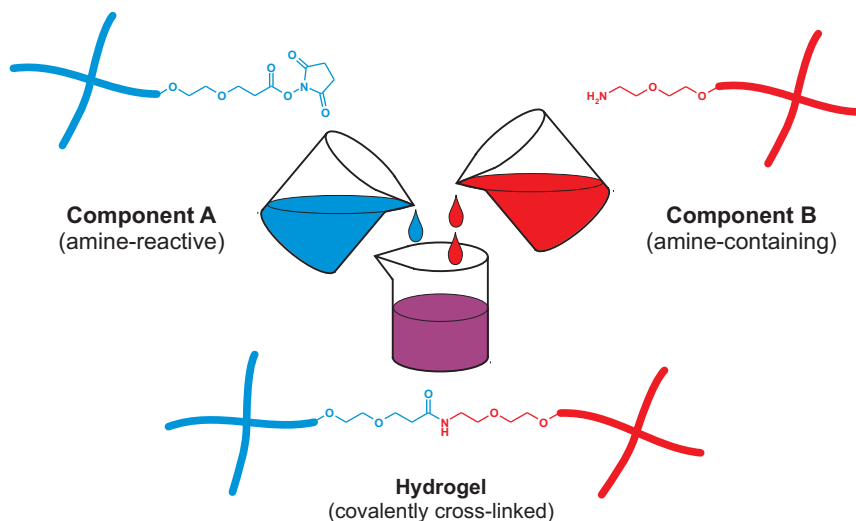


Figure 1.1: Principle of *in situ* forming hydrogels. An amine-reactive compound (A) is combined with an amine-containing component (B) e.g. by using a two-chamber syringe. Directly after mixing the liquid precursor solutions, the individual polymer chains are cross-linked to form a highly elastic hydrogel. Cells or drug molecules can be easily incorporated by suspending or dissolving them in one of the two precursor solutions.

In **Chapter 2**, the influence of environmental cues on cell proliferation and differentiation is, therefore, reviewed. Since most PEG-based hydrogels are biologically and chemically inert [10], the impact of physical factors on cell behavior is primarily stressed. To this end, the physical properties of hydrogels will be discussed, which include their gel forming characteristics, their mechanical properties, and degradation behavior. A short introduction to methods of characterizing the mechanical properties of hydrogels is also included. The chapter is completed by a detailed review of several *in vitro* studies that illustrate the complex interplay between substrate stiffness, degradability, cell differentiation, and tissue morphogenesis.

According to these theoretical considerations, the following work was focused on the development of *in situ* forming hydrogels for intraocular applications (**Chapter 3**). Age-related macular degeneration (AMD) and proliferative diabetic retinopathy (PDR) are among the leading causes of blindness in industrialized nations [18]. PDR is characterized by an abnormal growth of blood vessels into the vitreous body, a

virtually acellular, gel-like network of collagen fibrils and glycosaminoglycans that fills the posterior segment of the eye. In these patients, a total replacement of the affected vitreous may be required in order to prevent blindness or to restore vision. However, today's clinically used substitutes differ significantly from the natural vitreous body with regard to their physicochemical properties and mechanics. Some of these substances are also associated with severe side-effects when kept intravitreally over longer periods of time. Therefore, this work was aimed at developing a better tolerated, hydrogel-based vitreous substitute with mechanical properties similar to those of the natural vitreous body. Particular attention had to be paid to the biocompatibility, optical transparency, and injectability of the proposed hydrogels. The developed hydrogels are non-degradable and designed to act as inert space-filling agents over longer periods of time.

Apart from their potential application as vitreous substitutes, hydrogels would also be promising materials for the delivery of drugs to the posterior segment of the eye (e.g. to prevent the above described neovascularization). However, despite many favorable characteristics, hydrogel-based drug delivery systems still have some limitations. In fact, the high water content of most hydrogels often results in relatively rapid drug release over several hours to a few days. To overcome these limitations, efforts were made to extend the duration of drug release and to expand the range of molecules which can be effectively delivered by hydrogels (e.g. by increasing the average network mesh size). Since the resulting release profiles are hardly predictable, newly developed drug delivery systems are usually characterized by release experiments. However, these experiments are time-consuming and their reliability is often limited. In the next study, the significance of mechanical testing, swelling studies, fluorescence recovery after photobleaching (FRAP), and pulsed field gradient nuclear magnetic resonance (NMR) spectroscopy was, therefore, investigated for the characterization of hydrogel-based drug delivery systems (**Chapter 4**).

To prolong the release of incorporated peptides or proteins, the existing hydrogels had to be modified. For this purpose, the possibility of tethering drug substances to the hydrogel backbone was investigated. Ideally, hydrogel cross-linking and drug tethering would be performed simultaneously without requiring chemical modifications of the drug molecules. This would improve handling and flexibility of the developed drug delivery system, since any peptide or protein could be incorporated by simply dissolving

them together with the gel-forming polymers. To achieve this goal, biodegradable polymers were synthesized that readily react with amino groups of other polymers, peptides, or proteins (**Chapter 5**). During cross-linking, the drug molecules are covalently bound to the gel network, which effectively prevents their immediate release. Release kinetics is then controlled by the degradation of the anchor group; drug diffusivity only plays a secondary role. The anchor groups used for drug conjugation had to be carefully designed in order to prevent potential loss of bioactivity and to allow for the time-controlled release of incorporated molecules. The developed hydrogels were characterized by mechanical testing, the established FRAP technique, and release experiments.

Besides their use as inert space filling agents (**Chapter 3**) and drug delivery systems (**Chapter 4 and 5**), *in situ* forming hydrogels could also be applied as three-dimensional scaffolds in cell-based approaches. The developed hydrogels provide for effective cell encapsulation and unrestricted diffusion of nutrients and metabolites. For a successful application in regenerative medicine, hydrogel scaffolds must bear the occurring mechanical loads and provide a suitable microenvironment to promote cell proliferation and differentiation. Once placed at the application site, the scaffold should degrade in spatial and temporal synchrony with the formation of new tissue. For this purpose, the gel-forming polymers were functionalized with a synthetic tetrapeptide (Ala-Pro-Gly↓Leu) to make them susceptible to proteolytic breakdown (**Chapter 6**). These cell-responsive hydrogels mimic the proteolytic recognition of the natural ECM and are degraded by cell-secreted proteases. In the last study, these biointeractive hydrogels were seeded with 3T3-L1 preadipocytes to investigate the impact of substrate stiffness, adhesiveness, and degradability on cell proliferation and differentiation.

Chapter 2

Rational design of hydrogels for tissue engineering: Impact of physical factors on cell behavior

Ferdinand Brandl¹, Florian Sommer^{1,2}, Achim Göpferich¹

¹ *Department of Pharmaceutical Technology, University of Regensburg, 93040 Regensburg*

² *Boehringer Ingelheim Pharma GmbH & Co. KG, 88397 Biberach an der Riß*

Published in *Biomaterials* **28** (2), 134–146 (2007).

Abstract

When designing suitable biomaterials for tissue engineering applications, biological and chemical parameters are frequently taken into account, while the equally important physical design variables have often been neglected. For a rational design of biomaterials, however, all variables influencing cell function and tissue morphogenesis have to be considered. This review will stress the development of cross-linked hydrogels and outline the impact of their physical properties on cell function and tissue morphogenesis. In the first part, the principles of cellular mechanosensitivity, as well as the influence of substrate mechanics on cell behavior, will be discussed. Afterwards, methods to characterize the mechanical properties of biomaterials will be presented. The subsequent chapters will address hydrogels that allow for the control of their physical qualities followed by a discussion of their use in tissue engineering applications.

2.1 Introduction

The human organism is composed of around 10^{13} cells that are classified into more than 200 different cell types [19]. Cell function, tissue morphogenesis, and organ development are thought to be regulated by a fine-tuned interplay of chemical, physical, and topographical factors [19–21]. Many of the principles guiding embryogenesis *in vivo* are also considered to be involved in the regulation of tissue development *in vitro*. Despite the proliferation of this concept, the design of biomaterials for tissue engineering is still frequently guided by the principles of trial and error, rather than by rational considerations of the specific demands. Many biomaterials have been developed to meet particular biological and chemical requirements (e.g. biocompatibility, degradability, mediation of cell adhesion, etc.). Other design parameters, such as the physical properties of the biomaterial, were regarded with respect to the processing conditions, the mechanical load capacity, or the diffusivity of solutes, but not with respect to the biological response. This is probably at least in part due to the lack of adequate methods of measuring the physical attributes of tissues or tissue-engineered constructs.

For a rational design of biomaterials, however, all variables influencing cell function and tissue morphogenesis have to be considered. To understand the influence of each parameter, their individual signaling pathways have to be elucidated. Together, these fundamentals will reveal “set screws” for the design of biomaterials. Adjusting these parameters to the requirements of each specific application would allow for the creation of “custom-made” biomaterials that direct the development of desired tissues. Thereby, the inherent characteristics of biological tissues may serve as guides for this process [19–24].

This review was written to promote the rational design of hydrogels for tissue engineering applications with a special emphasis on physical properties. Hydrogels are highly hydrated networks that have been fabricated from a wide range of hydrophilic polymers [9, 10, 25]. They can be classified into ‘reversible’ or ‘physical’ gels and ‘permanent’ or ‘chemical’ gels. In physical gels, networks are held together by molecular entanglements and/or secondary forces including ionic cross-links, hydrogen bonds, and hydrophobic interactions. In contrast, chemical gels consist of covalently cross-linked networks [9].

In the first part of this review, we will discuss the basic principles of cellular mechanosensitivity. Theoretical considerations are illustrated by *in vitro* studies that elucidate the general cell responses on two-dimensional model substrates. Subsequently, we will outline the problems of characterizing the mechanical properties of biological tissues and hydrogels followed by a discussion on the rational design of hydrogels for tissue engineering applications. Finally, we will stress the impact of mechanical characteristics and degradability on cell function and tissue morphogenesis. For this purpose, we will present relevant *in vitro* studies as well as available *in vivo* data.

2.2 Environmental factors as morphogenetic guides

In tissues, cells are embedded within the extracellular microenvironment, a highly hydrated network that comprises three classes of stimuli or cues that stem from the following sources: insoluble hydrated macromolecules (e.g. fibrillar proteins, proteoglycans, or polymer chains), soluble molecules (e.g. growth factors or cytokines), and membrane-associated molecules of neighboring cells [8, 24]. As it is assumed that most interactions between cells and these extracellular effectors are determined by associations between receptors and corresponding ligands [26], we will concentrate here upon specific ligand-receptor interactions and disregard nonspecific effects, such as electrostatic interactions. Ligand-receptor interactions are considered as specific, as they depend on detailed topographical features of interacting structures (“lock-and-key principle”) [26].

Soluble receptor ligands, such as growth factors and cytokines, are thought to diffuse to their target receptors. The transmitted information will arise from the type of signaling molecule as well as its local concentration [19]. The resulting cellular response to that kind of stimulus is currently being investigated in detail; comprehensive reviews dealing with the application of growth factors in tissue engineering can be found in the literature [27–29]. By contrast, the pure biochemical information provided by ligands attached to an extracellular structure, such as the extracellular matrix (ECM), is supplemented by additional degrees of information including the spatial distribution of ligands and the mechanical properties of the structure the ligands are attached to [19]. Spatial variations in adhesiveness, for example, can lead to a directed cell movement towards regions of higher ligand density, a phenomenon

termed haptotaxis [30–32]. In the following paragraphs, however, we will focus on the impact of mechanical cues on such cell behavior.

2.2.1 Integrins as mechanoreceptors

In the past, great efforts have been made to elucidate how physical forces, applied to either the ECM or the cell surface, induce biochemical alterations inside the cell. Today, there is much evidence that mechanical signals are transferred into the cell across transmembrane molecules, such as integrins, which couple extracellular anchors to the cytoskeleton [33–35]. Integrins constitute a large family of transmembrane, heterodimeric receptors that bind to specific amino acid sequences, such as the arginine–glycine–aspartic acid (RGD) recognition motif, present in all major ECM proteins [36]. After binding to ECM ligands, integrins cluster together to form dot-like adhesive structures termed focal complexes. Depending on the stiffness of the underlying substrate, focal complexes can disappear or evolve into focal adhesions. These multi-molecular plaques anchor bundles of actin filaments (stress fibers) and mediate strong adhesion to the substrate. In turn, focal adhesions are considered to be a source for fibrillar adhesions, which are involved in matrix assembly into extracellular fibrils [37, 38]. Studying cell-matrix interactions in a three-dimensional (3-D) context, Cukierman et al. described distinctive “3-D matrix adhesions” that differed from both focal and fibrillar adhesions characterized on two-dimensional (2-D) substrates in structure, localization, and function. They further speculated that classically described *in vitro* adhesions are exaggerated precursors of those, more biologically relevant “3-D matrix adhesions” [39, 40].

To explain the molecular basis of mechanotransduction, Ingber et al. proposed the cellular tensegrity model [34, 35]. According to this model, living cells are thought to exist in a state of pre-stress, actively generated by myosin-II driven isometric contractions of the actin cytoskeleton. Structural elements that resist compression, notably internal microtubule struts and ECM adhesions, act as a counterbalance. As cell-ECM adhesions and microtubule struts resist cytoskeletal tension in a complementary manner, changes in ECM mechanics or extracellular perturbations generate mechanical forces within the cytoskeletal structure. In reaction to unbalanced forces, cells rearrange cell-matrix adhesions, reorganize their cytoskeleton, and immediately shift their shape. For example, if the stiffness of the ECM exceeds the stiffness of the

cytoskeleton, cells will flatten and spread. In the opposite case, cells will retract or become rounded. Biochemical responses are thought to be mediated by conformational changes of regulatory molecules within the adhesion plaque. These molecular events, in turn, trigger signal transduction cascades which ultimately regulate cell proliferation, differentiation, and apoptosis [33, 35].

2.2.2 Mechanical cues regulate cell behavior

Model considerations of cellular mechanosensitivity are also supported by experimental data. Using fibronectin-coated beads held in an optical trap, Choquet et al. demonstrated that cells strengthen their integrin-mediated contacts to the beads in proportion to the force restraining it. According to the authors, this mechanism might allow cells to migrate through the ECM in response to its mechanical properties [41]. In a later study, Lo et al. verified the idea of mechanotaxis by demonstrating that cell movement is guided by the rigidity of the substrate [42]. Similar results were found by Gray et al. They used a micropatterning technique to produce fibronectin-coated surfaces of varying stiffness and observed cell migration towards stiffer regions of the substrate (Figure 2.1) [43].

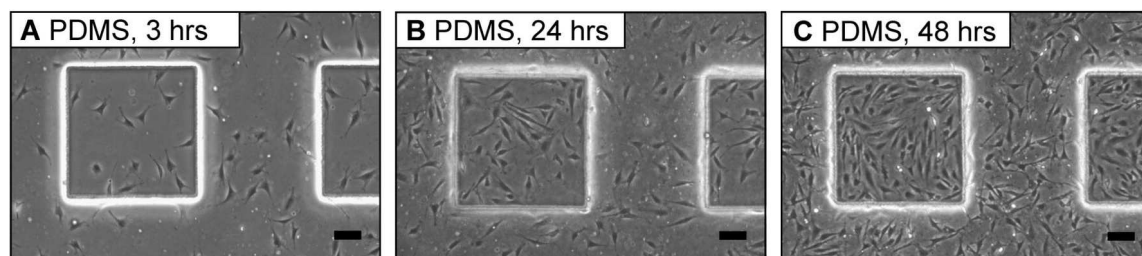


Figure 2.1: NIH/3T3 fibroblasts cultured on fibronectin-coated poly(dimethylsiloxane) (PDMS) substrates. The squares are stiff, whereas the regions surrounding the squares are compliant. Accumulation of cells on stiffer regions was found to be due to migration, not proliferation, of cells in response to the mechanical patterning (mechanotaxis). Scale bars represent 100 μm . Reprinted with permission from Gray et al. [43]. © 2003 John Wiley & Sons, Inc.

In addition to migration, a variety of other cell functions, such as cell spreading, growth, and differentiation, are also modulated by the substrate mechanics. Pelham et

al. reported that cells on flexible substrates showed reduced spreading and increased rates of motility compared to cells on rigid substrates [44]. Wang et al. found cell proliferation to be increased on culture substrates of higher mechanical stiffness. In contrast, the rate of apoptosis was increased on more flexible substrates [45]. Studying angiogenesis *in vitro*, Vailhe et al. demonstrated that the formation of capillary-like structures was influenced by the rigidity of the fibrin gels utilized [46]. Similar results were obtained by Deroanne et al., who could show that cell differentiation was affected by the mechanical properties of the supportive matrix: with decreasing substrate rigidity, the number of endothelial cells switching to a tube-like pattern increased [47]. Differentiation of neuronal cells also seems to be regulated by the mechanical properties of the culture substrate. According to Flanagan et al., the formation of neurite branches was enhanced by softer substrates [48].

As mechanosensitivity is related to cells' ability to rearrange adhesion ligands presented by the substrate and to apply traction forces to the material [49], substrate mechanics and adhesiveness should be regarded as coupled variables. Rowley et al. reported that myoblast differentiation on alginate gels was regulated by the mechanical properties of the substrate as well as the RGD density [50]. Investigating spreading of smooth muscle cells (SMCs) on collagen-coated polyacrylamide gels, Engler et al. showed matrix compliance and ligand density to be highly coupled variables that determine mean cell responses [51]. Finally, Peyton and Putnam reported a biphasic dependence of cell migration speed on ECM stiffness. In their study, the optimal stiffness at which cell migration speed is maximized was found to depend on the density of immobilized ECM ligands [52]. For more detailed information about the crucial role of substrate mechanics and adhesiveness in cell regulation, several comprehensive reviews are recommended [19–21].

2.3 Mechanical properties of materials and their characterization

The biochemical (e.g. adhesiveness) and physical properties (e.g. substrate stiffness) of the extracellular microenvironment have been recognized as interdependent fac-

tors that influence cell function and tissue morphogenesis in multiple ways [19–21]. Consequently, both biochemical and physical characteristics must be considered when designing hydrogels for tissue engineering applications [10, 25]. Hydrogels will act as morphogenetic guides if their biochemical and physical attributes are tailored to provide an appropriate environment for cell adhesion, migration, growth, and differentiation [8, 15–17, 24]. To determine the optimal parameters, the mechanical properties of tissues or remodeled ECM may serve as reference points [20, 21]. This, in turn, will require accurate methods of measuring the mechanical properties of tissues, fabricated hydrogels, and tissue-engineered constructs.

Amongst other methods, the mechanical properties of materials, including tissues [53] and hydrogels [54], are characterized by tensile tests, compression tests, and dynamic mechanical analysis (DMA). For uniaxial tensile testing, dog bone-shaped samples are placed between two clamps and stretched at constant extension rates. From these experiments, the *Young's modulus* of the material can be determined. It is defined as the ratio of tensile stress to tensile strain, whereas the maximal tensile stress carried by a material is defined as the *tensile strength*. Similarly, the *compressive modulus* is defined as the ratio of compressive stress to compressive strain. Testing is performed by uniaxial compression of cylindrical specimens between two smooth impermeable platens (unconfined compressive testing). In contrast to that, confined compressive testing is carried out in a confining chamber where the sample is loaded by a permeable piston. These experiments reveal the *aggregate modulus* of the material. Depending on the applied testing mode, the calculated values of the Young's modulus will differ: frictional effects and/or interdigitation of the sample into the platen pores may increase the moduli obtained in confined compression [55]. The *compressive strength* is defined as the maximal compressive stress that a sample can withstand. Both, Young's modulus and compressive modulus are a measure of the *stiffness* of a given material, which mirrors the resistance of an elastic body against the deflection of an applied force.

DMA is typically performed to measure the viscoelastic behavior of materials. In rheological terms, 'viscoelastic' means the concomitance of viscous ("liquid-like") and elastic ("solid-like") behavior. For a given material, the proportion of viscous to elastic properties will depend on the experimental conditions (e.g. timescale and temperature). DMA assessments require the application of a sinusoidal shear load on

the sample. A stress transducer measures the applied shear stress (σ^*). The strain induced in the sample (γ^*) is measured using a strain transducer. The *complex shear modulus* G^* is defined as follows:

$$G^* = G' + i \cdot G'' = \frac{\sigma^*}{\gamma^*} \quad (2.1)$$

G' is referred to as the real part of G^* (also elastic or storage modulus) and represents the relative degree of a material to recover (“elastic response”). G'' is referred to as the imaginary part of G^* (also viscous or loss modulus) and represents the relative degree of a material to flow (“viscous response”) [56]. Measuring G^* against the shear stress or shear strain, respectively, allows to determine the *stiffness* and *strength* of a given material.

Using tensile tests, compressive tests, or DMA, the elastic moduli of various tissues have been determined (Table 2.1) [53]. In general, the measured moduli range over several orders of magnitude; neuronal tissue [57] is much softer than cartilaginous tissue [58] or bone tissue [59], for example. However, the obtained values should be regarded just as rough estimates for the mechanical characteristics of biological tissues. Nevertheless, the observed differences imply that distinct mechanical microenvironments exist for different cell types and tissues [21].

Table 2.1: Mechanical properties of different biological tissues. Many other studies can be found elsewhere [53].

Specimen	Testing method	Results	Ref.
Bovine spinal cord (gray matter)	Tensile test	Tangent moduli ^{a,b} ranged between 63.9 ± 7.9 and 112.3 ± 10.2 kPa depending on the strain rate	[57]
Articular cartilage from human hip joints (femoral head)	Biphasic creep indentation test	Aggregate moduli ^a ranged between 0.679 ± 0.162 and 1.816 ± 0.868 MPa depending on the location	[58]
Cortical bone from human femoral diaphysis	Tensile test	Total average value of the Young’s modulus: 17.9 GPa (data obtained at strain rates of $4 \cdot 10^{-2} \text{ s}^{-1}$)	[59]

^aData are given as mean \pm standard deviation.

^bThe tangent modulus is defined as the slope of the tangent to the stress-strain curve at a specific point. Within the linear elastic region, the tangent modulus is equal to the Young’s modulus.

In biological tissues local regions of high stiffness exist beside regions that exhibit much lower values for the elastic modulus. These heterogeneities are due to the composite character and the ongoing remodeling of the ECM [20]. Admittedly, local differences in the mechanical properties will not be detected by bulk measurements, such as tensile tests, compressive tests, and DMA. But because cells respond to spatial variations in the substrate stiffness, which can be on the order of microns [19, 20, 43], the local mechanical properties rather than the bulk properties will be crucial for the design of hydrogels. In addition, tensile tests, compressive tests, and DMA may affect the structural integrity of the sample or even involve its destruction [54]. When surveying the mechanical properties of living tissues or tissue-engineered constructs, however, non-invasive and non-destructive methods with high spatial resolution would be preferred. In the next paragraphs, we will highlight some of these methods.

2.3.1 Atomic force microscopy

Atomic force microscopy (AFM) can be used not only for imaging the topography of surfaces, but also for measuring forces on a molecular level. To investigate the mechanical properties of soft matrices or thin films, the sample is compressed by the indenting AFM tip (Figure 2.2). The loading force is calculated from the deflection and the spring constant of the cantilever. To calculate the Young's modulus of the material, force-indentation-curves are recorded and fitted to the Hertz model, which describes the elastic deformation of two spherical surfaces under load [60, 61].

Engler et al. used AFM to investigate the mechanical environment seen by SMCs *in vivo* and correlated this with SMC responses on collagen-coated polyacrylamide (PAAM) gels. Surface probe measurements within the SMC-rich medial layer of sectioned arteries revealed an apparent Young's modulus of $\sim 5 - 8$ kPa; the Young's moduli of collagen-coated PAAM gels ranged between ~ 1 kPa and ~ 35 kPa. Spreading of SMCs on PAAM gels showed a hyperbolic dependence on the elastic modulus of the substrate. Remarkably, half-max spreading of SMCs occurred on gels that approximated the stiffness of the arterial media ($E_{\frac{1}{2}-spread} \approx E_{media}$). For this reason, $E_{\frac{1}{2}-spread}$ is regarded as a mechanical set point for SMCs. Engler et al. concluded from

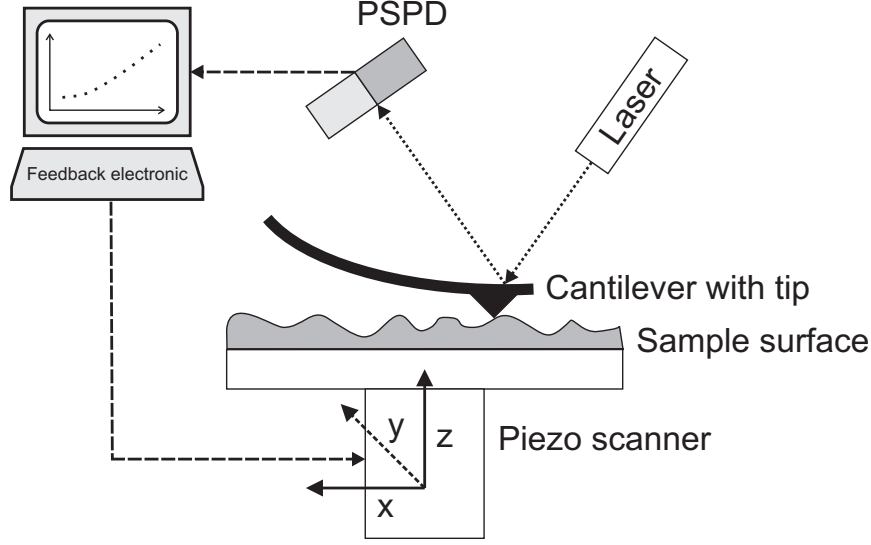


Figure 2.2: Diagram of AFM instrumentation [61]. A sharp tip at the free end of a microscale cantilever is used to probe the sample surface. The sample is mounted on a piezoelectric scanner that moves the sample in the x and y directions for scanning the surface and in the z direction for indenting the sample. A laser beam reflected from the back of the cantilever onto a position sensitive photodiode (PSPD) forms an optical lever system that measures the deflection of the cantilever. From this data and the spring constant of the cantilever the loading force can be calculated.

these experiments that surface probe measurements allow for an accurate assessment of the local mechanical properties of various materials including biological tissues [62].

2.3.2 Magnetic resonance elastography

Magnetic resonance elastography (MRE) is a non-invasive and non-destructive technique that visualizes spatial changes in mechanical properties. It has been successfully used to characterize the elastic properties of gel samples and tissue explants *ex vivo*. But MRE also provides information about the mechanical properties of soft tissue *in vivo*, which allows for the detection of pathological changes, such as soft tissue tumors, by a sensitive and safe method [63–65]. In this method, shear waves are generated within the sample using an electromechanical actuator coupled to the surface of the object. Using a magnetic resonance imaging (MRI) system with an additional motion sensitizing gradient, the displacement patterns corresponding to the shear

waves can be measured (Figure 2.3). The obtained “wave images” directly visualize the propagation of shear waves within the sample and allow the reconstruction of viscoelastic parameters at each location in the material [63, 64].

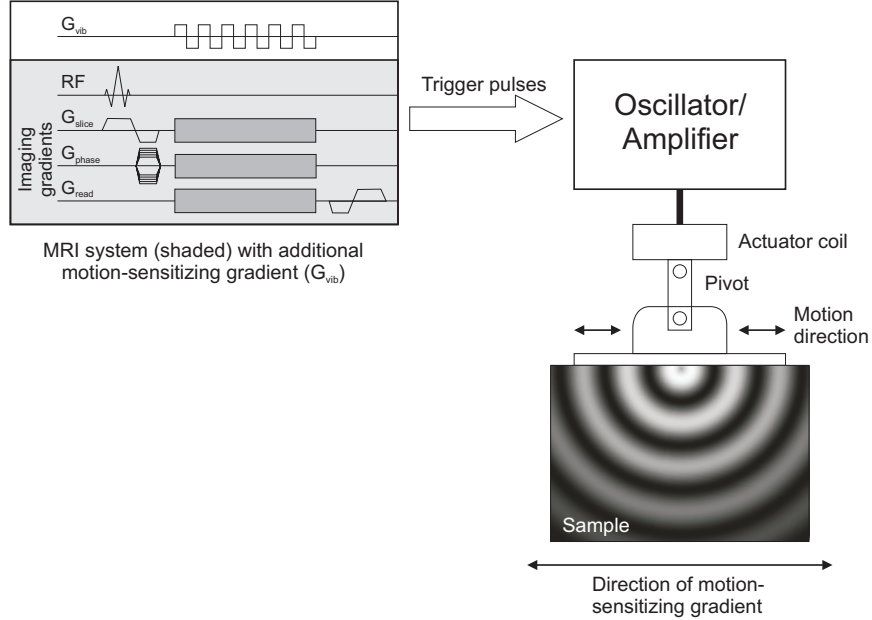


Figure 2.3: Schematic diagram of the MRE system [63]. A conventional MRI system operating with imaging gradients (G_{slice} , G_{phase} , and G_{read}) and radiofrequency (RF) pulses is equipped with an additional motion-sensitizing gradient (G_{vib}) (left). The imaging gradients are used to encode the spatial positions of the MR signal. Trigger pulses provided by the imager synchronize an oscillator that drives an electromechanical actuator coupled to the surface of the sample (right). In the presence of G_{vib} , the cyclic motion of the spins causes a measurable phase shift in the received MR signal. From this phase shift, the displacement in each volume element can be calculated. The data thus obtained are used to visualize the propagating shear waves within in the sample and to reconstruct the corresponding viscoelastic parameters.

Clinical magnetic resonance (MR) systems typically provide a spatial resolution of $1 \text{ mm} \times 1 \text{ mm} \times 10 \text{ mm}$, which would not be appropriate to survey the mechanical properties of small tissue-engineered constructs. In a recently published work, however, Othman et al. reported the development of an enhanced MRE method termed microscopic magnetic resonance elastography (μMRE). This technique has been used to image shear wave propagation with a microscopic resolution of $34 \mu\text{m} \times 34 \mu\text{m} \times 500 \mu\text{m}$. To evaluate the potential of μMRE for identifying the mechanical properties of

tissue-engineered constructs, Othman et al. cultured human bone marrow stromal cells (BMSCs) on gelatin sponges and differentiated them either into adipogenic or osteogenic cells. In preliminary experiments using μ MRE, the shear stiffness of adipogenic and osteogenic constructs was estimated to be ~ 1.2 and ~ 15 kPa, respectively. Although the algorithms used to reconstruct the material's properties still had to be adapted, the μ MRE technique provides a valuable tool to monitor the mechanical properties of tissue-engineered constructs during growth and differentiation [66].

2.3.3 Monitoring of cellular traction forces using fluorescence resonance energy transfer

Kong et al. [67] proposed a fluorescence resonance energy transfer (FRET) technique that may be adapted to study cell-material mechanics in three-dimensional culture. FRET occurs between a donor fluorochrome and an acceptor fluorochrome, if the emission wavelength of the donor and the excitation wavelength of the acceptor overlap. Furthermore, the spatial distance between donor and acceptor has to be less than 10 nm, such that the former can transfer energy to the latter (Figure 2.4) [68–70].

In their study, Kong et al. [67] coupled RGD-containing oligopeptides to sodium alginate and labeled the immobilized peptides with either Alexa Fluor 488 (green fluorescence) or Alexa Fluor 546 (red fluorescence). Hydrogels prepared by cross-linking equal volumes of differently labeled polymers with calcium were seeded with murine preosteoblasts and incubated in medium. Imaging was performed by laser scanning microscopy (excitation wavelength 488 nm). In these experiments, red fluorescence was limited to regions containing adherent cells, indicating that the labeled peptides not involved in cell adhesion were separated by a greater spacing than the critical distance required for FRET (Figure 2.4). With increasing substrate stiffness, the yield of red fluorescence first increased and then decreased. This is related to the capability of cells to cluster the adhesion peptides. The calculated force that cells exerted to displace the adhesion peptides, however, increased in proportion to the substrate stiffness. These results correlate very well with observed changes in cell phenotype, which have been reported to depend on cell adhesion stiffness. The FRET technique is, therefore, regarded as a molecular ruler to monitor displacements

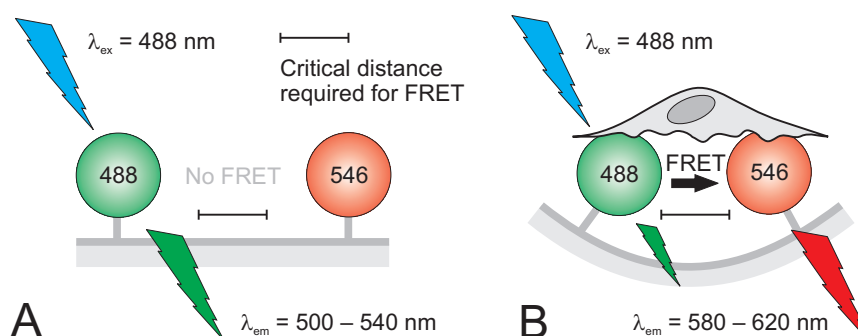


Figure 2.4: FRET is a process in which energy is transferred nonradiatively from an excited donor fluorophore to an acceptor fluorophore. It occurs with measurable efficiency if the two fluorophores are situated less than 10 nm apart [68–70]. (A) Excitation of the sample ($\lambda_{ex} = 488$ nm) results in green fluorescence ($\lambda_{em} = 500 - 540$ nm), as the corresponding fluorophores (RGD-containing oligopeptides labeled with either Alexa Fluor 488 or Alexa Fluor 546) are separated by a greater spacing than the critical distance required for FRET. (Alexa Fluor 546 is not excited at this wavelength.) (B) Seeded cells rearrange adhesion molecules presented from the substrate. Excitation of the sample leads to a reduction in the yield of green fluorescence, but increases the yield of red fluorescence ($\lambda_{em} = 580 - 620$ nm) [67].

between adhesion ligands and provides a valuable method to calculate cell traction forces without mechanical or chemical manipulations.

2.4 Rational design of hydrogels for tissue engineering considering physical aspects

Biochemical and physical parameters were identified as essential design variables of hydrogels used in tissue engineering applications [8, 10, 15–17, 22–25]. In this chapter, we will stress the physical properties of hydrogels, which include their gel forming characteristics, their mechanical or viscoelastic properties, respectively, and their degradation behavior. Below, we will present examples of current methods of controlling the physical properties of hydrogels. Alginates and poly(ethylene glycol) (PEG) serve as models, as their properties reflect those of many other gel forming polymers as well. The following considerations, however, can be applied to other polymers, too.

In general, all hydrogels used in biomedical applications must be biocompatible. Because the apparent mesh size of polymeric gels is typically much smaller than a cell's diameter, it would be useful to introduce cells into the liquid precursors of the gel, rather than to the preformed hydrogel itself. To accomplish this, gel forming methods have to be chosen that can be conducted in the presence of cells or *in vivo* without causing damage [10, 16, 25].

Alginates are naturally occurring polysaccharides and consist of guluronic acid (G) and mannuronic acid (M) organized into blocks of varying composition (G-blocks, M-blocks, and MG-blocks). Gels are formed when divalent cations (e.g. Ca^{2+}) interact with G-blocks to form ionic bridges between different polymer chains [71]. Because of their recognized biocompatibility and gentle gelling properties, hydrogels prepared from alginates are very attractive for many tissue engineering applications [10, 25]. PEG represents another type of polymer that is widely used in biomedical applications [10, 25]. Aqueous solutions of PEG macromers terminated with acrylate or methacrylate groups can be photo-polymerized in the presence of cells using UV or visible light, respectively, in combination with a proper initiating system to form covalently cross-linked hydrogels [72]. Besides ionic interactions and photo-polymerization, cross-linking is also accomplished by chemical reaction of complementary groups [73]. Vinylsulfone-functionalized PEG macromers can be cross-linked utilizing a Michael-type addition reaction between the vinylsulfone end groups and thiol-bearing compounds (Figure 2.5). These reactions can be conducted under physiological conditions and allow for the preparation of hydrogels in the presence of cells or *in vivo* [74]. Moreover, a variety of temperature-sensitive hydrogel systems are described in the literature [75]. Recently, important progress has also been made to form nanofibrillar matrices *in situ* by molecular self-assembly of synthetic peptides or proteins [76].

Due to their hydrophilic nature, most synthetic hydrogels are known to prevent the adsorption of ECM proteins. In addition, non-adhesiveness is accomplished because cells lack adhesion receptors for most hydrogel forming polymers [10, 25]. In order to design hydrogels that mediate attachment of cells, entire ECM proteins or synthetic peptide sequences capable of binding to cellular receptors have been covalently coupled to the polymer chains [8, 10, 15–17, 24, 25]. Incorporation of

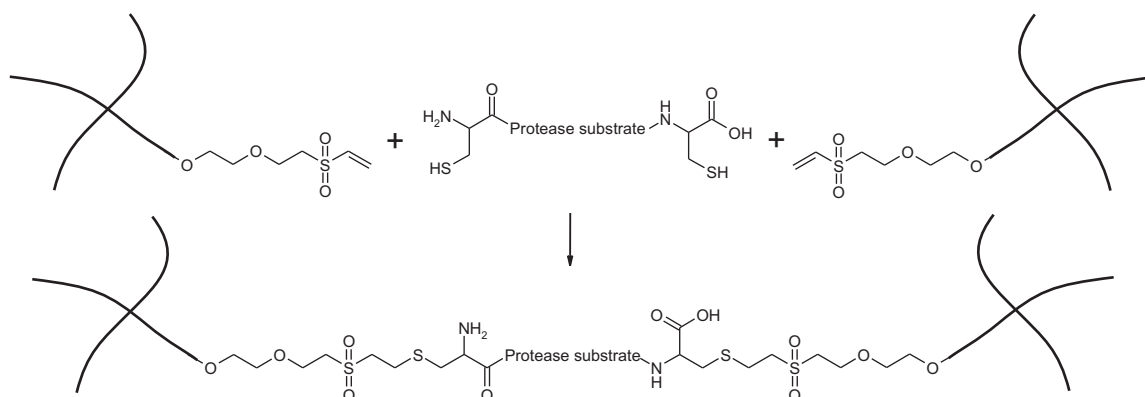


Figure 2.5: Michael-type addition reaction between vinylsulfone-functionalized PEG macro-mers and cysteine containing peptides. Cross-linking with enzymatically cleavable sequences renders the gels susceptible to proteolytic breakdown.

biologically active substances is another strategy by which hydrogels can be modified to regulate cell function and tissue morphogenesis [8–10, 15–17].

Once placed at the application site, the hydrogel scaffolds should be able to bear the local mechanical loads until the cells have produced their own functional ECM. Moreover, the hydrogel should provide an appropriate mechanical environment to support cell migration, proliferation, and differentiation [16, 74]. As each tissue provides its own mechanical microenvironment, the mechanical characteristics of hydrogels used in tissue engineering have to be adapted to the intended application: engineering neuronal tissue will require other mechanical conditions than cartilage or bone, for example. In part, the mechanical properties of hydrogels are predetermined by the inherent characteristics of the building blocks including their chemistry and molecular weight (MW). The gel strength can be further tailored by varying the concentration and composition of building blocks, by altering the method of cross-linking, and by adjusting the cross-link density or mesh size [54].

As only the G-blocks participate in ionic cross-linking, the gel strength of alginates depends on the monomeric ratio (M:G ratio) and the length of G-blocks [71]. Furthermore, the mechanical properties and swelling degree can be regulated by controlling the cross-link density (e.g. by altering the concentration of divalent cations) and using different principles of cross-linking (e.g. covalent cross-linking) [77]. Increasing the concentration of alginate also enhances the strength of alginate hydrogels [78].

Similarly, the mechanical properties of PEG gels are altered when the weight fraction of PEG diacrylate [79] or PEG dimethacrylate [80] increases. This is explained by the cyclization of macromers, which predominantly occurs at high solvent concentrations, finally leading to more loosely cross-linked hydrogels [80]. Furthermore, the molecular weight between cross-links and mesh size are also influenced by the molecular weight of the PEG macromer [81]. In contrast to PEG diacrylates and dimethacrylates, vinylsulfone-functionalized PEG macromers are typically branched. The mechanical properties and swelling ratio of hydrogels formed by the addition reaction of PEG vinylsulfones and cysteine containing oligopeptides are affected by the branching factor [82] and the molecular weight of the PEG macromer [74]. Additionally, the final network properties depend on the precursor concentration and the stoichiometry of reactive groups [74].

The network properties and swelling characteristics are further related to the mass transport characteristics of hydrogels [9, 10, 83, 84]. To accomplish a time-delayed release of small organic drugs or growth factors, for instance, it is necessary to limit the free diffusion out of the hydrogel carrier [9, 10, 85]. On the other hand, enhancing the supply of oxygen and nutrients as well as the removal of waste products is essential for the survival and growth of the implanted cells [83, 84, 86].

Besides appropriate mechanical properties and mass transport characteristics, degradation of the hydrogel is essential for many tissue engineering applications. Admittedly, most hydrogels formed by cross-linking of macromers exhibit a strong interdependency of cross-link density, mechanical properties, and degradation rate. With regard to the desired characteristics of the hydrogel, however, the independent control of degradation rate and mechanical properties will be crucial.

Ionically cross-linked hydrogels, such as alginate gels, normally undergo slow dissolution due to complexation of divalent cations or gradual exchange with monovalent cations present in the environment [78]. Reducing the molecular weight of alginate polymer chains [87] and introduction of hydrolytically labile acetal-like groups by oxidation [88, 89] allows for control of the degradation rate and mechanical properties in an almost independent manner. Hydrogels formed by photo-polymerization of PEG diacrylate or PEG dimethacrylate are non-degradable within the typical timescale of cell culture experiments. To render these hydrogels bioerodible, poly(α -hydroxy esters), such as poly(lactic acid) (PLA) or poly(glycolic acid) (PGA), have been grafted

to the PEG central block finally leading to triblock copolymers (PLA-*b*-PEG-*b*-PLA or PGA-*b*-PEG-*b*-PGA) with acrylate or methacrylate end groups. The degradation rate can be tailored by appropriate choice of the hydrolyzable poly(α -hydroxy esters) and by varying its block length [72]. Cross-linking of PEG vinylsulfone macromers with enzymatically cleavable peptides, such as matrix metalloproteinase (MMP) sensitive peptides, allows for the creation of hydrogels that are susceptible to proteolytic breakdown. The degradation kinetics were found to depend on the MMP activity of the incorporated substrate and the action of cell-secreted MMPs [90].

2.5 Physical parameters regulate tissue development in vitro and in vivo

Current research efforts focus on physical cues regulating cell function and tissue morphogenesis. Therefore, the physical characteristics of biomaterials used in tissue engineering applications should no longer be neglected with respect to their biological effects [22–24]. The subsequent chapters are to illustrate the impact of substrate stiffness and degradability on tissue engineering. Thereby, we will focus on the use of hydrogels and outline the effects of their inherent properties on tissue morphogenesis. The effects of externally applied forces on cells and tissues are reviewed elsewhere in detail [22, 24, 91, 92] and will, therefore, not be addressed here.

2.5.1 Impact of mechanical factors on cell function and tissue morphogenesis

In order to assess the impact of hydrogel pore size on neurite extension, Dillon et al. entrapped dorsal root ganglions (DRGs) into agarose gels of varying concentration. Concomitantly with increasing agarose concentration, the average pore size decreased exponentially as calculated from hydraulic permeability measurements. Similarly, the length of extended neurites decreased with increasing agarose concentration [93]. In a follow-up study, Balgude et al. correlated the rate of neurite extension to the mechanical stiffness of the hydrogel. They prepared agarose gels of varying

concentration and determined G^* by oscillatory rheometry. The magnitude of G^* was used to calculate the force exerted by the hydrogel network on the advancing neurite growth cones. Thereby, Balgude et al. found an inversely proportional relationship between the force exerted by the hydrogel and the rate of neurite extension [94].

Similar results were obtained by Gunn et al. who encapsulated PC12 cells, a commercially available rat pheochromocytoma cell line, into photo-cross-linkable hydrogels prepared from PEG diacrylate. The Young's modulus significantly increased when the weight fraction of PEG diacrylate was increased. To mediate cell attachment, hydrogels were further functionalized with various adhesion ligands. As a result of this study, neurite extension was found to depend on the type and concentration of adhesion ligand as well as the mechanical properties of the hydrogel. Compared to more flexible hydrogels, gels with higher modulus significantly decreased neurite extension [79].

To investigate the influence of cross-link density on cartilaginous tissue formation, Bryant et al. embedded bovine chondrocytes into hydrogels prepared from PEG dimethacrylate. Swelling studies revealed an increase in cross-link density with increasing macromer concentration. After cultivation, immunohistochemistry suggested an enhanced production of collagen type II in hydrogels of intermediate cross-link density. Deposited collagens and glycosaminoglycans (GAGs) were primarily located pericellularly, indicating that diffusion of macromolecules is restricted within these gels. Only in the most loosely cross-linked hydrogels GAGs were distributed homogeneously [80].

Cartilaginous tissue formation was also studied by Wong et al. using alginate hydrogels. In this study, the alginate type was shown to affect ECM accumulation, whereby gels containing intermediate amounts of guluronic acid showed the highest level of matrix synthesis. Among other possible reasons, such as impurities of the different alginate types, ECM production is thought to be influenced by the mechanical stiffness of the hydrogel, which results from the alginate type utilized [95].

Capillary morphogenesis has also been shown to depend on the substrate stiffness. Sieminski et al. cultured human blood outgrowth endothelial cells (HBOECs) and human umbilical vein endothelial cells (HUVECs) in collagen gels that were either free floating or bound to the bottom of the well. The apparent stiffness of the matrix is thought to depend on the collagen concentration as well as whether the gels are free

floating or attached to the rigid culture plastic. Generally, capillary morphogenesis seemed to be improved in more malleable environments. Furthermore, the apparent matrix stiffness that supported capillary morphogenesis to the highest extent was found to vary with different endothelial cells and their ability to contract the collagen matrix [96].

These examples illustrate the impact of mechanical cues on cell behavior and tissue morphogenesis. Cells embedded into hydrogels probably sense some sort of physical confinement that regulates growth, differentiation, and ECM accumulation. This confinement may be caused by the mechanical properties of the hydrogel itself as well as the pericellular accumulation of ECM macromolecules. The supply of nutrients, oxygen, and bioactive substances, as well as the removal of waste products, are also affected by the network properties and swelling characteristics of hydrogels [9, 10, 83, 84, 86]. This, in turn, may also contribute to the observed cellular responses.

2.5.2 Influence of degradation profile on tissue formation

As outlined above, tissue morphogenesis is strongly influenced by the mechanical properties of the supportive matrix. However, as most biomaterials used for tissue engineering applications are biodegradable, the initial mechanical properties are not retained over time. During the degradation of hydrogels, the average mesh size and swelling level increase, and the diffusion of macromolecules, e.g. ECM components, is facilitated. Concomitantly with the increase in mesh size, the mechanical properties of the degrading hydrogel decrease significantly.

To examine the effects of temporally changing physicochemical properties on tissue formation, Bryant et al. encapsulated bovine chondrocytes into photo-cross-linkable hydrogels prepared from varying ratios of degradable PLA-*b*-PEG-*b*-PLA diacrylate and nondegradable PEG dimethacrylate. After six weeks of cultivation, the total collagen and desoxyribonucleic acid (DNA) contents were significantly increased in gels with a high proportion of degradable macromers. The synthesis of collagen type II also seemed to be favored, as indicated by immunohistochemistry. Altogether, in highly degradable hydrogels, the composition of deposited ECM (collagens and GAGs) more closely approached those of native cartilage, compared to less degradable

gels. Additionally, the secreted ECM was distributed more homogeneously throughout the whole tissue, whereas, in gels with less degradable macromers, ECM was mainly located in the pericellular region [97].

Alsberg et al. compared irradiated, more rapidly degrading alginate hydrogels and non-irradiated, slowly degrading gels regarding their ability to support bone development *in vivo*. Rat-derived osteoblasts were encapsulated into RGD-modified, calcium cross-linked alginate gels and implanted into the backs of mice. Histological examinations, bone densitometry, and microcomputed tomography (μ CT) revealed that rapidly degrading gels dramatically improved the extent and quality of bone formation [87].

Similar results can be found by Kong et al., who used non-oxidized, high MW alginates and binary blends of oxidized, low and high MW alginates. Rat-derived BMSCs embedded in RGD-conjugated, calcium cross-linked alginate gels were implanted in the backs of mice. In order to promote differentiation of the BMSCs to osteoblasts, the hydrogels were loaded with bone morphogenic protein-2 (BMP-2) and transforming growth factor- β 3 (TGF- β 3). Compared to the more slowly degrading non-oxidized, high MW gels, the more rapidly degrading binary gels facilitated the formation of new bone tissue, indicated by histological sections [88].

However, tailoring the degradation rate not only provides control over tissue morphogenesis. In a recently published work, Mahoney et al. reported the temporal control of neural tissue formation by altering the degradation rate of methacrylate end-capped triblock copolymers of PLA, PGA, and PEG. During the first week of culture, photoencapsulated neural cells (precursor cells and neurons) assembled together and formed small micro-tissues, which are considered to be building blocks for the creation of functional neural circuits. After two weeks, the mesh size of the hydrogel exceeded a critical value and processes emerged to penetrate throughout the environment. Immunocytochemistry further revealed the presence of neurons and glial cells that were responsive to neurotransmitters. As the time-scale over which neural tissue develops could be tailored by incorporation of the cells into quickly degrading (PGA-*b*-PEG-*b*-PGA) or more slowly degrading networks (PLA-*b*-PEG-*b*-PLA), Mahoney et al. identified the degradation rate as a critical factor influencing process outgrowth and neural cell differentiation [98].

Degradability and degradation rate of the supportive matrix were identified as having a strong influence on cell migration, proliferation, differentiation, and morphology of the newly formed tissue. But the examples outlined above also illustrate that it may be hard to distinguish between effects of substrate degradability and substrate mechanics. The observed biological responses may be due to the given mechanical properties of the matrix or to the ongoing loss of material during degradation. Together, the presented studies imply that cell differentiation and tissue morphogenesis are supported by rapidly degrading matrices. This, however, may be a false conclusion, as the optimal degradation rate will depend on the intended application as well as the specifics of particular cells. The study of Meinel et al. illustrates this issue: too rapid of a degradation rate caused collagen scaffolds to collapse before substantial amounts of ECM were deposited by the cells [99]. Consequently, it would be beneficial to couple the rate of matrix degradation to the rate of ECM production in order to support cell differentiation and tissue integrity.

2.5.3 Cell-responsive hydrogels

Ideally, matrix degradation would occur in temporal and spatial synchrony with the formation of new tissue. In traditional biomaterials, however, degradation typically takes place by non-enzymatic cleavage of chemically labile bonds (e.g. by hydrolysis of ester bonds). Therefore, adapting the degradation rate to the rate of tissue formation is a challenging task. In contrast, cell-responsive biomaterials mimic the proteolytic recognition of natural ECMs and are degraded by cell-secreted and cell-activated proteases, such as MMPs and serine proteases. This creates a dynamic balance between matrix degradation and ECM deposition and allows for the remodeling of the biomaterial by encapsulated or invading cells [8, 15–17].

To study the invasion characteristics of human fibroblasts *in vitro*, Lutolf et al. attached integrin-binding domains (RGDSP) to vinylsulfone-functionalized PEGs and cross-linked the macromers with MMP-sensitive peptide sequences (Figure 2.6). The cell invasion rate was found to depend on the RGD ligand density, the MMP-sensitivity, and the cross-link density of the networks. At a constant RGD ligand

density, lowering the PEG molecular weight from 20 to 15 kDa decreased the invasion rate by almost a factor of four [90].

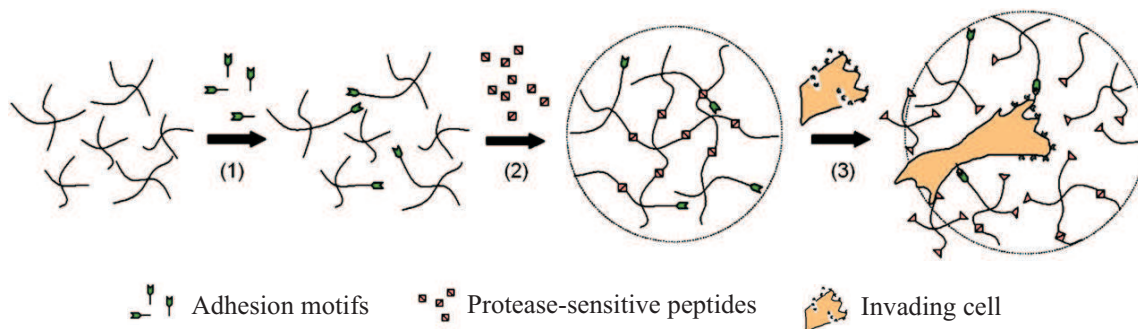


Figure 2.6: Michael-type addition reaction between four-armed PEG-vinylsulfones and cysteine containing peptides. Introduction of adhesion sequences (step 1). Gelation is performed in the presence of cells using protease-sensitive peptides as cross-linker (step 2). Networks are locally degraded by cellular proteases (step 3). Reprinted with permission from Lutolf et al. [90]. © 2003 National Academy of Sciences U.S.A.

To demonstrate the suitability of these biomaterials to induce tissue regeneration *in vivo*, similar gels were used to deliver physically entrapped BMP-2 to the site of critical-sized defects in rat crania. After five weeks, bone healing was assessed by analyzing cranial samples using μ CT. MMP-sensitive, BMP-2-bearing hydrogels promoted bone formation to a significantly higher extent than MMP-insensitive or BMP-2-lacking controls. Regarding the bone coverage, no significant differences could be observed between hydrogels composed of four-armed PEGs of 15 and 20 kDa molecular weight. However, cell infiltration was much more extensive in gels of lower cross-link density (higher MW), resulting in increased bone volume and connectivity [100].

In another study, Park et al. evaluated the suitability of MMP-sensitive PEG-based hydrogels as scaffolds for cartilage repair. Bovine chondrocytes were cultured for one month in hydrogels prepared from PEG-vinylsulfones and MMP-sensitive peptides (degradable gels) or PEG-vinylsulfones and PEG-dithiols (non-degradable gels). When eight-armed PEG-vinylsulfone is used instead of four-armed, the cross-linked hydrogels are stiffer and less swollen. The increased stiffness not only significantly reduced cell number and size of the cultured clusters, but also influenced the expression of ECM genes and the spatial distribution of deposited ECM. In degradable hydrogels, the expression level of collagen type II, collagen type XI, and aggrecan increased

with decreasing cross-link density, indicated by real-time polymerase chain reaction (PCR), and ECM fibrils extended far into the hydrogel. In contrast, non-degradable hydrogels generally led to lower expression levels of ECM genes and densely packed ECM fibrils, but supported the expression of MMP-13 genes. Due to these results, Park et al. concluded that cells obviously sense the matrix density or different levels of physical confinement and subsequently adapt their gene expression pattern [82].

The degradation rate of these cell-responsive hydrogels depends on the action of cellular proteases rather than environmental factors, such as the pH. Therefore, the mechanical properties of the gels are thought to be retained until cell-triggered remodeling is initiated. This enables the fabrication of hydrogels that provide an appropriate mechanical environment for cell migration, proliferation, and differentiation throughout their lifetime. The sustained mechanical integrity also prevents early failure of the scaffold in load bearing applications. Taken together, these hydrogel systems allow for an enormous versatility in design and might be useful in a variety of tissue engineering applications.

2.6 Concluding remarks

Physical factors are potent regulators of cell function and tissue morphogenesis. In most cases, however, the observed biological effects cannot be attributed to individual physical parameters: the network properties and swelling characteristics of hydrogels, for example, determine their mechanical properties as well as their mass transport characteristics. Consequently, the diffusivity of growth factors, oxygen, nutrients, or waste products will also contribute to the cellular response. In addition, the initial mechanical properties of biomaterials are not the only factors decisive for the cellular fate: over time, the substrate mechanics may significantly change due to degradation of the matrix and/or deposition of ECM macromolecules. To survey this process, non-invasive and non-destructive methods of measuring the mechanical properties are required. However, emerging techniques, such as AFM and MRE, are still far from being routine in tissue engineering. Therefore, the application of these methods has to be further propagated in order to allow for the systematic characterization of living tissues. Modeling of cell-biomaterial interactions in three-dimensional matrices may

also contribute to understand the complex interdependency of substrate mechanics and adhesiveness [19–21, 101]. Together, this enables the integration of chemical, physical, and topographical aspects and may have a powerful impact on the rational design of appropriate biomaterials for tissue engineering applications.

Chapter 3

Poly(ethylene glycol) based hydrogels for intraocular applications

Ferdinand Brandl¹, Matthias Henke¹, Stefan Rothschenk^{1,2},
Ruth Gschwind³, Miriam Breunig¹, Torsten Blunk¹, Jörg Teßmar¹,
Achim Göpferich¹

¹ *Department of Pharmaceutical Technology, University of Regensburg, 93040 Regensburg*

² *LTS Lohmann Therapie-Systeme AG, 56626 Andernach*

³ *Department of Organic Chemistry, University of Regensburg, 93040 Regensburg*

Published in *Advanced Engineering Materials* **9** (12), 1141–1149 (2007).

Abstract

Hydrogels are attractive materials for biomedical applications due to their versatility and excellent biocompatibility. In this study, we report the preparation of poly(ethylene glycol) (PEG) based hydrogels for intraocular applications. We synthesized branched PEG-succinimidyl propionates (10 kDa molecular weight) and different types of PEG-amines (linear and branched, 2 and 10 kDa molecular weight). Transparent hydrogels were formed *in situ* upon chemical reaction of these macromers. The gels were characterized by oscillatory rheometry and NMR experiments. By varying the concentration of macromers, the functionality of the PEG-amine, and the conditions during cross-linking, gels with adequate gelation times of approx. 5 – 10 min and gel strengths of approx. 350 – 1500 Pa were obtained. The cross-linked hydrogels showed no cytotoxic effects and may be used as vitreous substitutes or intraocular drug release systems.

3.1 Introduction

Hydrogels are highly hydrated networks of interacting polymer chains with viscoelastic properties similar to those of natural tissues. Due to their enormous versatility and excellent biocompatibility, they have been used for a variety of biomedical applications. In tissue engineering approaches, hydrogels were studied as cell carriers for the regeneration of a wide range of tissues including bone, cartilage, muscle, and neuronal tissue. They were also applied as controlled release systems for bioactive molecules (e.g. growth factors, nucleic acids, and various drugs) or as space filling scaffolds in plastic surgery [7, 8, 10, 102, 103].

When designing new biomaterials for such sophisticated applications, an exact knowledge of the biochemical and physicochemical requirements is essential. Hydrogels designed for intraocular applications, for example, need to have distinct optical and mechanical characteristics that are close to the properties of the vitreous body. The natural vitreous is a transparent, virtually acellular, gel-like network of collagen fibrils and glycosaminoglycans that fills the posterior segment of the eye. It acts as a shock absorber, maintains the shape of the eye, and assists in holding the neuronal retina in place [104, 105]. Dysfunctionalities of the vitreous body due to aging, traumatic injuries, tumors, or systemic diseases (e.g. diabetes mellitus) often result in severe visual impairment [105–107]. Proliferative diabetic retinopathy (PDR), for example, is a frequently occurring complication of diabetes mellitus and characterized by an abnormal growth of blood vessels into the vitreous body [108]. Besides age-related macular degeneration (AMD), cataract, and glaucoma, PDR is one of the leading causes of blindness in industrialized nations [18].

In such cases, a total replacement of the affected vitreous may be required in order to prevent blindness or to restore vision [105–107]. However, today’s clinically used substitutes (e.g. silicone oil, perfluorocarbon liquids, and gases) differ significantly from the natural vitreous body regarding their physicochemical properties and mechanics. Some of these materials are also associated with severe side-effects when kept intravitreally over longer periods of time [105, 106]. As alternatives, various gel-forming polymers (e.g. collagen, polysaccharides, and synthetic polymers) have been studied over the past decades, but none of them met clinical standards due to rapid degradation, fast clearance from the eye, and numerous other complications [105–107].

Cross-linked hydrogels, which are expected to exhibit longer retention times, also failed as vitreous substitutes as their mechanical properties are seriously impaired upon the injection process [107, 109]. It has been hypothesized that these difficulties could be avoided if low-viscous gels were used that solidify after injection into the vitreous cavity. Apart from their potential as vitreous substitutes, such hydrogels would be promising materials for the delivery of drugs to the posterior segment of the eye. As the pharmacologic treatment of vitreoretinal diseases, such as PDR and AMD, fairly advanced during the last years, therapeutic benefits can be expected from hydrogels loaded with anti-inflammatory or anti-proliferative agents [110, 111].

Hydrogels based on poly(ethylene glycol) (PEG) can be considered potential vitreous substitutes due to their excellent biocompatibility and transparency. Aqueous solutions of PEG macromers can be cross-linked *in situ*, if chemical reactions are used that are sufficiently gentle to be performed in the presence of cells or *in vivo* [73]. First studies that can be found in the literature are highly promising. Glucose-permeable hydrogels have been developed by cross-linking star-shaped PEG-amines with a di-succinimidyl ester of PEG. The gels formed in water without any catalysts or initiators and showed good biocompatibility when implanted subcutaneously in rats [112]. A rapidly gelling tissue sealant based on thiol-functionalized PEG macromers and PEG-succinimidyl glutarates has also been described [113]. Lutolf et al. prepared hydrogels by stepwise copolymerization of vinylsulfone-functionalized PEG macromers and cysteine containing peptides that were successfully applied in a variety of tissue engineering applications [74, 82, 100]. For ophthalmologic applications, hydrogels consisting of lysine-terminated dendrons and PEG-succinimidyl propionates have been proposed for the closure of scleral incisions [114].

Despite their promise for other applications, the described hydrogels would be less suited for intraocular applications due to their high polymer content of up to 40 % (w/v) and their high mechanical stiffness of several thousand Pascal. Furthermore, most of these gels solidify within a few seconds, which would impede their injection into the eye. In this paper, we report the synthesis and preparation of hydrogels cross-linked *in situ* by chemical reaction of branched PEG-succinimidyl propionates with PEG-amines. As the two macromers are linked together by amide bonds, the obtained hydrogels are expected to be stable over an extended period of time. Gelation kinetics and mechanical strength were analyzed by oscillatory shear experiments and adjusted

to the requirements of potential vitreous substitutes. The effectiveness of cross-linking was further evaluated by nuclear magnetic resonance (NMR) experiments. *In vitro* cytotoxicity of the cross-linked gels was investigated using a standard cell proliferation assay. In a final experiment, we studied the suitability of the prepared hydrogels as potential drug carrier systems which would be interesting for the pharmacotherapy of common eye diseases, such as PDR and AMD.

3.2 Materials and Methods

3.2.1 Materials

Acrylonitrile, *N,N'*-dicyclohexylcarbodiimide (DCC), diisopropyl azodicarboxylate (DIAD), Dulbecco's modified Eagle's medium (DMEM), fetal bovine serum (FBS), fluoresceine isothiocyanate (FITC)-dextran, N-hydroxysuccinimide (NHS), poly(ethylene glycol) (molecular weight 2 kDa, PEG2k-OH), and sodium dodecyl sulfate (SDS) were purchased from Sigma-Aldrich (Taufkirchen, Germany). Phthalimide was obtained from Acros Organics (Geel, Belgium). Four-armed poly(ethylene glycol) (molecular weight 10 kDa, 4armPEG10k-OH) was purchased from Nektar Therapeutics (Huntsville, AL). Diethyl ether, ethanol, and methylene chloride were of technical grade and used without purification. Deuterated chloroform (CDCl_3) and deuterium oxide (D_2O) were purchased from Deutero GmbH (Kastellaun, Germany). FluoSpheres[®] and phosphate buffered saline (PBS) were purchased from Invitrogen GmbH (Karlsruhe, Germany). All other chemicals were of analytical grade and purchased from Merck KGaA (Darmstadt, Germany). Water was obtained using a Milli-Q water purification system from Millipore (Schwalbach, Germany).

3.2.2 Synthesis of PEG-amines

PEG-amines were synthesized according to a procedure described by Mongondry et al. [115]. For a typical synthesis, PEG2k-OH (5 mmol), phthalimide (15 mmol), and triphenylphosphine (PPh_3) (15 mmol) were dissolved in 50 mL of tetrahydrofuran

(THF). Then, a solution of DIAD (15 mmol) in THF (15 mL) was added dropwise (Figure 3.1A). For the synthesis of branched PEG-amines, 4armPEG10k-OH (1 mmol) was used instead of PEG2k-OH and the excess of reagents was decreased to 1.2 times. After 48 h of stirring at room temperature, the solvent was evaporated under reduced pressure. For purification, the raw product was dissolved in water again, filtered, and washed with diethyl ether. After the water had been removed under reduced pressure, the oily product was dissolved in methylene chloride and subsequently precipitated by dropping into ice cold diethyl ether. The precipitate was collected by filtration and dried under vacuum overnight.

The obtained phthalimido-PEGs (4 mmol) were dissolved in ethanol (50 mL) and treated with hydrazine monohydrate (40 mmol) under reflux for 5 h. After cooling to room temperature, hydrochloric acid (3 M) was added up to pH 2 – 3 and the formed precipitate was removed by filtration. The solvent was evaporated, the obtained raw product was dissolved in water, and the pH of the aqueous solution was adjusted with sodium hydroxide (3 M) to 9 – 10. The product was then extracted with methylene chloride. After drying over anhydrous sodium sulfate, the solution was concentrated under reduced pressure and dropped into ice cold diethyl ether. The precipitated polymer was collected and dried under vacuum.

$^1\text{H-NMR}$ (PEG2k-NH₂, CDCl₃, 300 MHz): δ 2.95 ppm (t, 4H, $-\text{OCH}_2\text{CH}_2\text{NH}_2$), 3.65 ppm (s, $-\text{OCH}_2\text{CH}_2\text{O}-$). $^1\text{H-NMR}$ (4armPEG10k-NH₂, CDCl₃, 600 MHz): δ 2.87 ppm (t, 8H, $-\text{OCH}_2\text{CH}_2\text{NH}_2$), 3.41 ppm (s, 8H, $\text{R}_3\text{CCH}_2\text{O}-$), 3.64 ppm (s, $-\text{OCH}_2\text{CH}_2\text{O}-$). The degree of end-group conversion ranged from 95 to 100 %, as determined by NMR.

3.2.3 Synthesis of branched PEG-succinimidyl propionates

PEG-propionic acid was synthesized as described by Sedaghat-Herati et al. [116]. For the synthesis of branched succinimidyl esters (Figure 3.1B), the experimental procedure was modified as follows: 4armPEG10k-OH (1 mmol) was dissolved in water (15 mL) containing potassium hydroxide (0.20 g). After cooling to 0 °C, acrylonitrile (20 mmol) was added stepwise. The reaction mixture was stirred for 2.5 h at 0 °C and then kept in the refrigerator overnight. After neutralizing with hydrochloric

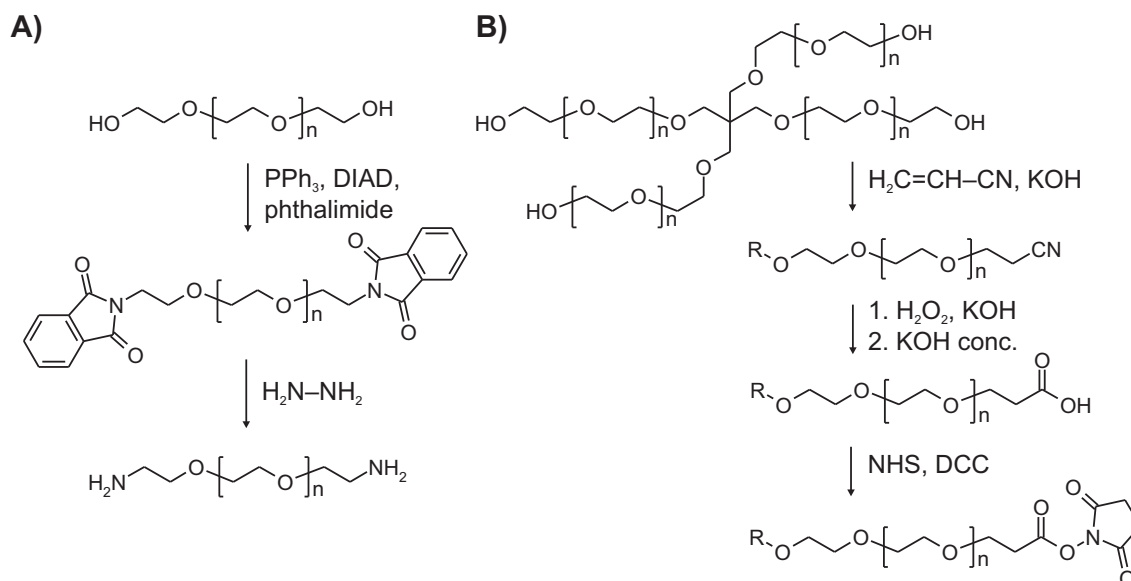


Figure 3.1: Synthesis of PEG2k-NH₂ (A) and 4armPEG10k-SPA (B).

acid (3 M), the aqueous solution was extracted with methylene chloride. The combined organic phases were washed with a saturated solution of sodium chloride and dried over anhydrous sodium sulfate. The organic solution was concentrated under reduced pressure and dropped into ice cold diethyl ether. The precipitated product was collected by filtration and dried under vacuum.

To obtain the PEG-propionic acid, PEG-propionitrile was dissolved in water (50 mL) containing potassium hydroxide (0.18 g). This solution was cooled to 0 °C and 2.70 mL of a hydrogen peroxide solution (30 %) were added stepwise. The reaction mixture was stirred at room temperature overnight. Then, 1.5 g of sodium thiosulfate and 250 mL of a potassium hydroxide solution (6 %) were added. After stirring for 48 h at room temperature, the reaction mixture was placed in an ice bath and neutralized with hydrochloric acid (3 M). The product was extracted and precipitated as described for PEG-propionitrile.

For the synthesis of the corresponding succinimidyl ester, PEG-propionic acid (0.2 mmol) and NHS (1.6 mmol) were dissolved in 15 mL of dry methylene chloride. DCC (1.6 mL) was separately dissolved in 5 mL of the same solvent. The carbodiimide solution was then added to the solution of PEG-propionic acid and kept under stirring at room temperature overnight. The mixture was filtrated to remove precipitated

dicyclohexylurea, concentrated under reduced pressure and dropped into ice cold diethyl ether. The precipitated polymer was collected and dried under vacuum.

^1H -NMR (4armPEG10k-SPA, CDCl_3 , 600 MHz): δ 2.84 ppm (s, 14H, $-\text{CH}_2\text{CH}_2\text{COOSu}$), 2.90 ppm (t, 7H, $-\text{CH}_2\text{CH}_2\text{COOSu}$), 3.41 ppm (s, 8H, $\text{R}_3\text{CCH}_2\text{O}-$), 3.64 ppm (s, $-\text{OCH}_2\text{CH}_2\text{O}-$), 3.85 ppm (t, 7H, $-\text{CH}_2\text{CH}_2\text{COOSu}$). The degree of substitution was about 90 %, with the remaining 10 % being PEG-propionic acid, as determined by NMR spectroscopy.

3.2.4 Preparation and rheological characterization of hydrogels

Gelation kinetics and gel strength were studied by performing oscillatory shear experiments on a TA Instruments AR 2000 rheometer (TA Instruments, Eschborn, Germany) with parallel plate geometry under humidified atmosphere. For the preparation of hydrogels, specified amounts of PEG-amines were dissolved in buffer solutions of defined pH (Table 3.1); 4armPEG10k-SPA was dissolved in PBS or water, respectively. The solutions of 4armPEG10k-SPA were filtrated (0.20 μm syringe filter, Corning Costar, Bodenheim, Germany) to remove traces of water-insoluble impurities. The two precursor solutions were mixed and immediately cast onto the lower plate of the rheometer.

The evolution of storage (G') and loss moduli (G'') was recorded as a function of time at designated temperatures (Table 3.1), 1 Hz oscillatory frequency, and 10 μNm torque (20 mm steel plate, measuring gap size 1000 μm). The crossover of G' and G'' was regarded as the gel point. The gel strength was determined by recording the complex shear modulus (G^*) at a constant frequency of 1 Hz as a function of the applied stress. If measurements were affected by the existent system inertia, G' and G'' were recorded at 0.5 Hz oscillatory frequency and 10 μNm torque (40 mm steel plate, measuring gap size 500 μm).

3.2.5 Characterization of hydrogels by NMR

For NMR measurements, 4armPEG10k-SPA and PEG2k- NH_2 were dissolved in D_2O in concentrations of 10 % (w/v) and 4 % (w/v), respectively. Samples were prepared

Table 3.1: Composition of hydrogels and conditions of gel preparation

Gel	4armPEG10k-SPA	PEG-amine		pH	Temperature	Ratio r^a
	Concentration	Concentration	Type			
1	5 % (w/v)	1 % (w/v)	linear (2 kDa)	7.4 ^b	25 °C	2.00
2	5 % (w/v)	1.5 % (w/v)	linear (2 kDa)	7.4 ^b	25 °C	1.33
3	5 % (w/v)	2 % (w/v)	linear (2 kDa)	7.4 ^b	25 °C	1.00
4	5 % (w/v)	2.5 % (w/v)	linear (2 kDa)	7.4 ^b	25 °C	0.80
5	10 % (w/v)	3 % (w/v)	linear (2 kDa)	7.4 ^b	25 °C	1.33
6	10 % (w/v)	4 % (w/v)	linear (2 kDa)	7.4 ^b	25 °C	1.00
7	5 % (w/v)	1.5 % (w/v)	linear (2 kDa)	6.0 ^c	25 °C	1.33
8	5 % (w/v)	1.5 % (w/v)	linear (2 kDa)	6.5 ^c	25 °C	1.33
9	5 % (w/v)	1.5 % (w/v)	linear (2 kDa)	7.0 ^c	25 °C	1.33
10	5 % (w/v)	1.5 % (w/v)	linear (2 kDa)	7.5 ^c	25 °C	1.33
11	5 % (w/v)	2 % (w/v)	linear (2 kDa)	7.0 ^d	15 °C	1.00
12	5 % (w/v)	2 % (w/v)	linear (2 kDa)	7.0 ^d	25 °C	1.00
13	5 % (w/v)	2 % (w/v)	linear (2 kDa)	7.0 ^d	35 °C	1.00
14	2 % (w/v)	2 % (w/v)	4arm (10 kDa)	7.0 ^d	25 °C	1.00
15	3 % (w/v)	3 % (w/v)	4arm (10 kDa)	7.0 ^d	25 °C	1.00

^aThe stoichiometric ratio r is defined as the molar ratio of succinimidyl ester to amino groups.

Calculations are performed assuming quantitative conversion of end-groups.

^bPhosphate buffered saline (both macromers dissolved in PBS)

^c250 mM phosphate buffer (PEG-amine in 500 mM phosphate buffer, 4armPEG10k-SPA in water)

^d25 mM phosphate buffer (PEG-amine in 50 mM phosphate buffer, 4armPEG10k-SPA in water)

from equal volumes of the filtrated precursor solutions. ¹H-NMR and ¹³C-NMR spectra were recorded at 600 and 150 MHz, respectively, on a Bruker Avance 600 (Bruker BioSpin GmbH, Rheinstetten, Germany). To follow the cross-linking of hydrogels, a time series of ¹H-NMR spectra was recorded over a total time of 180 min.

3.2.6 Cytotoxicity of cross-linked hydrogels

NIH 3T3 fibroblasts (LGC Promochem GmbH, Wesel, Germany) were grown in T-75 cell culture flasks containing 10 mL DMEM supplemented with 10 % FBS at standard cell culture conditions (37 °C, 95 % relative humidity, and 5 % CO₂).

The cytotoxicity of the cross-linked hydrogels was evaluated by a medium extraction test. 300 μL of hydrogels consisting of 2 % (w/v) 4armPEG10k-SPA and 2 % (w/v) 4armPEG10k-NH₂ were cast into 24-well plates (surface area approx. 2 cm²). After 60 min of cross-linking, the gels were covered with 1 or 2 mL DMEM and incubated under standard cell culture conditions (see above) for 24 h (surface area to fluid volume 1 and 2 cm²/mL). Prior to cytotoxicity testing, the cells were replated at 90 % confluency and seeded into 96-well plates at a density of 12,000 cells per well. Twenty hours after seeding, the culture medium was replaced by the extraction medium (100 μL /well), followed by incubation for 24 h. Cells treated with 0.01 % SDS served as positive control.

Cell viability was evaluated using the CellTiter 96[®] AQueous One Solution Cell Proliferation Assay (Promega GmbH, Mannheim, Germany). 20 μL of Cell Titer 96[®] AQueous One Solution containing the tetrazolium salt 3-(4,5-dimethylthiazol-2-yl)-5-(3-carboxymethoxyphenyl)-2-(4-sulfophenyl)-2H-tetrazolium (MTS) were added to each well. After 3 h of incubation under standard cell culture coconditions (see above), the amount of soluble formazan produced by cellular reduction of MTS was quantified by recording the absorption at 490 nm using a TitertekPlus Microplate Reader (Friedrich S. Bartolomey Labortechnik, Rheinbach, Germany). Cell viability was normalized to that of fibroblasts cultured in medium without extracts. All experiments were carried out in triplicate and the results are expressed as means \pm standard deviation.

3.2.7 Release of FITC-dextrans and fluorescent nanospheres

For release experiments, fluorescein isothiocyanate labeled dextrans (FITC-dextrans) and orange fluorescent nanospheres (FluoSpheres[®]) were used as model substances. FITC-dextrans of 4 and 150 kDa molecular weight were dissolved in 50 mM phosphate buffer pH 7.0 at 1 % (w/v). FluoSpheres[®] (bead diameter 100 nm) were supplied as aqueous suspensions containing 2 % solids. To prepare hydrogels, aliquots of these three solutions were mixed with a 4 % (w/v) solution of 4armPEG10k-NH₂ in 50 mM phosphate buffer pH 7.0. Subsequently, an equal volume of a 4 % (w/v) solution of 4armPEG10k-SPA in water was added. The resulting mixture was vortexed; samples

of 500 μL were then cast into glass vials (inner diameter 24 mm) and allowed to gel for 60 min. In order to determine the in vitro release kinetics, samples (1.1 mm height \times 24 mm diameter) were covered with 5 mL of 50 mM phosphate buffered saline pH 7.4 (containing 0.025 % sodium azide) and maintained at 37 °C on an orbital shaker (\sim 50 rpm). At specified time intervals, 400 μL of the supernatant were collected and replaced with fresh buffer. The amounts of released FITC-dextran ($\lambda_{ex} = 490$ nm, $\lambda_{em} = 520$ nm) and FluoSpheres[®] ($\lambda_{ex} = 540$ nm, $\lambda_{em} = 560$ nm) were determined on a PerkinElmer LS 55 Fluorescence Spectrometer (PerkinElmer, Rodgau-Jügesheim, Germany). All experiments were carried out in triplicate and the results are expressed as means \pm standard deviation.

3.3 Results and discussion

3.3.1 Preparation and rheological characterization of hydrogels

Hydrogels were prepared by step-growth polymerization of branched PEG-succinimidyl propionates with PEG-amines. Figure 3.2 shows a typical rheogram for a gel formed by reaction of 5 % (w/v) 4armPEG10k-SPA and 2 % (w/v) PEG2k-NH₂ at pH 7.0 and 25 °C (Table 3.1, gel 12). Directly after mixing the two precursor solutions, the sample behaved like a free-flowing liquid ($G'' > G'$). This quality is of special advantage, as it would enable the injection into the eye using small-gauge needles. The cross-over of G' and G'' after approx. 10 min was regarded as the gel point. In the course of time, cross-linking further proceeded as indicated by the steadily increasing value of G' . After approx. 30 min, highly elastic gels had formed ($G' \gg G''$); the value of G' exceeded that of G'' by several orders of magnitude. Mechanically, these hydrogels would be suitable for vitreous substitution, as they are expected to assist in holding the neuronal retina in place after the natural vitreous has failed. The mechanical energy generated by external forces, such as rubbing or hitting, or by heart beats and eye movements, would be stored and then dissipated slowly [105, 107, 109]. More importantly, the mechanical properties will be unaffected by the injection process as cross-linking is performed in the vitreous cavity. Therefore, failure of

the substitute due to liquefaction, as observable for hydrogels cross-linked prior to injection [107, 109], can be avoided.

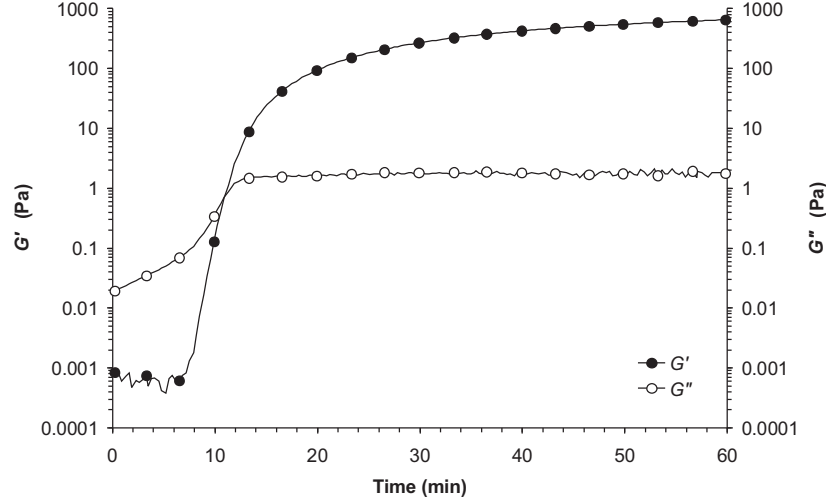


Figure 3.2: Rheogram of a gel formed by polymerization of 5 % (w/v) 4armPEG10k-SPA with 2 % (w/v) PEG2k-NH₂ at pH 7.0 and 25 °C (Table 3.1, gel 12). The measurement was performed at 0.5 Hz oscillatory frequency using a 40 mm steel plate with 500 μ m gap size.

As shown in Figure 3.3A, gelation was accelerated with decreasing stoichiometric ratio r of reactive groups. At $r = 2.00$, solidification occurred after more than 90 min. An exact value could not be determined, as the rheological measurements were run over 90 min only. The highest cross-linking rate was observed at $r = 0.80$. Under these conditions, the gel point was reached within 17 min. The stoichiometric ratio r also affected the strength of the prepared hydrogels. With decreasing r , the stiffness of the gels first increased, reached an optimum at $r = 1.00$, and then decreased again. This is attributed to structural defects in the network architecture that occur upon mixing of nonstoichiometric ratios of reactants [117]. At high stoichiometric ratios, cross-linking will be inefficient due to the relative excess of succinimidyl ester groups. In contrast, an excess of amino groups at low stoichiometric ratios will promote the formation of cyclizations and elastically inactive dangling ends. Both phenomena increase the average molecular weight between cross-links and lead to mechanically weaker gels.

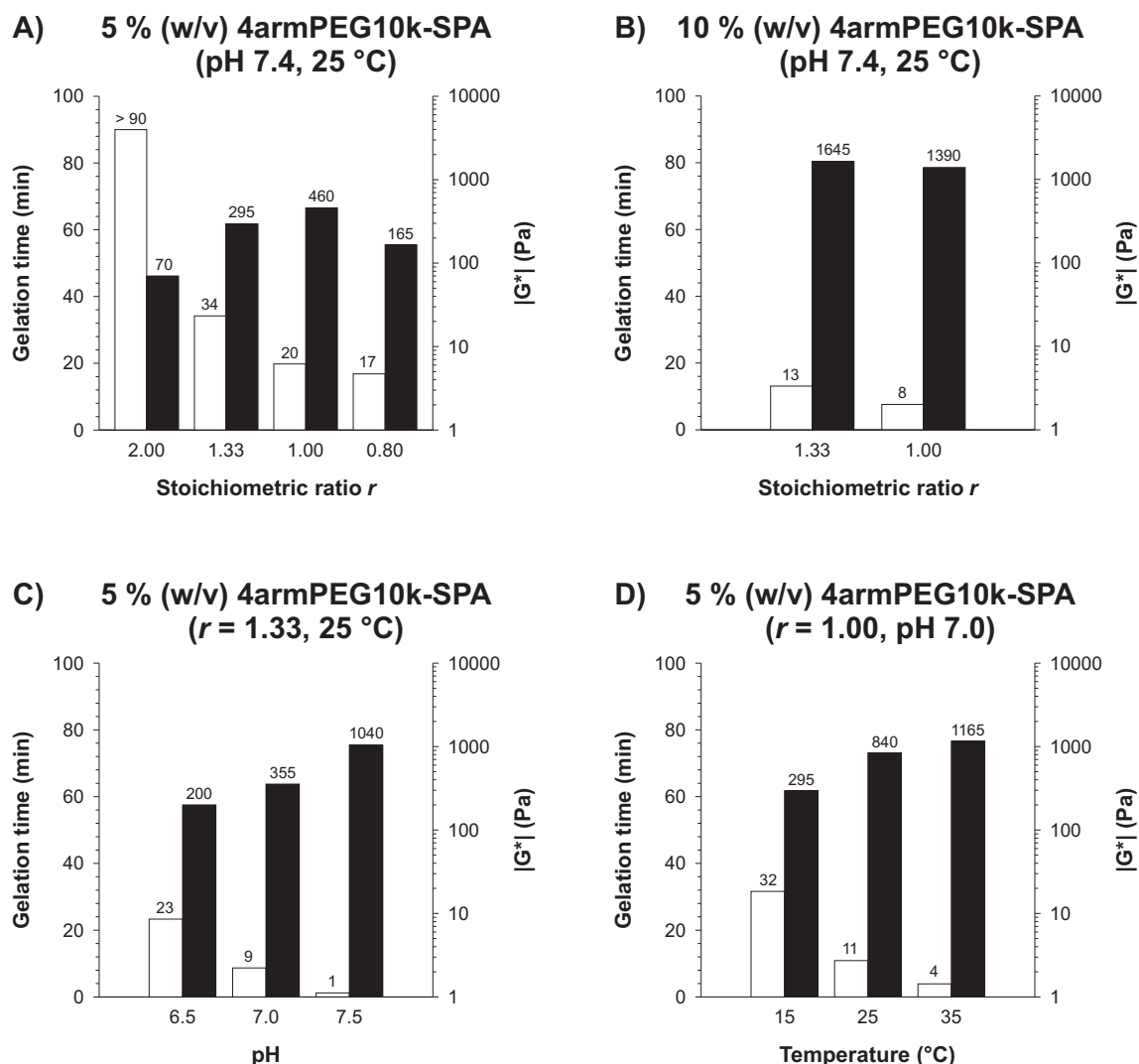


Figure 3.3: Dependence of gelation time (white bars, left y-axis) and gel strength (black bars, right y-axis) on the stoichiometric ratio r of reactive groups, pH, and temperature. (A) Gels were formed from 5 % (w/v) 4armPEG10k-SPA and varying concentrations of PEG10k-NH₂ in PBS (pH 7.4) at 25 °C. (B) Gels were formed from 10 % 4armPEG10k-SPA and two different concentrations of PEG2k-NH₂ in PBS at 25 °C. (C) Gels were formed from 5 % (w/v) 4armPEG10k-SPA and 1.5 % (w/v) PEG2k-NH₂ in 250 mM phosphate buffer solutions at 25 °C. (D) Gels were formed from 5 % (w/v) 4armPEG10k-SPA and 2 % (w/v) PEG2k-NH₂ at pH 7.0 (25 mM phosphate buffer). These measurements were performed at 0.5 Hz oscillatory frequency using a 40 mm steel plate with 500 μ m gap size.

Gelation time and gel strength also depended on the used concentrations of macromers. Gels formed from 10 % (w/v) 4armPEG10k-SPA (Figure 3.3B) solidified more than twice as fast as the corresponding gels containing 5 % (w/v) 4armPEG10k-SPA (Figure 3.3A). The mechanical strength was also dramatically increased. These findings can again be explained by the architecture of the formed polymer networks [117]. At low concentrations of 4armPEG10k-SPA, the overall concentration of succinimidyl ester groups is correspondingly low. The local concentration of succinimidyl ester functions upon one PEG macromer, however, is independent of the overall concentration. Thus, low concentrations of 4armPEG10k-SPA (Figure 3.3A) favor intramolecular cyclizations that decrease the cross-link density and mechanical rigidity of the formed networks. In contrast, higher concentrations of 4armPEG10k-SPA (Figure 3.3B) favor intermolecular reactions as the probability increases that cross-links are formed between two different 4armPEG macromers.

To investigate the influence of pH on the gelation rate, gels were made from solutions of 4armPEG10k-SPA in water and solutions of PEG2k-NH₂ in 500 mM phosphate buffer solutions of defined pH (Figure 3.3C). Even though the ionic strength of these buffers is far from being physiological, this high salt concentration was necessary to ensure a constant pH during cross-linking. At pH 6.0, no gelation occurred within 180 min (data not shown). By increasing the pH from 6.5 to 7.5, the gelation time was reduced from 23 min to approx. 1 min. Concomitantly, the stiffness increased by a factor of 5. This pH dependency is attributed to the basic character of PEG2k-NH₂ and the assumption that only free amine bases are able to react with succinimidyl ester groups. Compared to pH 6.5, the amount of free amine bases is increased 10-fold at pH 7.5. Obviously, this is sufficient to enhance the polymerization rate and the resulting gel strength. Adjusting the pH is, therefore, seen as a valuable tool for controlling the gel properties in future applications.

The cross-linking temperature was expected to be another important parameter influencing gel properties. At 35 °C, the gel point was reached after approx. 4 min. With decreasing temperature, the polymerization rate was reduced: at 25 and 15 °C it took about 11 and 32 min, respectively, until gelation occurred (Figure 3.3D). At 15 °C, cross-linking was still incomplete even after 90 min (data not shown).

When comparing the gels formed in PBS (Figure 3.3A) with those prepared in stronger buffer solutions (Figure 3.3C and D), significant differences became obvious.

The former were mechanically weaker and showed lower polymerization rates than the latter. This is associated with the fact that 4armPEG10k-SPA was dissolved in PBS instead of water. As the hydrolysis rate of succinimidyl ester groups is higher in PBS than in pure water (data not shown), some loss of 4armPEG10k-SPA during sample preparation might explain the observed differences. Moreover, the pH was found to slightly decrease during cross-linking, probably due to the acidic reaction of released NHS (data not shown). Due to its low buffer capacity, PBS is not able to compensate this drop in pH, which finally slows down the cross-linking rate.

To cope with the problem of inefficient cross-linking due to formation of intramolecular cyclizations and elastically inactive dangling ends, hydrogels were formed upon reaction of 4armPEG10k-SPA with branched PEG-amines. The overall concentration of macromers was 4 % (w/v) and 6 % (w/v), respectively. Due to the higher functionality of 4armPEG10k-NH₂ (4 vs. 2), the cross-linking rate of these hydrogels was increased compared to gels made from PEG2k-NH₂. The gelation time was approx. 5 min for gels containing 2 % (w/v) 4armPEG10k-NH₂ and 2 min for those containing 3 % (w/v). The stiffness reached values of about 1485 and 3220 Pa, respectively. This high gel strength most likely originates from the reduced mesh size of these networks (theoretically 5 kDa), which is lower than those of networks formed from 4armPEG10k-SPA and PEG2k-NH₂ (theoretically 7 kDa). Further, elastically inactive cyclizations will not be generated if two branched macromers are used.

With respect to intraocular applications, hydrogels with an intermediate gelation time are preferred, since these gels would be suitable for injection but solidify in an appropriate period of time (approx. 5 – 10 min). This would be an essential feature of potential vitreous substitutes, as it avoids their own drainage through retinal breaks and ensures a proper position of the retina [105, 107]. Regarding the stiffness of potential vitreous replacements, values similar to those of the natural vitreous body would be desired. Defining these values, however, might be a challenging task, as the mechanical properties of the vitreous change with age, species, and preparation method. The reported values of the storage modulus G' ranged from a few Pascal for porcine vitreous up to several hundred Pascal for goat vitreous [118, 119]. Indeed, the stiffness of the developed hydrogels ranges at the upper limit of the reported values but still can be adjusted by varying the gel composition and conditions during cross-linking.

Due to their high water content of approx. 96 %, ideal gelation time, and appropriate mechanical stability, hydrogels prepared from 2 % (w/v) 4armPEG10k-SPA and 2 % (w/v) 4armPEG10k-NH₂ were favored and used for cytotoxicity testing and release experiments (see below).

3.3.2 Characterization of hydrogels by NMR

To investigate polymerization kinetics and cross-linking efficiency, a time series of ¹H-NMR spectra was recorded. The first spectrum was obtained approx. 5 min after mixing the two precursor solutions and showed the characteristic signals of 4armPEG10k-SPA and PEG2k-NH₂. The protons of the succinimidyl group (Figure 3.4, signal *c*) were found at 2.87 ppm. The methylene protons neighboring the succinimidyl ester group (Figure 3.4, signal *d*) and amino group (Figure 3.4, signal *e*) were identified at 2.95 and 3.13 ppm, respectively. The signal at 3.42 ppm (Figure 3.4, signal *g*) corresponded to the pentaerythritol core of 4armPEG10k-SPA and was used for the calibration of integrals. The methylene protons of the PEG backbone were found at about 3.62 ppm (not shown in Figure 3.4). Moreover, 3 further signals (Figure 3.4, signals *a*, *b* and *f*) appeared that were neither detected in the spectrum of pure 4armPEG10k-SPA nor in that of pure PEG2k-NH₂. The signal *b* at about 2.65 ppm stemmed from the methylene protons of released NHS; signals *a* and *f* at 2.46 and 3.32 ppm were assigned to the methylene protons neighboring the newly formed amide bond. This was confirmed by HMBC spectra showing an interaction between these protons and the carbonyl carbon atom at 174 ppm (data not shown).

Integration of the aforementioned signals revealed that a large fraction of succinimidyl ester groups had already reacted during preparation and acquisition of the first spectrum. This, however, does not conflict with the rheological measurements, as it is possible that in early stages of polymerization, weakly cross-linked polymer strands or smaller aggregates are formed rather than percolating networks. Thus, the cross-linking density might increase for a long time without enhancing the gel strength significantly.

Within the observation period, the signals *c*, *d* and *e* decreased by approx. 30 %. Concomitantly, the signals *a*, *b* and *f* increased by approx. 30 %, which is consistent

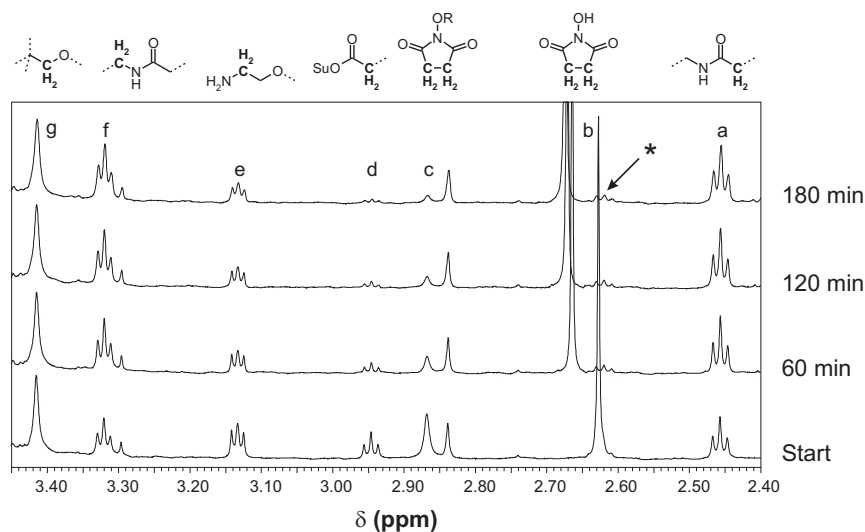


Figure 3.4: ^1H -NMR spectra of a hydrogel formed by reaction of 5 % (w/v) 4armPEG10k-SPA and 2 % (w/v) PEG2k-NH₂ (D₂O, 600 MHz, 300 K). The first spectrum (start) was obtained approx. 5 min after mixing the two precursor solutions. Then, spectra were recorded for 180 min.

with the supposed mechanism of cross-linking. At later time-points, another signal was recognized at 2.62 ppm that had been overlapped by signal *b* before (see asterisk in Figure 3.4). This signal most likely corresponds to the PEG-propionic acid protons and suggests occurring hydrolysis of the succinimidyl ester group. Furthermore, the integral of signal *e* stayed somewhat higher than expected. This indicates a nonstoichiometric consumption of amino groups probably due to hydrolysis of succinimidyl ester groups. As a consequence, the cross-linked hydrogels contain small amounts of carboxylic acid and ammonium groups; cross-linking efficiency and mechanical stability are, therefore, somewhat lower than expected from theory. Altogether, NMR spectroscopy was found to be a valuable method to monitor the process of gel formation on a molecular level.

3.3.3 Cytotoxicity of cross-linked hydrogels

Although the described hydrogels are being developed for intraocular applications, this study was carried out with fibroblasts. Fibroblasts are widely accepted for cytotoxicity testing [120] and used as a standard cell type in order to determine the

general biocompatibility of materials. To assess cytotoxicity, hydrogels consisting of 2 % (w/v) 4armPEG10k-SPA and 2 % (w/v) 4armPEG10k-NH₂ were evaluated by a medium extraction test. The cytotoxic effects of extracted products are presented in Figure 3.5. The tested hydrogels showed no adverse effects on the viability of fibroblasts, where the minimum viability was 98 ± 4 %. Therefore, it can be concluded that no toxic products (e.g. byproducts of the synthesis) are leached out of the incubated gels. Detrimental effects due to shifts in pH or osmotic pressure can be excluded. In future experiments, the biocompatibility with ocular tissues will be investigated using a perfusion culture model of full-thickness porcine retina, an *in vitro* model suitable for the evaluation of biomaterials in more organotypical environments [121, 122].

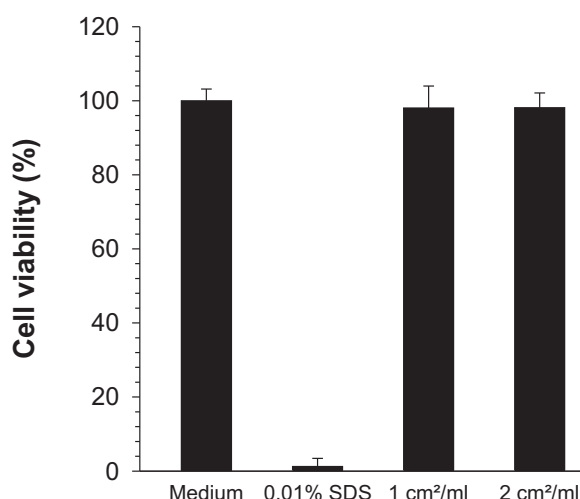


Figure 3.5: Cell viability after exposure to extracts of hydrogels prepared from 2 % (w/v) 4armPEG10k-SPA and 2 % (w/v) 4armPEG10k-NH₂ (surface area to fluid volume 1 and 2 cm²/mL). Data represent mean \pm standard deviation ($n = 3$ for each group).

3.3.4 Release of FITC-dextran and fluorescent nanospheres

The *in vitro* release properties of hydrogels were studied using FITC labeled dextrans (molecular weight 4 and 150 kDa) and fluorescent nanospheres (FluoSpheres[®], bead diameter 100 nm) as macromolecular model substances. Hydrogels were formed from 2 % (w/v) 4armPEG10k-SPA and 2 % (w/v) 4armPEG10k-NH₂ (water content: 96 %). FITC-dextrans with a molecular weight of 4 kDa were released very rapidly, indicating that the size of these molecules was smaller than the mesh size of the prepared hydrogels (theoretically 5 kDa). After an initial burst, the release continued

and was completed after approx. 10 h (Figure 3.6). The release exceeded 100 % probably due to small measuring errors that propagate in the calculation of the cumulative release data. However, this is not significant as it was the aim of this study to characterize the overall release kinetics of model substances rather than the absolute amounts released. The release rate of larger FITC-dextrans (molecular weight 150 kDa) was considerably lower. Over a period of 10 h, the gels had released approx. 70 % of the incorporated FITC-dextrans (Figure 3.6). Unlike smaller dextrans, the release was completed only after 48 h. In contrast to the tested FITC-dextrans, no significant release of FluoSpheres[®] was observed within 96 h (data not shown). The used FluoSpheres[®] consist of polystyrene and have a bead diameter of 100 nm. Most likely, they are trapped within the hydrogels and will not be released until the mesh size increases due to degradation of the gels. In future studies, this could be investigated using hydrogels prepared from biodegradable macromers.

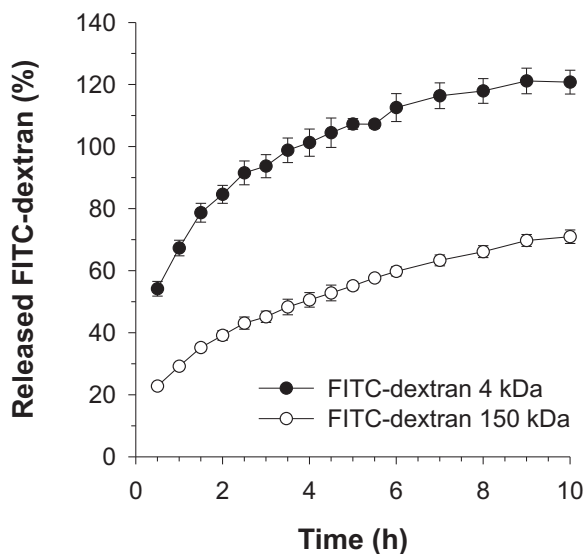


Figure 3.6: Cumulative amount of FITC-dextrans (molecular weight 4 kDa and 150 kDa) released from hydrogels consisting of 2 % (w/v) 4armPEG10k-SPA and 2 % (w/v) 4armPEG10k-NH₂. Data are represented as means \pm standard deviations ($n = 3$ for each group).

These findings are of special interest regarding potential ophthalmologic applications of the developed hydrogels. Similar to the natural vitreous body, the gels would allow the diffusion of nutrients, metabolites, and soluble proteins to or from the adjacent tissues. On the other hand, the hydrogels could be used as injectable carriers for nanoparticulate drug delivery systems in order to treat common eye diseases such as AMD or PDR, for example [110, 123].

3.4 Conclusion

We successfully prepared optically transparent hydrogels by step-growth polymerization of branched PEG-succinimidyl propionates with two different types of PEG-amines. Gelation time and gel strength were found to depend on the macromer concentration, the PEG-amine functionality, and the conditions during cross-linking. By adjusting these parameters, we obtained hydrogels with ideal gelation times of approx. 5 – 10 min and mechanical properties similar to those of the natural vitreous body. The tested hydrogels showed no cytotoxic effects *in vitro* and may be used as injectable vitreous substitutes. The gels allow for further functionalization by incorporation of nanoparticulate drug delivery systems or by attachment of peptides, proteins, and other bioactive substances, yielding biomimetic materials [124]. In future applications, it would also be possible to load these hydrogels with cells naturally occurring in the cortex of the vitreous body. These so called hyalocytes were shown to accumulate collagen and hyaluronic acid *in vitro* and may be used in tissue engineering approaches for the regeneration of the natural vitreous body [125].

Chapter 4

Hydrogel-based drug delivery systems: Comparison of drug diffusivity and release kinetics

Ferdinand Brandl¹, Fritz Kastner², Ruth Gschwind³, Torsten Blunk¹,
Jörg Teßmar¹, Achim Göpferich¹

¹ *Department of Pharmaceutical Technology, University of Regensburg, 93040 Regensburg*

² *Center for Chemical Analysis, University of Regensburg, 93040 Regensburg, Germany*

³ *Department of Organic Chemistry, University of Regensburg, 93049 Regensburg, Germany*

Published in the *Journal of Controlled Release*, in press.

Abstract

Hydrogels are extensively studied as matrices for the controlled release of macromolecules. To evaluate the mobility of embedded molecules, these drug delivery systems are usually characterized by release studies. However, these experiments are time-consuming and their reliability is often poor. In this study, gels were prepared by step-growth polymerization of poly(ethylene glycol) (PEG) and loaded with fluoresceine isothiocyanate (FITC) labeled dextrans. Mechanical testing and swelling studies allowed prediction of the expected FITC-dextran diffusivity. The translational diffusion coefficients (D) of the incorporated FITC-dextrans were measured by fluorescence recovery after photobleaching (FRAP) and pulsed field gradient NMR spectroscopy. Because the determined values of D agreed well with those obtained from release studies, mechanical testing, FRAP, and pulsed field gradient NMR spectroscopy are proposed as alternatives to release experiments. The applied methods complemented each other and represented the relative differences between the tested samples correctly. Measuring D can therefore be used to rapidly evaluate the potential of newly developed drug delivery systems.

4.1 Introduction

Hydrogels have been studied as injectable drug delivery systems for the controlled release of macromolecules, including therapeutic peptides, proteins, and nucleic acids [7, 11, 12, 126]. However, despite their many favorable characteristics, these drug delivery systems still have not found their way into broad clinical applications. One reason is that the quantity and homogeneity of drug loading are still a matter of concern [11, 12]. Moreover, the high water content of most hydrogels often results in relatively rapid drug release over a few hours to several days. This not only shortens the efficacy of the applied drug delivery system, but also carries the risk of provoking harmful side-effects [7, 11, 12]. Therefore, research focuses on extending the duration of drug release, and expanding the range of molecules which can be effectively delivered [11, 12]. Because the resulting release profiles are hardly predictable, the developed formulations are usually characterized by release studies. The reliability of these experiments is, however, limited. The results depend on a number of parameters, such as the geometry of the dosage form, its swelling capacity, and the type and amount of release medium [127, 128]. Furthermore, release experiments are often time-consuming, and require relatively large drug loads. Depending on the expected release kinetics, the sampling time can last up to several days. For these reasons, screening large libraries of potential drug delivery formulations can be a challenging task. A wider range of fast and reliable analytical methods that directly assess drug diffusivity would certainly aid further research and accelerate the development of new hydrogel-based drug delivery systems.

Fluorescence recovery after photobleaching (FRAP) is a well-established analytical method that has been widely used to study the translational diffusion of molecules [129–131]. The basic instrumentation for FRAP experiments consists of an optical microscope equipped with a light source to bleach arbitrary regions within the sample. Furthermore, some of the probe molecules must be fluorescently labeled. After bleaching the probe molecules within the region of interest, the fluorescence recovery due to diffusion of unbleached molecules is recorded; the diffusion coefficients can then be calculated from the resulting recovery profiles. Although FRAP experiments have already been used for the characterization of hydrogel-based drug delivery systems [132–136], the relevance of these data for the expected release profiles has

yet to be proven. Therefore, systematic comparisons between the measured diffusion coefficients and the resulting release kinetics will be required until FRAP experiments and other analytical techniques are generally accepted.

In this study, hydrogels were prepared by step-growth polymerization of branched poly(ethylene glycol) (PEG) and loaded with fluoresceine isothiocyanate (FITC) labeled dextrans as macromolecular model drugs. Because of their well defined architecture [74, 117], these gels can be considered model systems for hydrogel-based drug delivery formulations. To get an estimate of the expected FITC-dextran diffusivity, the gels were characterized by mechanical testing and equilibrium swelling studies. Subsequently, the translational diffusion coefficients of the incorporated FITC-dextrans were determined by FRAP. In one sample, FITC-dextran diffusivity was also measured by pulsed field gradient nuclear magnetic resonance (NMR) spectroscopy, an independent analytical method to study the translational diffusion of molecules [137, 138]. To complete the experimental data, the apparent diffusion coefficients of the incorporated FITC-dextrans were also calculated from release experiments. By comparing these values, we show the significance of mechanical testing and FRAP experiments for the characterization of hydrogel-based drug delivery systems. Furthermore, we discuss the limits of these techniques and comment on the possibility of predicting entire release profiles from the obtained diffusion coefficients.

4.2 Materials and methods

4.2.1 Materials

Acrylonitrile, *N,N'*-dicyclohexylcarbodiimide (DCC), diisopropyl azodicarboxylate (DIAD), fluoresceine isothiocyanate (FITC) labeled dextrans (FITC-dextrans), and N-hydroxysuccinimide (HOSu) were purchased from Sigma-Aldrich (Taufkirchen, Germany). Hexane and phthalimide were obtained from Acros Organics (Geel, Belgium). Four-armed poly(ethylene glycol) (molecular weight 10 kDa, 4armPEG10k-OH) was purchased from Nektar Therapeutics (Huntsville, AL). Deuterium oxide (D₂O) was obtained from Deutero GmbH (Kastellaun, Germany). Phosphate buffered

saline (PBS) was purchased from Invitrogen GmbH (Karlsruhe, Germany). All other chemicals were of analytical grade and purchased from Merck KGaA (Darmstadt, Germany). Deionized water was obtained from a Milli-Q water purification system from Millipore (Schwalbach, Germany).

4.2.2 Synthesis of polymers

Branched PEG-succinimidyl propionates (4armPEG10k-SPA) were synthesized as previously described [139]. In brief, PEG-propionic acid was obtained through Michael-type addition reaction of 4armPEG10k-OH onto acrylonitrile and subsequent hydrolysis under alkaline conditions. The obtained carboxylic acid groups were then converted to amine-reactive succinimidyl ester groups using HOSu and DCC. The synthesis of branched PEG-amines (4armPEG10k-NH₂) also followed a previously established procedure [139]. First, phthalimido-PEGs were synthesized by reaction of 4armPEG10k-OH, phthalimide, triphenylphosphine, and DIAD. The phthalimido groups were then converted into primary amines by hydrazinolysis.

4.2.3 Rheological characterization of hydrogels

Gelation kinetics and gel strength were studied at 25 °C by performing oscillatory shear experiments using a TA Instruments AR 2000 rheometer (TA Instruments, Eschborn, Germany) with parallel plate geometry. For the preparation of hydrogels, defined amounts of 4armPEG10k-NH₂ (25 or 50 mg) were dissolved in 1000 µL of 25 mM phosphate buffer, pH 7.0. Immediately before starting the experiment, the polymer solution was added to an equal amount of 4armPEG10k-SPA (25 or 50 mg). After vigorous stirring, the precursor solution was poured onto the bottom plate of the rheometer. The upper plate (20 mm in diameter) was then lowered to a gap size of 1000 µm, and the measurement was started. The evolution of storage (G') and loss moduli (G'') was recorded as a function of time at 1 Hz oscillatory frequency and a constant strain of 0.05. A solvent trap was used in order to prevent the evaporation of water. The cross-over of G' and G'' was regarded as the gel point. After 120 min, the complex shear modulus (G^*) was determined. The gel disks were then removed

from the rheometer, immersed in 10 mL of PBS, and incubated at 37 °C for 24 h. To measure G^* in the swollen state, the hydrogel disks were again placed in the center of the lower plate and the measuring gap was slowly closed until a normal force of approx. 150 mN was reached. The resulting compression was sufficient to prevent slippage. The following frequency sweep was conducted at constant strain (0.05) as a function of frequency (from 0.1 to 10 Hz). Finally, an amplitude sweep (from 0.1 to 10,000 Pa oscillatory stress) was performed in order to confirm that all previous measurements were conducted within the linear viscoelastic region of the sample. All experiments were carried out in triplicate and the results are expressed as means \pm standard deviations.

4.2.4 Equilibrium swelling of hydrogels

For the swelling studies, defined amounts of 4armPEG10k-NH₂ (25 or 50 mg) were dissolved in 1000 μ L of phosphate buffer (25 mM, pH 7.0) and added to an equal amount of 4armPEG10k-SPA (25 or 50 mg). After vortexing, 250 μ L of the precursor solution were cast into cylindrical glass molds (7 mm inner diameter) and allowed to gel for 2 h. The samples were then weighed in air and hexane before and after swelling for 24 h in 10 mL of PBS using a density determination kit (Mettler-Toledo, Gießen, Germany). Using Archimedes' principle, the gel volumes after cross-linking (V_{gc}) and after swelling (V_{gs}) were determined. The volume of the dry polymer (V_p) was calculated from the mass of the freeze-dried hydrogel and the density of the polymer in the dry state (taken as the density of PEG, 1.12 g \cdot cm⁻³). With these parameters, the polymer fraction of the gel after cross-linking, $v_{2c} = V_p/V_{gc}$, and in the swollen state, $v_{2s} = V_p/V_{gs}$, was calculated. The reciprocal of v_{2s} is usually called the volumetric swelling ratio (Q). All experiments were carried out in triplicate and the results are expressed as means \pm standard deviations.

4.2.5 Calculation of hydrogel network mesh size

The number of moles of elastically active chains in the hydrogel network, ν_e , can be calculated from equilibrium swelling measurements using a modified version of the classical Flory-Rehner equation [140–142]:

$$\nu_e = -\frac{V_p}{V_1 v_{2c}} \cdot \frac{[\ln(1 - v_{2s}) + v_{2s} + \chi_1 v_{2s}^2]}{\left[\left(\frac{v_{2s}}{v_{2c}} \right)^{\frac{1}{3}} - \frac{2}{f} \left(\frac{v_{2s}}{v_{2c}} \right) \right]} \quad (4.1)$$

In this equation, χ_1 is the Flory-Huggins interaction parameter for PEG in water (taken as 0.43), V_1 is the molar volume of the solvent ($18 \text{ cm}^3 \cdot \text{mol}^{-1}$), and f is the functionality of the cross-links (4 in the case of four-armed PEG). In the case of perfectly formed condensation gels, the average molecular weight between cross-links, \bar{M}_c , can be calculated by $\bar{M}_c = m_p / \nu_e$, where m_p is the total mass of PEG in the hydrogel [142]. Using this parameter, the average mesh size (ξ) can be calculated by [143]:

$$\xi = v_{2s}^{-\frac{1}{3}} l \left(\frac{2\bar{M}_c}{M_r} \right)^{\frac{1}{2}} C_n^{\frac{1}{2}} \quad (4.2)$$

where l is the bond length along the polymer backbone (taken as 0.146 nm), M_r is the molecular mass of the PEG repeating unit ($44 \text{ g} \cdot \text{mol}^{-1}$), and C_n is the Flory characteristic ratio (here taken as 4 for PEG) [144].

Alternatively, information about the network structure can be derived from the equilibrium modulus, G_e , which provides an independent estimate of ν_e . The elastic behavior of gel networks thereby falls between two idealized limits, affine and phantom, which relate the network structure to the elastic deformation under applied stress [145]. It has been shown, however, that for gels cross-linked at low concentrations, the agreement between the phantom model and the experimental observations appears to be satisfactory [146]. Utilizing the following expression, ν_e can be obtained from G_e [145, 146]:

$$G_e = RT \left(\frac{\nu_e - \mu_e}{V_{gc}} \right) v_{2c}^{-\frac{1}{3}} v_{2s}^{\frac{1}{3}} \quad (4.3)$$

Here, R is the molar gas constant ($8.3145 \text{ J} \cdot \text{mol}^{-1} \cdot \text{K}^{-1}$), T the absolute temperature (298.16 K), and μ_e refers to the number of moles of cross-links. For a network with only one type of cross-link, $\nu_e - \mu_e = \nu_e(1 - 2/f)$ [145].

4.2.6 Fluorescence recovery after photobleaching (FRAP)

To investigate the mobility of incorporated macromolecules, the hydrogels were loaded with different FITC-dextran (20, 150, and 2,000 kDa molecular weight). The samples were prepared by dissolving defined amounts of 4armPEG10k-NH₂ (12.5 or 25 mg) in 450 μL of phosphate buffer (25 mM, pH 7.0). Subsequently, 50 μL of the respective FITC-dextran stock solution (prepared in the same buffer, $c = 10 \text{ mg/mL}$) were added. This mixture was then added to an equal amount of 4armPEG10k-SPA (12.5 or 25 mg), vigorously stirred, and cast into cylindrical glass molds (5 mm inner diameter, 5 mm height). After gelling for 2 h, the samples were removed from the glass molds, placed into a Lab-TekTM II Chambered Coverglass (Thermo Fisher Scientific, Langenselbold, Germany), warmed to 37 °C, and positioned on the microscope stage.

The FRAP experiments were performed on a Zeiss Axiovert 200 M microscope coupled to a LSM 510 META scanning device (Carl Zeiss MicroImaging GmbH, Jena, Germany). A Plan-Neofluar 10 \times objective lens with a numerical aperture of 0.30 was used. All bleaching experiments were performed using the 488 nm-line of a 30 mW Ar-ion laser operating at 25 % output power. The confocal pinhole was opened completely in order to detect as much fluorescence as possible. After the location of interest was brought into focus, a time-series of digital images with a resolution of 512×128 pixel was recorded using a highly attenuated laser beam (0.2 % transmission). The interval between two consecutive images was between 1 and 4 s, depending on the expected diffusion time of the used FITC-dextran. After the acquisition of five prebleach images, a uniform disk with a diameter of 36 μm was bleached at maximum laser intensity (100 % transmission). The bleaching phase usually took 0.8 – 1.6 s, which should be sufficiently short to avoid fluorescence recovery during bleaching [130, 131]. Immediately after bleaching, a stack of 75 images was acquired at low laser intensity (0.2 % transmission) in order to measure the recovery of fluorescence inside the bleached area. To extract the experimental

recovery curve from the image stack, the mean fluorescence intensities inside the bleached region, $I_{frap}(t)$, and inside a reference region, $I_{ref}(t)$, were calculated for each time point t using the NIH software ImageJ. In the next step, $I_{frap}(t)$ was normalized to the prebleach intensity, $I_{frap}(pre)$, and corrected for any bleaching effects that might have occurred during image acquisition:

$$f(t) = \frac{I_{ref}(pre)}{I_{ref}(t)} \cdot \frac{I_{frap}(t)}{I_{frap}(pre)} \quad (4.4)$$

Here, $f(t)$ is the normalized fluorescence intensity inside the bleached region, and $I_{ref}(pre)$ is the fluorescence intensity inside the reference region before bleaching. In the following step, $f(t)$ was further normalized to the full scale using:

$$F(t) = \frac{f(t) - f(0)}{f(pre) - f(0)} \quad (4.5)$$

where $f(0)$ is the normalized fluorescence intensity immediately after bleaching, and $f(pre)$ the normalized fluorescence intensity before bleaching. Finally, the characteristic diffusion time τ_D and the mobile fraction k were determined by a least-squares fit of the following expression to the experimental recovery curve:

$$F(t) = k \cdot e^{-\frac{\tau_D}{2t}} \left[I_0 \left(\frac{\tau_D}{2t} \right) + I_1 \left(\frac{\tau_D}{2t} \right) \right] \quad (4.6)$$

where I_0 and I_1 are the modified Bessel functions of the first kind of zero and first order. This FRAP model has been described earlier by Soumpasis for a uniform disk bleached in two-dimensional samples [147]. However, if an objective lens of low numerical aperture is used for bleaching, Equation (4.6) can also be used to describe the fluorescence recovery in three-dimensional samples [130]. The diffusion coefficient (D) was then calculated by $D = w^2/\tau_D$, where w is the radius of the bleached spot (18 μm in all experiments).

In order to measure the diffusion coefficients also in the swollen state of the hydrogels, the samples were immersed in 500 μL of PBS which contained 1 mg/mL of the respective FITC-dextran. After 24 and 48 h of incubation at 37 $^\circ\text{C}$, the swollen gels were removed, rinsed with PBS, and placed into a Lab-TekTM II Chambered Coverglass again. The FRAP experiments were then repeated as described above.

4.2.7 Nuclear magnetic resonance (NMR) spectroscopy

For the NMR experiments, hydrogels were prepared in deuterated buffer solutions. For this purpose, 68.05 mg KH_2PO_4 were dissolved in 20 mL of D_2O . This solution was adjusted with NaOH to a pH meter reading of 7.0 and lyophilized; the lyophilisate was then reconstituted with 20 mL of D_2O . To prepare a hydrogel, 25 mg 4armPEG10k- NH_2 were dissolved in 900 μL of this buffer solution and mixed with 100 μL of a solution containing 10 mg/mL FITC-dextran (molecular weight 20 kDa). This mixture was then added to 25 mg 4armPEG10k-SPA, vortexed, transferred into a NMR tube, and allowed to gel for 2 h.

Diffusion ordered NMR spectroscopy (DOSY) experiments were performed on a Bruker AVANCE 600 spectrometer (Bruker BioSpin GmbH, Rheinstetten, Germany) operating at 600.13 MHz. As pulse sequence, a stimulated echo diffusion experiment with bipolar gradients, longitudinal eddy current delay, and two spoil gradients was chosen. Preparatory experiments revealed that transversal relaxation was not critical (data not shown). To minimize the eddy current effects after long gradients, sinusoidal gradient shapes were selected. The gradient strength was varied linearly from 5 % to 95 % of the maximal available 53.5 G/cm. To study FITC-dextran diffusivity, DOSY spectra were acquired at 300 K, and the attenuation of the NMR signal at 4.98 ppm was observed. Typical values of the parameters were 2 s for the relaxation delay, 150 ms for the diffusion time (Δ), and 8.5 ms for the gradient pulse length (δ). Diffusion coefficients were extracted out of the signal decay curve using the SimFit algorithm of the Bruker TopSpin Software.

4.2.8 Release of FITC-dextrans

As described for the FRAP experiments, the hydrogels were loaded with different FITC-dextrans (molecular weight 20, 150, and 2,000 kDa). To prepare the gel samples, defined amounts of 4armPEG10k- NH_2 (12.5 or 25 mg) were dissolved in 450 μL of phosphate buffer (25 mM, pH 7.0) and mixed with 50 μL of the respective FITC-dextran stock solution (prepared in the same buffer, $c = 10$ mg/mL). This mixture was then added to an equal amount of 4armPEG10k-SPA (12.5 or 25 mg) and vigorously stirred. In each case, 100 μL of this precursor solution were cast into

cylindrical glass molds (5 mm inner diameter, 5 mm height) and allowed to gel for 2 h. Afterwards, the gels were removed from the glass molds, immersed in 500 μL of PBS which contained 1 mg/mL of the respective FITC-dextran, and incubated for 24 h at 37 °C. After swelling, the gels were removed, rinsed with PBS and measured using a slide rule. The gels were placed into glass vials, covered with 10 mL of PBS (containing 0.025 % sodium azide), and maintained at 37 °C in a shaking water bath (approx. 50 rpm). At specified time intervals, 500 μL of the release medium were collected and replaced with fresh buffer. The amounts of released FITC-dextran ($\lambda_{ex} = 490 \text{ nm}$, $\lambda_{em} = 520 \text{ nm}$) were determined on a PerkinElmer LS 55 Fluorescence spectrometer (PerkinElmer, Wiesbaden, Germany) using standard calibration curves.

Considering perfect sink conditions throughout the experiment and the fact that FITC-dextran release is purely diffusion controlled, the following solution of Fick's second law of diffusion can be used to describe the experimental release profiles [128, 148]:

$$\frac{M_t}{M_\infty} = 1 - \frac{32}{\pi^2} \sum_{n=1}^{\infty} \frac{1}{q_n^2} \exp\left(-\frac{q_n^2}{r^2} Dt\right) \cdot \sum_{p=0}^{\infty} \frac{1}{(2p+1)^2} \exp\left(-\frac{(2p+1)^2 \pi^2}{h^2} Dt\right) \quad (4.7)$$

where M_t and M_∞ represent the absolute cumulative amounts of FITC-dextran released at time t and infinity, respectively; the q_n are the roots of the Bessel function of the first kind of zero order, and r and h denote the radius and height of the gel cylinders. By a least squares fit of Equation (4.7) to the experimental release profiles, the apparent diffusion coefficients (D) of the FITC-dextran were determined.

4.3 Results and discussion

4.3.1 Physicochemical characterization of hydrogels

Hydrogels were prepared by step-growth polymerization of branched PEG-amines with branched PEG-succinimidyl propionates. At the beginning of the experiments, all samples behaved like free-flowing liquids ($G'' > G'$). Gelation occurred after $8.1 \pm 0.2 \text{ min}$ for gels containing 5 % polymer, and $3.2 \pm 0.1 \text{ min}$ for gels containing 10 % polymer (Table 4.1). During the course of the experiment, cross-linking further

proceeded as indicated by the steadily increasing value of G' . After approx. 120 min, the value of G' reached a plateau and exceeded that of G'' by several orders of magnitude ($G' \gg G''$). The gel strength ($|G^*|$) was 2134 ± 89 Pa for hydrogels containing 5 % polymer, and 6808 ± 145 Pa for gels containing 10 % polymer (Table 4.1). After swelling in PBS, G^* was measured at constant strain as a function of frequency. Within the studied range, the absolute value of G^* was almost insensitive to the oscillatory frequency, which is typical for covalently cross-linked networks [149]. In the swollen state, the gel strength (determined at a frequency of 1 Hz) was 1873 ± 183 Pa for gels containing 5 % polymer, and 5767 ± 149 Pa for those containing 10 % polymer (Table 4.1). In amplitude sweep measurements, both gel types showed a broad linear viscoelastic region up to an oscillatory stress of approx. 300 and 750 Pa, respectively, indicating that all previous experiments were run well within the linear viscoelastic region of the samples.

Table 4.1: Physicochemical characteristics of the prepared hydrogels

	5 % Polymer	10 % Polymer
Gelation time (min)	8.1 ± 0.2	3.2 ± 0.1
Gel strength $ G^* $ after cross-linking (Pa)	2134 ± 89	6808 ± 145
Gel strength $ G^* $ after swelling (Pa)	1873 ± 183	5767 ± 149
Volumetric swelling ratio (Q)	32.2 ± 0.1	24.0 ± 0.1
\bar{M}_c ($\text{g} \cdot \text{mol}^{-1}$) calculated from swelling data	6652 ± 70	6547 ± 57
ξ (nm) calculated from swelling data	16.1 ± 0.1	14.5 ± 0.1
\bar{M}_c ($\text{g} \cdot \text{mol}^{-1}$) calculated from G_e	35279	18775
ξ (nm) calculated from G_e	37.2	24.6

In general, the absolute value of G^* of hydrogels containing 10 % polymer was approx. three times higher than that of gels containing only 5 % polymer. In a defect-free, end-linked network, however, the mechanical characteristics should be independent of the precursor concentration [74]. As this was obviously not the case, network defects seem to play a significant role in the structure of the prepared hydrogels. At low precursor concentrations, the concentration of elastically active chains is probably reduced by non-reacted groups and loops, whereas it is increased by entanglements at higher precursor concentrations.

A similar trend was observed in the volumetric swelling ratio. The value of Q decreased from 32.2 ± 0.1 (5 % polymer) to 24.0 ± 0.1 (10 % polymer). Using a modified version of the Flory-Rehner equation, \bar{M}_c was calculated to be $6652 \pm 70 \text{ g} \cdot \text{mol}^{-1}$ for gels containing 5 % polymer, and $6547 \pm 57 \text{ g} \cdot \text{mol}^{-1}$ for those containing 10 % polymer. These values correspond to an average mesh size (ξ) of 16.1 ± 0.1 and $14.5 \pm 0.1 \text{ nm}$, respectively (Table 4.1). Given the large differences in the absolute values of G^* , however, it seems unlikely that the real values of ξ are close to each other. The problems associated with the estimation of ξ can be attributed to the fact that the Flory-Huggins interaction parameter (χ_1) has not been experimentally determined. The value of χ_1 (0.43) was originally calculated for linear PEG chains in water [150] and might differ for the macromers used in this study. Furthermore, Equation (4.1) does not account for any network defects (such as elastically inactive dangling ends) as this would require the number of non-reacted groups [151]. For these reasons, the network parameters were also calculated from the equilibrium modulus (G_e) of the hydrogels. Since G^* was almost constant within the studied frequency range, the absolute value of G^* determined at 1 Hz oscillatory frequency was taken as equal to G_e . The resulting values of ξ were 37.2 and 24.6 nm for gels prepared from 5 % and 10 % polymer, respectively (Table 4.1). These values seem to be more realistic given the observed experimental data.

4.3.2 Estimation of diffusion coefficients

Three different FITC-dextran with molecular weights of 20, 150, and 2,000 kDa were used as macromolecular model compounds in order to evaluate the mass transport characteristics of the prepared hydrogels. Their hydrodynamic radii, r_H , were calculated according to Braeckmans et al. [130]. Knowing these values, a theoretical estimate of their diffusion coefficients in water (D_0) can be made with the Stokes-Einstein equation:

$$D_0 = \frac{kT}{6\pi\eta r_H} \quad (4.8)$$

where k is the Boltzmann constant ($1.38 \cdot 10^{-23} \text{ J} \cdot \text{K}^{-1}$), T the absolute temperature (310.16 K), and η the dynamic viscosity of water ($0.001 \text{ Pa} \cdot \text{s}$). The results are summarized in Table 4.2.

Table 4.2: Hydrodynamic radii (r_H) and diffusion coefficients in water (D_0) of FITC-dextran. The values of D_0 were estimated using Equation (4.8).

FITC-dextran	20 kDa	150 kDa	2,000 kDa
r_H (nm)	2.9	8.3	32.8
D_0 ($\mu\text{m}^2/\text{s}$)	79.6	27.4	7.0

Based on a free-volume approach proposed by Lustig and Peppas [126, 152], the diffusivity of incorporated molecules (D_g) can be related to the structure of the hydrogel network:

$$\frac{D_g}{D_0} = \left(1 - \frac{r_H}{\xi}\right) \cdot \exp\left(-Y \left(\frac{v_{2s}}{1 - v_{2s}}\right)\right) \quad (4.9)$$

Here, Y is defined as the ratio of the critical volume required for a translational movement of the encapsulated molecule and the average free volume per solvent molecule. For correlation purposes, a good approximation of Y is unity [126]. With this equation, the FITC-dextran diffusivities were estimated based on the determined values of ξ (derived from mechanical testing), and the results are presented in Table 4.3. According to the calculated values, the smaller FITC-dextran (20 and 150 kDa molecular weight) should be able to move almost freely within the formed hydrogels ($D_g \sim D_0$). For the larger FITC-dextran (2,000 kDa molecular weight), however, Equation (4.9) predicts strongly restricted diffusivities. In case of gels prepared from 10 % polymer, the average network mesh size was lower than the hydrodynamic radius of the FITC-dextran ($\xi < r_H$) and D_g could not be calculated.

4.3.3 Determination of diffusion coefficients by FRAP

After these theoretical considerations, the diffusion coefficients (D) of the incorporated FITC-dextran were measured. A typical FRAP experiment is illustrated in Figure 4.1A. After acquisition of the image stacks, the mobile fractions k and the

diffusion coefficients (D) were determined by least-squares fits of Equation (4.6) to the experimental recovery profiles (see Figure 4.1B). The coefficients of determination were generally very high ($R^2 > 0.99$), except for gels loaded with 2,000 kDa FITC-dextran (10 % polymer), where slightly lower values were obtained ($R^2 > 0.89$).

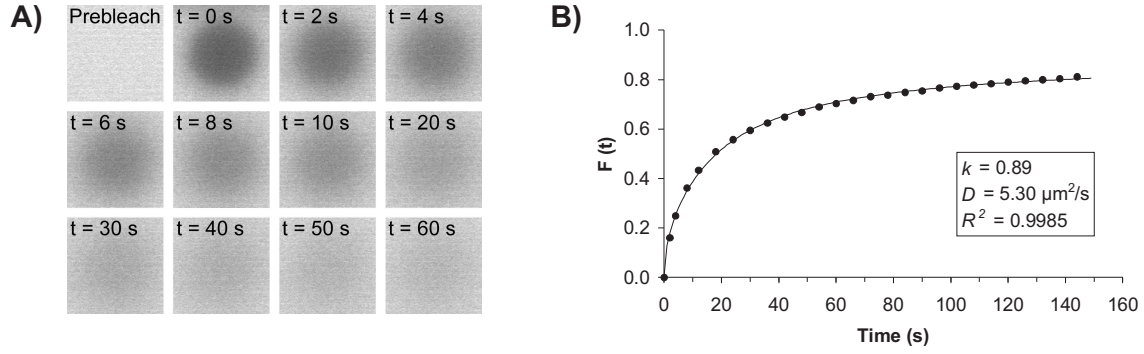


Figure 4.1: (A) Image stack of a typical FRAP experiment (5 % polymer, FITC-dextran 150 kDa). The first image shows the sample before bleaching (prebleach image). Immediately before taking the second image, a uniform disk is bleached. Then, the laser intensity is reduced again, and fluorescence recovery is recorded over multiple images. (B) An image processing program extracts the recovery curve from the image stack. The experimental data are indicated by symbols (●). A least-squares fit (solid line) of Equation (4.6) yields the mobile fraction k and the diffusion coefficient D .

Remarkably, the values of k did not vary significantly over the course of the experiment. In case of the 20 kDa FITC-dextran, all molecules were mobile, regardless of the polymer concentration (see Table 4.3). This was expected, as the hydrodynamic diameter of this molecule was well below the average network mesh size of the hydrogels. In contrast, the mobility of the 150 kDa FITC-dextran was restricted to some extent ($k = 0.89$ and $k = 0.66$ for gels containing 5 % and 10 % polymer, respectively). This effect was even more pronounced in hydrogels loaded with 2,000 kDa FITC-dextran ($k = 0.20$ and $k = 0.24$ for 5 % and 10 % polymer, respectively); this can also be explained by the size of these molecules. Their hydrodynamic diameters exceeded the average hydrogel mesh size by approximately a factor of two (Table 4.1 and 4.2). The calculated diffusion coefficients D (after swelling for 48 h) are presented in Table 4.3.

For all studied FITC-dextran, the diffusion coefficients were generally slightly lower in hydrogels containing 10 % polymer than in gels prepared from only 5 % polymer. As shown in Figure 4.2, an increase in D during hydrogel swelling was

Table 4.3: Measurement of the mobile fraction k and diffusion coefficient D ($\mu\text{m}^2/\text{s}$) of FITC-dextrans incorporated into hydrogels. Data are presented as means \pm standard deviations ($n = 3$ for each group). For comparison, the expected diffusion coefficients D_g ($\mu\text{m}^2/\text{s}$) are also included.

FITC-dextran Polymer conc.	20 kDa		150 kDa		2,000 kDa	
	5 %	10 %	5 %	10 %	5 %	10 %
D_g (expected) ^a	71.1	67.3	20.6	17.3	0.8	–
k (FRAP) ^{b,c}	1.04	1.03	0.89	0.66	0.20	0.24
D (FRAP) ^c	20.2 ± 0.2	18.1 ± 0.1	15.2 ± 0.1	12.8 ± 0.1	0.9 ± 0.1	0.1 ± 0.0
D (DOSY)	30.4	–	–	–	–	–
D (release)	47.7 ± 1.1	44.7 ± 1.2	24.5 ± 0.6	25.8 ± 0.7	3.7 ± 0.7	2.2 ± 0.7

^aCalculated from the average network mesh size using Equation (4.9)

^bData are presented as means; standard deviations (values < 0.03) are not shown for clarity

^cDetermined after swelling in PBS for 48 h

observed for all smaller FITC-dextrans (20 and 150 kDa molecular weight). After approx. 48 h, however, the diffusion coefficients had levelled off to their final values. As expected, the diffusion coefficients of the largest FITC-dextran (2,000 kDa molecular weight) were very low (0.9 ± 0.1 and $0.1 \pm 0.0 \mu\text{m}^2/\text{s}$ for gels containing 5 % and 10 % polymer, respectively). In case of the 150 kDa FITC-dextrans, the measured values of D also correlated well with the predicted values (15.2 ± 0.1 vs. $20.6 \mu\text{m}^2/\text{s}$ for gels containing 5 % polymer, and 12.8 ± 0.1 vs. $17.3 \mu\text{m}^2/\text{s}$ for hydrogels prepared from 10 % polymer, Table 4.3). However, the FRAP technique yielded lower values for the diffusion coefficients of the 20 kDa FITC-dextrans than expected (20.2 ± 0.2 and $18.1 \pm 0.2 \mu\text{m}^2/\text{s}$ for gels prepared from 5 % and 10 % polymer, respectively). Since these molecules were expected to diffuse very fast in the gels ($D_g = 71.1$ and $67.3 \mu\text{m}^2/\text{s}$, Table 4.3), significant recovery of fluorescence might have occurred during the bleaching phase, which would consequently lead to an underestimation of D .

4.3.4 Determination of diffusion coefficients by NMR

To get more accurate values of D for the smallest FITC-dextran (20 kDa molecular weight), the diffusivity of this macromolecule was examined by pulsed field gradient

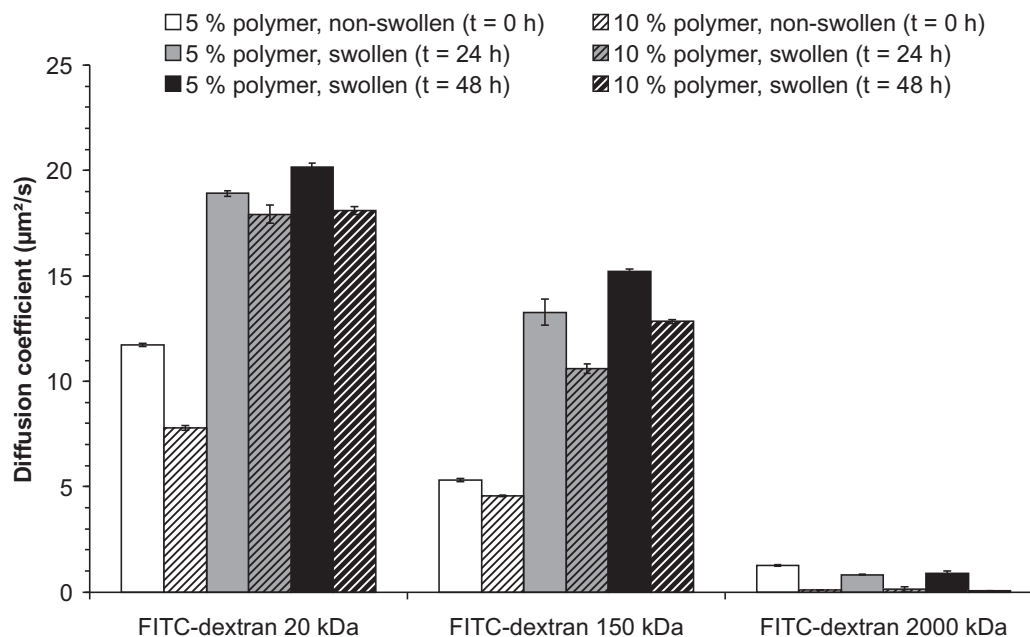


Figure 4.2: Diffusion coefficients (D) of FITC-dextran determined by FRAP. Data are shown as means \pm standard deviations ($n = 3$).

NMR spectroscopy. Using a magnetic field gradient, the probe molecules get spatially labeled according to their position in the NMR tube. If diffusion occurs, the NMR signal intensity is attenuated depending on the diffusion time (Δ), the length of the gradient (δ), and the gradient strength. In two-dimensional DOSY experiments, usually the strength of the magnetic field gradient is varied, whereas Δ and δ are kept constant. In the resulting spectra, the chemical shifts are plotted along the F2 axis and the diffusion coefficients along the F1 axis.

For the studied FITC-dextran, a diffusion coefficient of $30.38 \mu\text{m}^2/\text{s}$ was extracted from the signal decay curve. Although non-swollen gel samples were used for NMR measurements, the calculated value of D was considerably higher than that determined by FRAP after 48 h of swelling (Table 4.3). Therefore, it can be expected that the measured values of D have good chances to agree with the predicted ones, if NMR measurements could be performed in swollen hydrogel samples. Altogether, pulsed field gradient NMR spectroscopy is regarded as a valuable and robust method to determine the diffusion coefficients of comparatively fast-diffusing molecules. In addition, it is particularly advantageous as non-fluorescent probe molecules can also

be studied. In the case of slow-diffusing macromolecules, however, DOSY experiments are less well suited, as the signal intensity will not decay sufficiently within acceptable limits of Δ and δ . For this reason, the diffusion coefficients of the two larger FITC-dextran (150 and 2,000 kDa molecular weight) could not be determined by pulsed field gradient NMR spectroscopy.

4.3.5 Release of FITC-dextran

In the final experiment, the *in vitro* FITC-dextran release was studied. For this purpose, FITC-dextran loaded gel cylinders were prepared and incubated in a comparatively large amount of PBS in order to assure sink conditions. To calculate the diffusion coefficients of the incorporated FITC-dextran, an analytical solution of Fick's second law of diffusion [Equation (4.7)] was fitted to the experimentally determined release kinetics. Since this theory does not account for hydrogel swelling (diameter and height of the gel cylinder are assumed to be constant), all samples were pre-swollen in PBS which contained 1 mg/mL of the respective FITC-dextran. As a consequence of this, the exact amount of FITC-dextran loading was unknown (actual FITC-dextran load per hydrogel $\geq 100 \mu\text{g}$), and only the absolute values of the released quantities were represented.

As can be seen in Figure 4.3, good agreement between theoretical values (solid lines) and experimental data (symbols) was obtained in all cases ($R^2 > 0.98$). The apparent diffusion coefficients of the investigated FITC-dextran (20, 150, and 2,000 kDa molecular weight) are listed in Table 4.3. As already observed in the FRAP experiments, the differences between the two polymer concentrations (5 % and 10 %) were generally very small. In all cases, the determined values of D were also significantly higher than the values measured by FRAP. Such discrepancies have been described in the literature and are most likely due to the experimental setup [132, 135, 136]. In release experiments, mass transport occurs along concentration gradients (classical Fickian diffusion), whereas FRAP experiments investigate processes of self-diffusion (diffusion in the absence of concentration gradients). Furthermore, the larger FITC-dextran (2,000 kDa molecular weight) in particular show a relatively broad molecular weight distribution [153]. Therefore it might be possible that two different populations of

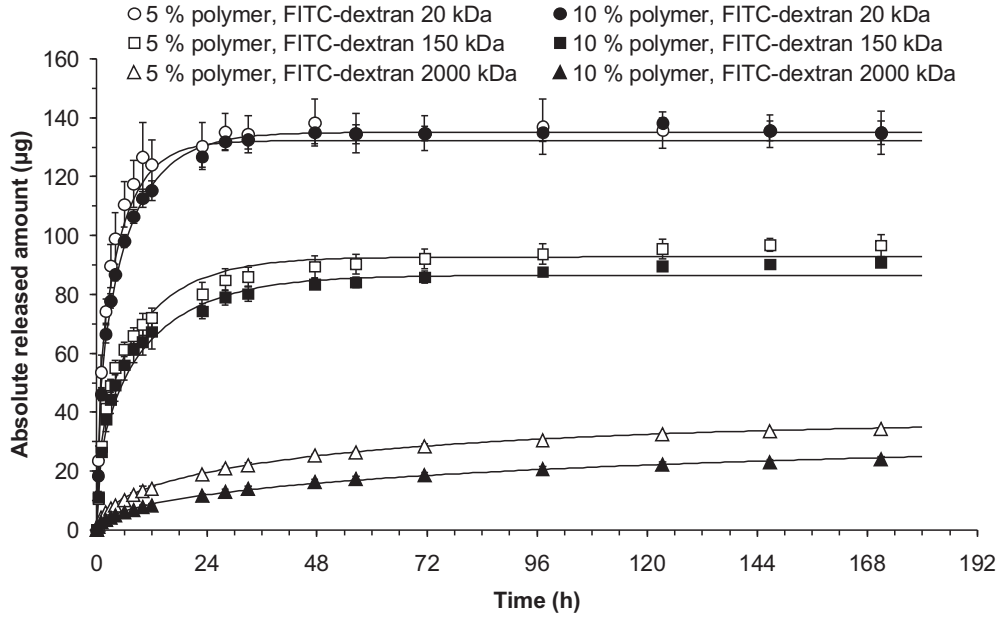


Figure 4.3: Absolute cumulative amounts of released FITC-dextrans. Data are shown as means \pm standard deviations ($n = 3$). Symbols represent the experimental data, solid lines the theoretical values obtained from Equation (4.7).

FITC-dextrans are present within the hydrogels: a low molecular weight fraction with D almost equal to that in water, and a high molecular weight fraction with restricted mobility. As outlined in section 4.3.3, the fraction of low molecular weight FITC-dextrans probably diffuses too fast in order to determine D using FRAP. Consequently, only molecules with restricted mobility will account for the recovery profile, which results in lower values of D .

4.4 Conclusion

Hydrogels were prepared by step-growth polymerization of branched PEG-amines with branched PEG-succinimidyl propionates and loaded with three different FITC-dextrans (20, 150, and 2,000 kDa molecular weight) as macromolecular model drugs. Mechanical tests and swelling studies allowed prediction of the FITC-dextran mobility. The actual diffusion coefficients D inside the gels were measured by fluorescence

recovery after photobleaching (FRAP) and pulsed field gradient NMR spectroscopy. In a final experiment, the apparent diffusion coefficients of incorporated FITC-dextran were determined by least-squares fits of appropriate model equations to experimentally obtained release profiles. FRAP proved to be suitable to measure the diffusion coefficients of slow-diffusing molecules, whereas pulsed field gradient NMR spectroscopy appears to be especially suited to determine D of fast-diffusing substances. Furthermore, FRAP could be used to follow changes in drug diffusivity during hydrogel swelling and degradation or to measure local diffusion coefficients in inhomogeneous samples. Altogether, mechanical testing, FRAP, and pulsed field gradient NMR spectroscopy proved to be valuable tools for the characterization of hydrogel-based drug delivery systems. Although the determined values of D did not match the apparent diffusion coefficients exactly, the relative differences between the two polymer concentrations and the different FITC-dextran were represented correctly. Measuring D will, therefore, allow evaluation of the potential of newly developed drug delivery systems within a few minutes. This is a clear advantage over traditional release experiments which often span a period up to several days. Provided that appropriate mathematical models exist and the mechanisms controlling drug release are known, entire release profiles could be predicted. This might contribute to a better understanding of hydrogel-based materials and accelerate the development of marketable drug delivery systems.

Chapter 5

Biodegradable hydrogels for time-controlled release of tethered peptides or proteins

Ferdinand Brandl¹, Jörg Teßmar¹, Torsten Blunk¹, Achim Göpferich¹

¹ *Department of Pharmaceutical Technology, University of Regensburg, 93040 Regensburg*

Submitted to *Biomacromolecules*.

Abstract

Tethering drug substances to a gel network is an effective way of controlling the release kinetics of hydrogel-based drug delivery systems. Here, we report on *in situ* forming, biodegradable hydrogels that allow for the covalent attachment of peptides or proteins. Hydrogels were prepared by step-growth polymerization of branched poly(ethylene glycol). The gel strength ranged from 1075 to 2435 Pa; the degradation time varied between 24 and 120 h. Fluorescence recovery after photobleaching showed that fluorescently labeled bovine serum albumin (FITC-BSA) was successfully bound to the gel network during gel formation. Within 168 h, the mobility of the tethered molecules gradually increased due to polymer degradation. Using FITC-BSA and lysozyme as model proteins, we showed the potential of the developed hydrogels for time-controlled release. The obtained release profiles had a sigmoidal shape and matched the degradation profile very well; protein release was complete after 96 h.

5.1 Introduction

Over the past decades, hydrogels have been extensively used as matrices for controlled drug delivery and tissue engineering applications [7, 10–12, 102, 154]. The popularity of these materials is based on their enormous chemical versatility, which allows for the design of a broad range of hydrogels with varying properties [10–12, 154]. Furthermore, hydrogel-based materials generally show excellent biocompatibility because of their physicochemical similarity to the native extracellular matrix [10–12, 154]. Finally, compared to other commonly used biomaterials, such as poly(lactic acid) or poly(lactide-*co*-glycolide), hydrophilic polymers are well suited for the entrapment of biomolecules due to their lack of hydrophobic interactions, which can affect the activity of these fragile species [11, 154].

Despite this multitude of advantageous characteristics, hydrogels also have several limitations. As a result of their high water content, most hydrogels usually restrict the mobility of encapsulated peptides or proteins only moderately. Consequently, a large amount of the incorporated molecules will be released within a few hours, which illustrates the necessity for more sophisticated strategies in order to prolong drug release [7, 11, 12]. Adjusting the cross-linking density is a common approach to reduce gel permeability and slow down the release kinetics. However, this approach is only effective in controlling the release of relatively large molecules, such as proteins with molecular weights of several thousand Daltons. Furthermore, increasing the cross-linking density often results in decreased hydrophilicity and hence decreased biocompatibility [11]. Tethering drug substances to the gel network via degradable anchor groups would be a further strategy to effectively control drug release. In these systems, the release kinetics is ideally controlled by the degradation of the anchor group while drug diffusivity only plays a secondary role [7, 11, 12, 155]. However, the drug molecules often need to be chemically modified in order to allow for their covalent attachment, which makes these drug delivery systems highly complex [156–158]. Furthermore, drug conjugation may also decrease bioactivity, especially when peptides or proteins are the target therapeutics [11]. In addition, the anchor groups have to be carefully designed in order to avoid unwanted side-effects during degradation *in vivo* [11].

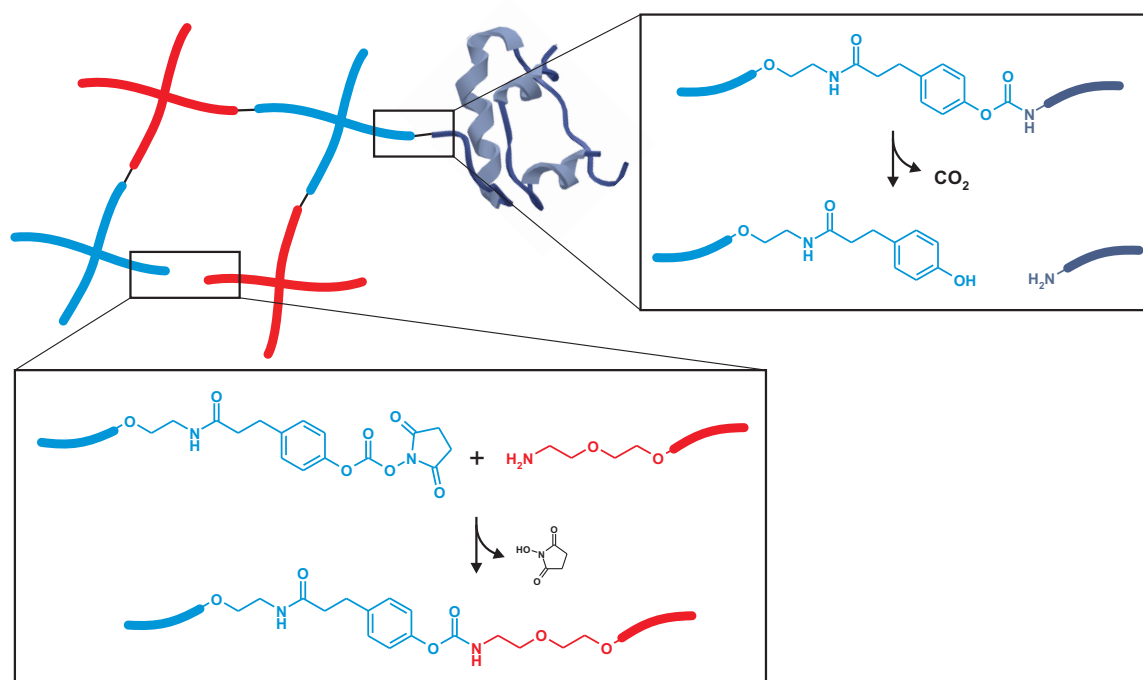


Figure 5.1: Schematic illustration of hydrolytically degradable hydrogels for time-controlled release of tethered peptides or proteins. For gel formation, branched PEG-succinimidyl carbonates are reacted with branched PEG-amines (lower inset). The same chemistry allows for the immobilization of dissolved peptides or proteins via pendant PEG chains. During gel degradation, these anchoring PEG-chains are cleaved, and the unmodified peptide or protein will be released into solution (upper inset).

In this paper, we report the preparation and characterization of *in situ* cross-linkable, biodegradable hydrogels for time-controlled release of peptides or proteins. For this purpose, branched poly(ethylene glycol) (PEG) was functionalized with aromatic succinimidyl carbonate groups that readily react with amino groups of other polymers, peptides, or proteins under formation of biodegradable carbamate bonds. Aromatic succinimidyl carbonates have been originally described as linking groups for the reversible PEGylation of proteins [159, 160]. While extensively applied for the preparation of soluble protein prodrugs, this chemistry has never been used for the formation of hydrogels. For the preparation of covalently cross-linked hydrogels, PEG-succinimidyl carbonates were reacted with branched PEG-amines (Figure 5.1, lower inset). Since the chemical environment of the reacting amino groups was expected to influence gel formation and degradation, the PEG-amines were further

modified with alanine, 6-aminohexanoic acid, and lysine. These amino acid moieties were chosen to represent the different amino groups available in proteins (amino terminus and ϵ -amino groups of lysine residues). During gelation, dissolved peptides or proteins are expected to be immobilized within the gel network via pendant PEG chains (Figure 5.1). This will improve handling and flexibility of the drug delivery system, since any peptide or protein could be incorporated without requiring chemical modifications of these molecules. Similar to soluble prodrugs, the anchoring PEG chains are cleaved during gel degradation, and the native peptide or protein will be released into solution (Figure 5.1, upper inset) [159–162]. Non-degradable gels served as a control group. The prepared hydrogels were characterized with respect to their mechanical properties, swelling capacities, and degradation rates. To prove their suitability as potential drug delivery systems, the gels were loaded with fluoresceine isothiocyanate (FITC) labeled bovine serum albumin (BSA) and lysozyme as model proteins. The successful immobilization and subsequent liberation of FITC-BSA was investigated by fluorescence recovery after photobleaching (FRAP) experiments. And finally, the *in vitro* release kinetics of FITC-BSA and lysozyme were determined.

5.2 Materials and methods

5.2.1 Materials

Hexane, 3-(4-hydroxyphenyl)propionic acid, methylene chloride (DCM), and phthalimide were purchased from Acros Organics (Geel, Belgium). Boc-protected alanine (Boc-Ala-OH), Boc-6-aminohexanoic acid, and di-Boc protected lysine dicyclohexylammonium salt (Boc-Lys(Boc)-OH · DCHA) were obtained from Bachem GmbH (Weil am Rhein, Germany). Deuterated chloroform (CDCl_3) was obtained from Deutero GmbH (Kastellaun, Germany). Phosphate buffered saline (PBS) was purchased from Invitrogen GmbH (Karlsruhe, Germany). Four-armed poly(ethylene glycol) (molecular weight 10 kDa, 4armPEG10k-OH) was purchased from Nektar Therapeutics (Huntsville, AL). Acetonitrile, Coomassie Brilliant Blue G250, *N,N'*-dicyclohexylcarbodiimide (DCC), fluoresceine isothiocyanate (FITC) labeled bovine serum albumin (BSA), FITC-

dextran (150 kDa molecular weight), N-hydroxysuccinimide (HOSu), diisopropyl azodicarboxylate, *N,N'*-diisopropylethylamine (DIPEA), lysozyme (from chicken egg white), Sigmacote[®], and *N,N'*-discuccinimidyl carbonate (DSC) were obtained from Sigma-Aldrich (Taufkirchen, Germany). Ethanol, ethyl acetate, and diethyl ether were of technical grade and used without further purification. All other chemicals were of analytical grade and purchased from Merck KGaA (Darmstadt, Germany). Deionized water was obtained using a Milli-Q water purification system from Millipore (Schwalbach, Germany).

5.2.2 Synthesis of PEG-amines

Branched PEG-amines (10 kDa molecular weight, 4armPEG10k-NH₂) were synthesized as previously described [139]. First, phthalimido-PEGs were obtained by reaction of 4armPEG10k-OH, phthalimide, triphenylphosphine, and diisopropyl azodicarboxylate. The phthalimido groups were then converted into primary amines by hydrazinolysis.

5.2.3 Synthesis of non-degradable PEG-succinimidyl carbonates (4armPEG10k-SC)

2.0 g of 4armPEG10k-OH (0.2 mmol) and 0.82 g of DSC (3.2 mmol) were dissolved in 20 mL of dried acetonitrile. Then, 520 μ L of pyridine (6.4 mmol) were added, and the reaction mixture was stirred overnight at room temperature. The next day, the solvent was evaporated under reduced pressure, and 20 mL of DCM were added to the residue. The insoluble residue was filtered off, and the solution was concentrated under reduced pressure. The product was crystallized at 0 °C under vigorous stirring by drop-wise addition of diethyl ether. For further purification, the crystallization step was repeated. The precipitate was collected by filtration, washed with cold diethyl ether, and dried under vacuum to yield 1.9 g (90 %) of 4armPEG10k-SC (Figure 5.2A).

¹H-NMR (4armPEG10k-SC, DMSO-d₆, 600 MHz): δ 2.80 ppm (s, 16H, -C(O)CH₂-CH₂C(O)-), 3.30 ppm (s, 8H, R₃CCH₂O-), 3.50 ppm (s, -OCH₂CH₂O-), 3.69 ppm (t, 8H, -OCH₂CH₂OC(O)O-), 4.39 ppm (t, 8H, -OCH₂CH₂OC(O)O-)

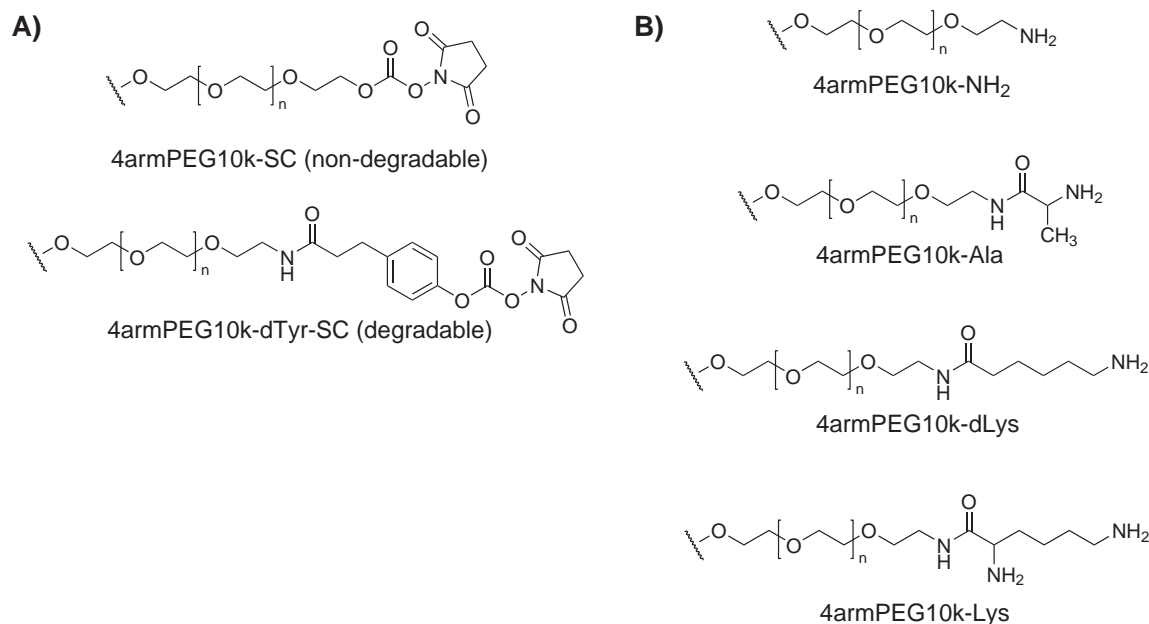


Figure 5.2: Polymers derived from branched poly(ethylene glycol). Amine-reactive PEG-succinimidyl carbonates (A) and amino acid-modified PEG-amines (B).

5.2.4 Synthesis of degradable PEG-succinimidyl carbonates (4armPEG10k-dTyr-SC)

In the first step, 0.67 g of 3-(4-hydroxyphenyl)propionic acid (4.0 mmol), 0.46 g of HOSu (4.0 mmol), and 0.83 g of DCC (4.0 mmol) were dissolved in 20 mL of dried 1,4-dioxane and stirred overnight at room temperature. The next day, the reaction mixture was passed through a glass filter funnel to remove precipitated *N,N'*-dicyclohexylurea (DCU), combined with a solution of 4armPEG10k-NH₂ (5.0 g, 0.5 mmol) and NaHCO₃ (0.19 g, 2.2 mmol) in water (20 mL), and stirred overnight at 50 °C. Afterwards, the solvent was evaporated and the residue was dissolved in water. The raw product was then extracted with DCM. The combined organic phases were dried over anhydrous Na₂SO₄, and the solution was concentrated under reduced pressure. The intermediate was crystallized at 0 °C under vigorous stirring by drop-wise addition of diethyl ether. The precipitate was collected by filtration, washed with cold diethyl ether, and dried under vacuum to yield 5.1 g (96 %) of 4armPEG10k-dTyr. Thin layer chromatography (TLC) indicated that the product was free of 4armPEG10k-NH₂, 3-(4-hydroxyphenyl)propionic acid, and HOSu.

$^1\text{H-NMR}$ (4armPEG10k-dTyr, CDCl_3 , 600 MHz): δ 2.43 ppm (t, 8H, $-\text{C}(\text{O})\text{CH}_2\text{CH}_2-$), 2.87 ppm (t, 8H, $-\text{C}(\text{O})\text{CH}_2\text{CH}_2-$), 3.41 ppm (s, 8H, $\text{R}_3\text{CCH}_2\text{O}-$), 3.64 ppm (s, $-\text{OCH}_2\text{CH}_2\text{O}-$), 6.13 ppm (t, 4H, $-\text{NHC}(\text{O})-$), 6.76 ppm (d, 8H, $-\text{C}_6\text{H}_4\text{OH}$), 7.03 ppm (d, 8H, $-\text{C}_6\text{H}_4\text{OH}$)

The phenolic hydroxyl groups were then converted into amine-reactive succinimidyl carbonate groups. For a typical synthesis, 5.3 g of 4armPEG10k-dTyr (0.5 mmol) and 2.05 g of DSC (8.0 mmol) were dissolved in 50 mL of dried acetonitrile. Then, 1300 μL of pyridine (16.0 mmol) were added, and the reaction mixture was stirred overnight at room temperature. The next day, the solvent was evaporated under reduced pressure, and 50 mL of DCM were added to the residue. The insoluble residue was filtered off, and the solution was concentrated under reduced pressure. The product was crystallized at 0 $^\circ\text{C}$ under vigorous stirring by drop-wise addition of diethyl ether. For further purification, the crystallization step was repeated. The precipitate was collected by filtration, washed with cold diethyl ether, and dried under vacuum to yield 5.2 g (93 %) of 4armPEG10k-dTyr-SC (Figure 5.2A).

$^1\text{H-NMR}$ (4armPEG10k-dTyr-SC, CDCl_3 , 600 MHz): δ 2.48 ppm (t, 8H, $-\text{C}(\text{O})\text{CH}_2\text{CH}_2-$), 2.88 ppm (s, 16H, $-\text{C}(\text{O})\text{CH}_2\text{CH}_2\text{C}(\text{O})-$), 2.98 ppm (t, 8H, $-\text{C}(\text{O})\text{CH}_2\text{CH}_2-$), 3.41 ppm (s, 8H, $\text{R}_3\text{CCH}_2\text{O}-$), 3.64 ppm (s, $-\text{OCH}_2\text{CH}_2\text{O}-$), 6.36 ppm (t, 4H, $-\text{NHC}(\text{O})-$), 7.17 ppm (d, 8H, $-\text{C}_6\text{H}_4\text{OSu}$), 7.26 ppm (d, 8H, $-\text{C}_6\text{H}_4\text{OSu}$)

5.2.5 Synthesis of alanine-modified PEG-amines (4armPEG10k-Ala)

In the coupling step, 1.51 g of Boc-Ala-OH (8.0 mmol) and 0.83 g of DCC (4.0 mmol) were dissolved in 20 mL of dried DCM. After stirring for 30 min at room temperature, the solution was passed through a glass filter funnel to remove precipitated DCU, and combined with a solution of 4armPEG10k-NH₂ (5.0 g, 0.5 mmol) in dried DCM (50 mL). Then, 700 μL of DIPEA (4.0 mmol) were added, and the mixture was stirred for 1.5 h at room temperature. The solution was concentrated under reduced pressure and placed into an ice bath. The intermediate was crystallized at 0 $^\circ\text{C}$ under vigorous stirring by drop-wise addition of diethyl ether. The precipitate was collected

by filtration, washed with cold diethyl ether, and dried under vacuum to yield 5.1 g (97 %) of 4armPEG10k-Ala-Boc.

$^1\text{H-NMR}$ (4armPEG10k-Ala-Boc, CDCl_3 , 300 MHz): δ 1.36 ppm (d, 12H, $-\text{CH}(\text{NH-Boc})\text{CH}_3$), 1.44 ppm (s, 36H, $-\text{OtBu}$), 3.41 ppm (s, 8H, $\text{R}_3\text{CCH}_2\text{O}-$), 3.64 ppm (s, $-\text{OCH}_2\text{CH}_2\text{O}-$), 4.15 ppm (4H, $-\text{CH}(\text{NHBoc})\text{CH}_3$), 5.20 ppm (4H, $-\text{CH}(\text{NHBoc})-\text{CH}_3$), 6.66 ppm (4H, $-\text{NHC}(\text{O})-$)

To deprotect the amino acid moiety, 5.1 g of 4armPEG10k-Ala-Boc (0.5 mmol) were dissolved in 55 mL of methanolic HCl (prepared by dropping 5 mL of acetyl chloride into 50 mL of ice-cooled methanol). After stirring for 30 min at room temperature, the solvent was evaporated, and the residue was dissolved in 25 mL of water. The raw product was extracted with DCM. The combined organic phases were dried over anhydrous Na_2SO_4 , and the solution was concentrated under reduced pressure. 4armPEG10k-Ala was crystallized at 0 °C under vigorous stirring by drop-wise addition of diethyl ether. The precipitate was collected, washed with cold diethyl ether, and dried under vacuum to yield 4.7 g (96 %) of the product (Figure 5.2B).

$^1\text{H-NMR}$ (4armPEG10k-Ala, CDCl_3 , 600 MHz): δ 1.34 ppm (d, 12H, $-\text{CH}(\text{NH}_2)-\text{CH}_3$), 3.41 ppm (s, 8H, $\text{R}_3\text{CCH}_2\text{O}-$), 3.64 ppm (s, $-\text{OCH}_2\text{CH}_2\text{O}-$), 7.55 ppm (t, 4H, $-\text{NHC}(\text{O})-$)

5.2.6 Synthesis of 6-aminohexanoic acid-modified PEG-amines (4armPEG10k-dLys)

4armPEG10k-dLys (Figure 5.2B) was synthesized from 4armPEG10k- NH_2 and Boc-6-aminohexanoic acid with a 95 % yield as described for 4armPEG10k-Ala.

$^1\text{H-NMR}$ (4armPEG10k-dLys, CDCl_3 , 600 MHz): δ 1.36 ppm (m, 8H, $-\text{CH}_2\text{CH}_2-\text{CH}_2\text{CH}_2\text{CH}_2\text{NH}_2$), 1.47 ppm (m, 8H, $-\text{CH}_2\text{CH}_2\text{CH}_2\text{CH}_2\text{CH}_2\text{NH}_2$), 1.66 ppm (m, 8H, $-\text{CH}_2\text{CH}_2\text{CH}_2\text{CH}_2\text{CH}_2\text{NH}_2$), 2.19 ppm (t, 8H, $-\text{CH}_2\text{CH}_2\text{CH}_2\text{CH}_2\text{CH}_2\text{NH}_2$), 2.70 ppm (t, 8H, $-\text{CH}_2\text{CH}_2\text{CH}_2\text{CH}_2\text{CH}_2\text{NH}_2$), 3.41 ppm (s, 8H, $\text{R}_3\text{CCH}_2\text{O}-$), 3.64 ppm (s, $-\text{OCH}_2\text{CH}_2\text{O}-$), 6.23 ppm (t, 4H, $-\text{NHC}(\text{O})-$)

5.2.7 Synthesis of lysine-modified PEG-amines (4armPEG10k-Lys)

5.0 g of Boc-Lys(Boc)-OH · DCHA (9.5 mmol) were suspended in 50 mL of ethyl acetate. A solution of 10 % citric acid in water was added until a clear mixture was obtained. After stirring for 30 min at 0 °C, the aqueous phase was separated and extracted with ethyl acetate. The combined organic phases were washed with water until neutral and dried over anhydrous Na₂SO₄. After evaporation of the solvent, Boc-Lys(Boc)-OH was dried under vacuum to yield 3.2 g (97 %). 4armPEG10k-Lys was prepared from 4armPEG10k-NH₂ and Boc-Lys(Boc)-OH in a similar manner to that of 4armPEG10k-Ala with a 95 % yield (Figure 5.2B).

¹H-NMR (4armPEG10k-Lys, CDCl₃, 600 MHz): δ 1.32 – 1.54 ppm (m, 20H, $-CH_2CH_2CH_2CH_2NH_2$), 1.76 – 1.85 ppm (m, 4H, $-CH_2CH_2CH_2CH_2NH_2$), 2.69 ppm (t, 8H, $-CH_2CH_2CH_2CH_2NH_2$), 3.32 ppm (4H, $-NHC(O)CH(NH_2)-$), 3.39 ppm (s, 8H, R₃CCH₂O-), 3.61 ppm (s, $-OCH_2CH_2O-$), 7.54 ppm (4H, $-OCH_2CH_2NHC(O)-$)

5.2.8 Preparation and rheological characterization of hydrogels

Gelation kinetics and gel strength were studied by performing oscillatory shear experiments on a TA Instruments AR 2000 rheometer (TA Instruments, Eschborn, Germany) with parallel plate geometry. For the preparation of hydrogels, accurately weighed amounts of the amine component were dissolved in 1000 μ L of 25 mM phosphate buffer (Table 5.1) and cooled to 5 °C. Immediately before starting the experiment, this polymer solution was added to the PEG-succinimidyl carbonate (Table 5.1). The stoichiometric ratio between succinimidyl carbonate and amino groups was balanced, and the overall polymer concentration was 5 % (w/v) for all hydrogels. After vortexing, the precursor solution was poured onto the bottom plate of the rheometer which was also cooled to 5 °C. The upper plate (20 mm in diameter) was then lowered to a gap size of 1000 μ m, the temperature was raised to 25 °C, and the measurement was started. The evolution of storage (G') and loss moduli (G'') was recorded as a function of time at 1 Hz oscillatory frequency and a constant strain of 0.05. A solvent trap was used in order to prevent the evaporation of water. The cross-over of G' and G'' was regarded as the gel point. After 90 min, the absolute

value of the complex shear modulus ($G^* = G' + i \cdot G''$) was determined as a measure for the gel strength. All experiments were carried out in triplicate and the results are expressed as means \pm standard deviations.

Table 5.1: Composition of the prepared hydrogels. The amine component was dissolved in 1000 μ L of 25 mM phosphate buffer and added to the PEG-succinimidyl carbonate. The stoichiometric ratio between succinimidyl carbonate and amino groups was balanced.

Group	Polymer conc.	pH	Amine component	PEG-succinimidyl carbonate
PEG-dLys	5 %	8.0	4armPEG10k-dLys (25 mg)	4armPEG10k-dTyr-SC (25 mg)
PEG-NH ₂	5 %	7.4	4armPEG10k-NH ₂ (25 mg)	4armPEG10k-dTyr-SC (25 mg)
PEG-Ala	5 %	6.8	4armPEG10k-Ala (25 mg)	4armPEG10k-dTyr-SC (25 mg)
PEG-Lys	5 %	6.4	4armPEG10k-Lys (17 mg)	4armPEG10k-dTyr-SC (33 mg)
Control	5 %	7.0	4armPEG10k-NH ₂ (25 mg)	4armPEG10k-SC (25 mg)

5.2.9 Equilibrium swelling of hydrogels and determination of network parameters

For the swelling studies, accurately weighed amounts of the amine component were dissolved in 1000 μ L of 25 mM phosphate buffer, and added to the PEG-succinimidyl carbonate (Table 5.1). The stoichiometric ratio between succinimidyl carbonate and amino groups was balanced, and the overall polymer concentration was again 5 % (w/v) for all gels. After vortexing, 250 μ L of the precursor solution were cast into cylindrical glass molds (7 mm inner diameter) and allowed to gel for 2 h. The samples were then weighed in air and hexane before and after swelling for 24 h in 10 mL of PBS using a density determination kit (Mettler-Toledo, Gießen, Germany). To minimize hydrogel degradation, the samples were incubated at 5 °C. Based on Archimedes' principle, the gel volumes after cross-linking (V_{gc}) and after swelling (V_{gs}) were determined. The volume of the dry polymer (V_p) was calculated from the mass of the freeze-dried hydrogel and the density of the polymer in the dry state (taken as the density of PEG, $1.12 \text{ g} \cdot \text{cm}^{-3}$). With these parameters, the polymer fraction of the gel after cross-linking, $v_{2c} = V_p/V_{gc}$, and in the swollen state, $v_{2s} = V_p/V_{gs}$,

was calculated. The reciprocal of v_{2s} is usually termed as the volumetric swelling ratio (Q).

The number of moles of elastically active chains in the hydrogel network, ν_e , was calculated using a modified version of the classical Flory-Rehner equation [140–142]:

$$\nu_e = -\frac{V_p}{V_1 v_{2c}} \cdot \frac{[\ln(1 - v_{2s}) + v_{2s} + \chi_1 v_{2s}^2]}{\left[\left(\frac{v_{2s}}{v_{2c}} \right)^{\frac{1}{3}} - \frac{2}{f} \left(\frac{v_{2s}}{v_{2c}} \right) \right]} \quad (5.1)$$

Here, χ_1 is the Flory-Huggins interaction parameter for PEG in water (taken as 0.43), V_1 is the molar volume of the solvent ($18 \text{ cm}^3 \cdot \text{mol}^{-1}$), and f is the functionality of the cross-links (4 in the case of four-armed PEG). Assuming a defect-free network, the average molecular weight between cross-links, \bar{M}_c , was calculated by $\bar{M}_c = m_p / \nu_e$, where m_p is the total mass of PEG in the hydrogel. With this parameter, the average network mesh size (ξ) was estimated by [143]:

$$\xi = v_{2s}^{-\frac{1}{3}} l \left(\frac{2\bar{M}_c}{M_r} \right)^{\frac{1}{2}} C_n^{\frac{1}{2}} \quad (5.2)$$

where l is the bond length along the polymer backbone (taken as 0.146 nm), M_r is the molecular mass of the PEG repeating unit ($44 \text{ g} \cdot \text{mol}^{-1}$), and C_n is the Flory characteristic ratio (here taken as 4 for PEG) [144]. All experiments were carried out in triplicate and the results are expressed as means \pm standard deviations.

5.2.10 Degradation of hydrogels

The gel samples were prepared as described in section 5.2.9. After gelation, the initial weight of each hydrogel was determined. To study the degradation of the gel networks, the samples were immersed in 10 mL of PBS (containing 0.025 % sodium azide) and incubated at 37 °C in a shaking water bath (approx. 50 rpm). Every day, the samples were poured out over 24 mm Netwell™ Inserts (Corning GmbH, Kaiserslautern, Germany) with a 500 μm mesh size polyester membrane and weighed. Degradation was assumed to be complete when the sample passed through the Netwell™ Insert and no remaining material could be detected.

5.2.11 Mobility of incorporated macromolecules determined by fluorescence recovery after photobleaching (FRAP)

To investigate the mobility of incorporated macromolecules with and without amino groups, the hydrogels were loaded with FITC-BSA (66 kDa molecular weight) and FITC-dextran (150 kDa molecular weight). The samples were prepared by dissolving 12.5 mg of 4armPEG10k-NH₂ in 450 μ L of 25 mM phosphate buffer, pH 7.4. Subsequently, 50 μ L of the FITC-BSA or FITC-dextran stock solution (prepared in the same buffer, $c = 10$ mg/mL) were added. The mixture was then added to 12.5 mg of 4armPEG10k-dTyr-SC (degradable gels) or 12.5 mg of 4armPEG10k-SC (non-degradable control gels), vigorously stirred, and cast into Lab-TekTM II Chambered Coverglasses (Thermo Fisher Scientific, Langenselbold, Germany). After 2 h of gelation, the samples were positioned on the microscope stage.

The FRAP experiments were performed on a Zeiss Axiovert 200 M microscope coupled to a LSM 510 META scanning device (Carl Zeiss MicroImaging GmbH, Jena, Germany). A Plan-Neofluar 20 \times objective lens with a numerical aperture of 0.50 was used. All bleaching experiments were performed using the 488 nm-line of a 30 mW Ar-ion laser operating at 50 % output power. After the region of interest was brought into focus, a time series of digital images with a resolution of 512 \times 128 pixel was recorded using a highly attenuated laser beam (0.5 % transmission). The interval between two consecutive images was 2 s. After acquisition of five prebleach images, a uniform disk with a diameter of 36 μ m was bleached at maximum laser intensity (100 % transmission). Immediately after bleaching, the laser intensity was switched back to the previous value (0.5 % transmission), and a series of 75 images was acquired in order to measure the recovery of fluorescence. To extract the experimental recovery curve from the image stack, the mean fluorescence intensities inside the bleached region, $I_{frap}(t)$, and inside a reference region were calculated for each time point using the NIH software ImageJ. In the next step, $I_{frap}(t)$ was normalized to the prebleach intensity, corrected for any bleaching effects that might have occurred during image acquisition, and normalized to the full scale.

In order to follow changes in the macromolecular mobility during gel degradation, the samples were covered with 500 μ L of PBS (containing 0.025 % sodium azide) and incubated at 37 °C. At predetermined time points ($t = 48$ h, 96 h, and 168 h), the FRAP experiments were repeated as described above.

5.2.12 Release of FITC-BSA and lysozyme

The hydrogels were loaded with FITC-BSA (66 kDa molecular weight) and lysozyme (14 kDa molecular weight) in order to evaluate their suitability as potential drug delivery systems. These two proteins were chosen because of their different mass and different number of amino groups, and serve as model compounds for therapeutic peptides or proteins. To prepare the gel samples, 25 mg of 4armPEG10k-NH₂ were dissolved in 900 μ L of 25 mM phosphate buffer, pH 7.4 and mixed with 100 μ L of the respective protein stock solution (prepared in the same buffer, $c = 10$ mg/mL). This mixture was then added to 25 mg of 4armPEG10k-dTyr-SC and vigorously vortexed. In each case, 250 μ L of these precursor solutions were cast into cylindrical glass molds (7 mm inner diameter) and allowed to gel for 2 h. The protein loading was 250 μ g per gel. Afterwards, the gels were removed from the glass molds, immersed in 10 mL of PBS (containing 0.025 % sodium azide), and maintained at 37 °C in a shaking water bath (approx. 50 rpm). All vials were treated with Sigmacote[®] to prevent the adsorption of proteins. At specified time intervals, 500 μ L of the release medium were collected and replaced with fresh buffer. Blank hydrogels without protein and protein solutions (250 μ g in 10 mL of PBS) served as control groups.

The released protein amounts were determined as described by Bradford [163]. In brief, 100 μ L of sampled release buffer were pipetted into a microtiter plate and incubated with 100 μ L of Bradford reagent for 10 min. The protein content was quantified by measuring the absorption at 595 nm using a Shimadzu CS-9301PC 96-well plate reader (Shimadzu GmbH, Duisburg, Germany). Calibration curves were obtained from known concentrations of FITC-BSA and lysozyme. All experiments were carried out in triplicate and the results are expressed as means \pm standard deviations.

5.2.13 Statistical analysis

The results from mechanical testing, swelling studies, and FRAP experiments were compared using single-factor analysis of variance (ANOVA) and Tukey's multiple comparison test. $p < 0.05$ was regarded as statistically significant. Statistical analysis was performed using SigmaStat 3.0 software (Systat Software, San Jose, CA).

5.3 Results and discussion

The aim of the present study was to prepare *in situ* forming hydrogels that allow for the time-controlled release of incorporated proteins. For this purpose, branched PEG-succinimidyl carbonates were synthesized (Figure 5.2A). These polymers react with primary amino groups of other polymers, peptides, or proteins under formation of carbamate bonds. In case of proteins, succinimidyl carbonates typically react with N-terminal amino acids and ϵ -amino groups of lysine residues [164]. Since bond formation and cleavage may vary depending on the chemical environment of the reacting amino groups, the polymers used for gel formation were further modified with alanine (mimicking the amino terminus of proteins), 6-aminohexanoic acid, and lysine (Figure 5.2B). All syntheses were straightforward and the desired products were obtained with high yields. End-groups were almost fully converted, as indicated by $^1\text{H-NMR}$ spectra.

5.3.1 Physicochemical characterization of hydrogels

Hydrogels were prepared by step-growth polymerization of branched, amino acid-modified PEG-amines with branched PEG-succinimidyl carbonates. As it was expected, gelation kinetics and gel strength were strongly dependent on the polymers used for gel preparation. In preliminary tests, the buffer pH value was therefore adjusted for each gel type (Table 5.1). When the buffer pH value was too low, polymerization was slow and the gel strength remained comparatively low. On the other hand, if the pH value was too high, the gels solidified immediately and could no longer be placed on the rheometer.

Non-degradable hydrogels were prepared from 4armPEG10k-SC and 4armPEG10k-NH₂ at pH 7.0. At the beginning of the experiment, the sample behaved like a free flowing liquid ($G'' > G'$); gelation occurred after 9.2 ± 0.4 min. During the course of the experiment, cross-linking further proceeded as indicated by the steadily increasing value of G' (Figure 5.3). After 90 min, the value of G' exceeded that of G'' by several orders of magnitude ($G' \gg G''$); the gel strength was 2429 ± 73 Pa (Table 5.2). These data agreed very well with those reported previously for gels prepared from branched PEG-succinimidyl propionates and PEG-amines [139]. For the preparation

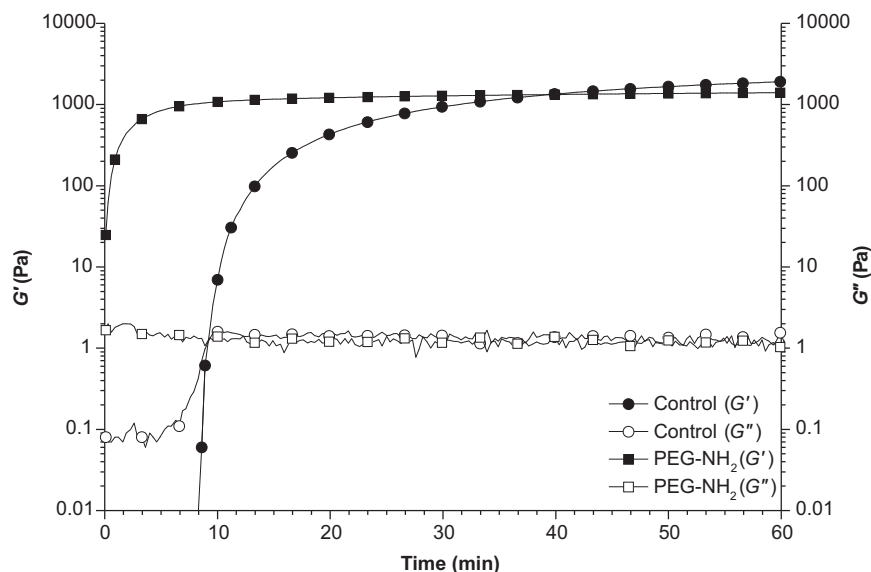


Figure 5.3: Typical rheograms of degradable (■/□) and non-degradable hydrogels (●/○). Both gels were prepared from 4armPEG10k-NH₂ at pH 7.4 (degradable gel) and pH 7.0 (non-degradable gel). The closed symbols (■/●) represent G' , the open symbols (□/○) represent G'' .

of biodegradable gels, 4armPEG10k-NH₂ was polymerized with 4armPEG10k-dTyr-SC at pH 7.4. These samples solidified in less than 1 min and the gel strength was 1486 ± 132 Pa (Table 5.2). Compared to 4armPEG10k-SC, the reactivity of 4armPEG10k-dTyr-SC seemed to be considerably increased (Figure 5.3). This could explain both the accelerated polymerization as well as the lower strength of these gels. With increasing reactivity of succinimidyl carbonate groups, their susceptibility to hydrolysis will simultaneously increase [160]. This will result in lower cross-linking densities and hence reduced gel strengths. In case of 4armPEG10k-dLys, the buffer pH value was increased to pH 8.0. This was required because of the high pK_a value of the 6-aminohexanoic acid moiety (10.6 ± 0.1). The prepared hydrogels solidified after 1.1 ± 0.2 min and the absolute value of G^* was 1075 ± 68 pascal (Table 5.2). However, when 4armPEG10k-Ala and 4armPEG10k-Lys were used for gel preparation, the buffer pH value was decreased to pH 6.8 and pH 6.4, respectively. Otherwise, gelation occurred within a few seconds and the samples could not be placed on the rheometer. The high reactivity of 4armPEG10k-Ala was attributed to the comparatively low pK_a value of the alanine moiety (8.2 ± 0.3). And in case of 4armPEG10k-Lys, gelation

was most likely facilitated by the increased number of amino groups per macromer (8 vs. 4). The stiffness was 2137 ± 55 Pa for gels prepared from 4armPEG10k-Ala, and 2435 ± 105 Pa for those prepared from 4armPEG10k-Lys (Table 5.2).

Table 5.2: Gel strength ($|G^*|$), volumetric swelling ratio (Q), molecular weight between cross-links (\bar{M}_c), and average network mesh size (ξ) of the prepared hydrogels. Data are represented as means \pm standard deviations ($n = 3$). The differences in the mean values are statistically significant ($p < 0.05$).

Group	$ G^* $ (Pa)	Q	\bar{M}_c (g \cdot mol $^{-1}$)	ξ (nm)
PEG-dLys	1075 ± 68	36.8 ± 0.5	10477 ± 202	21.2 ± 0.3
PEG-NH ₂	1486 ± 132	34.7 ± 0.1	9300 ± 82	19.6 ± 0.1
PEG-Ala	2137 ± 55	32.2 ± 0.3	7905 ± 123	17.6 ± 0.2
PEG-Lys	2435 ± 105^a	30.9 ± 0.3^b	–	–
Control	2429 ± 73^a	30.6 ± 0.8^b	6946 ± 122	16.3 ± 0.2

^aStatistically not significant ($p > 0.05$)

^bStatistically not significant ($p > 0.05$)

When compared to each other, the gels prepared from 4armPEG10k-dLys had the lowest cross-linking density of all degradable hydrogels (estimated by G^*), whereas those made from 4armPEG10k-Lys showed the highest value. This corresponded well with the results of equilibrium swelling studies. The volumetric swelling ratio Q was inversely related to gel strength and was highest for hydrogels prepared from 4armPEG10k-dLys and lowest for those prepared from 4armPEG10k-Lys (Table 5.2). Using Equations (5.1) and (5.2), these data also allowed for the calculation of the average network mesh size (ξ). The gels with the lowest cross-linking density showed the highest value of ξ (21.2 ± 0.3 nm); hydrogels with higher stiffness and hence higher cross-linking density exhibited lower values of ξ (Table 5.2). For gels prepared from 4armPEG10k-Lys, the average network mesh size could not be calculated, as these gels contained macromers of two different functionalities and Equation (5.1) can only be applied for gels containing one single type of cross-links [140–142].

5.3.2 Degradation of hydrogels

Samples were incubated in PBS at 37 °C and weighed at predetermined time points to study hydrogel degradation. As expected, the gels of the control group did not degrade within the observation period. During the first 24 h, the wet weight of these samples first increased due to swelling. However, after the non-degradable gels were swollen to equilibrium, their wet weight remained constant (Figure 5.4). In these networks, the individual macromers are linked together by aliphatic carbamate bonds, which are stable under the experimental conditions [165]. In degradable gels, however, the polymer chains were held together by aromatic carbamate groups. These carbamates hydrolyze in neutral and basic solutions by an E1cB elimination reaction involving the intermediate formation of an unstable isocyanate [165, 166]. The isocyanate readily reacts with water and disintegrates into a primary amine and carbon dioxide (see Figure 5.1 for comparison) [165, 166].

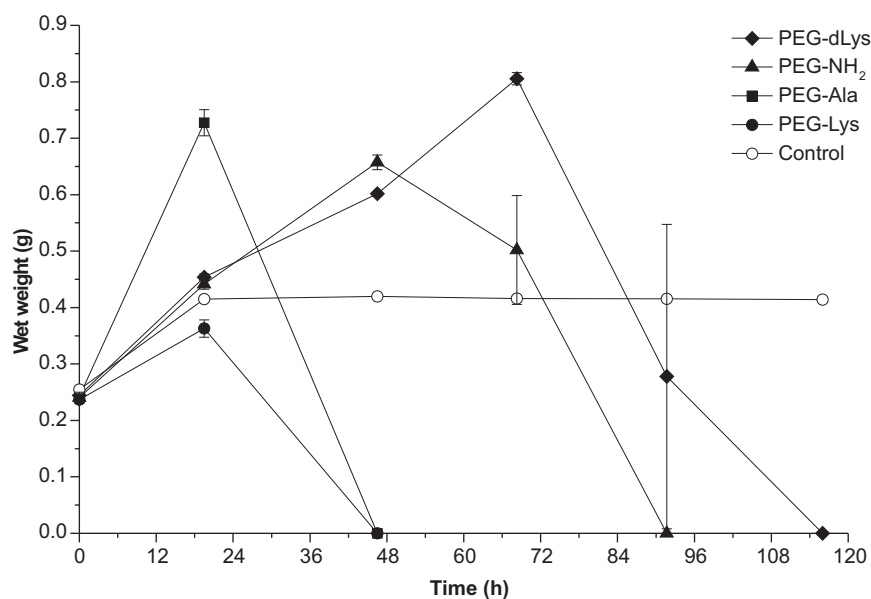


Figure 5.4: Degradation of hydrogels. Gels prepared from 4armPEG10k-Lys (●) and 4armPEG10k-Ala (■) degraded within 48 h. Hydrogels made from 4armPEG10k-NH₂ (▲) and 4armPEG10k-dLys (◆) disintegrated over 4 and 5 days, respectively. The non-degradable gels (○) remained stable over the observation period. The experiments were carried out in triplicate and the results are presented as means ± standard deviations.

During the initial phase of the study, the wet weight of the degradable samples first increased (Figure 5.4). The hydrolysis of carbamate groups obviously enlarged the average network mesh size of these hydrogels which resulted in an increased swelling capacity. After a critical amount of bonds had been cleaved, the wet weight decreased and the gels dissolved slowly. Interestingly, the two gels prepared from 4armPEG10k-Lys and 4armPEG10k-Ala disintegrated within the first 48 h. This was not expected, as these hydrogels had the highest cross-linking density of all biodegradable gels. In contrast to that, the hydrogels containing 4armPEG10k-NH₂ and 4armPEG10k-dLys were stable over 72 h and 96 h, respectively, and dissolved within the following 24 h (Figure 5.4).

Obviously, the nature of the amino groups not only influenced gelation kinetics and gel strength but also affected degradation rate. It is known from the literature that the reactivity of phenyl carbamates increases with increasing polar effects within the N-substituent. Phenyl carbamates of amino acid amides or dipeptides, for example, were hydrolyzed within a few hours. Phenyl N-ethylcarbamates, however, showed a half-life of several days [166]. The same effects could account for the degradation profiles of the different hydrogels. In case of 4armPEG10k-Lys and 4armPEG10k-Ala, the amino group is in close proximity to an amide linkage, which makes the resulting carbamates more susceptible to hydrolysis. In contrast to that, the chemical structures of 4armPEG10k-NH₂ and 4armPEG10k-dLys resemble those of phenyl N-ethylcarbamates, which can explain the better hydrolytic resistance of the corresponding hydrogels.

As a compromise between both, gel strength and degradation time, hydrogels prepared from 4armPEG10k-NH₂ were chosen for all further experiments. In future studies it may be also possible to prolong the degradation time by introducing strongly electropositive carboxylic acid moieties into the N-substituent, since these groups were reported to increase the hydrolytic resistance of phenyl carbamates [166].

5.3.3 Mobility of incorporated macromolecules

To show their suitability as drug delivery system, the developed hydrogels were loaded with FITC-BSA (66 kDa molecular weight) and FITC-dextran (150 kDa

molecular weight). The hydrodynamic diameters of these two macromolecules were 7.2 nm [167] and 16.6 nm [168], respectively. When comparing these values with the average network mesh sizes of non-degradable (16.3 nm) and degradable gels (prepared from 4armPEG10k-NH₂, 19.6 nm), the diffusivity of both macromolecules should be restricted only to a minor extent. The diffusivity of the incorporated FITC-dextran served as benchmark and allowed for the evaluation of the successful immobilization of FITC-BSA.

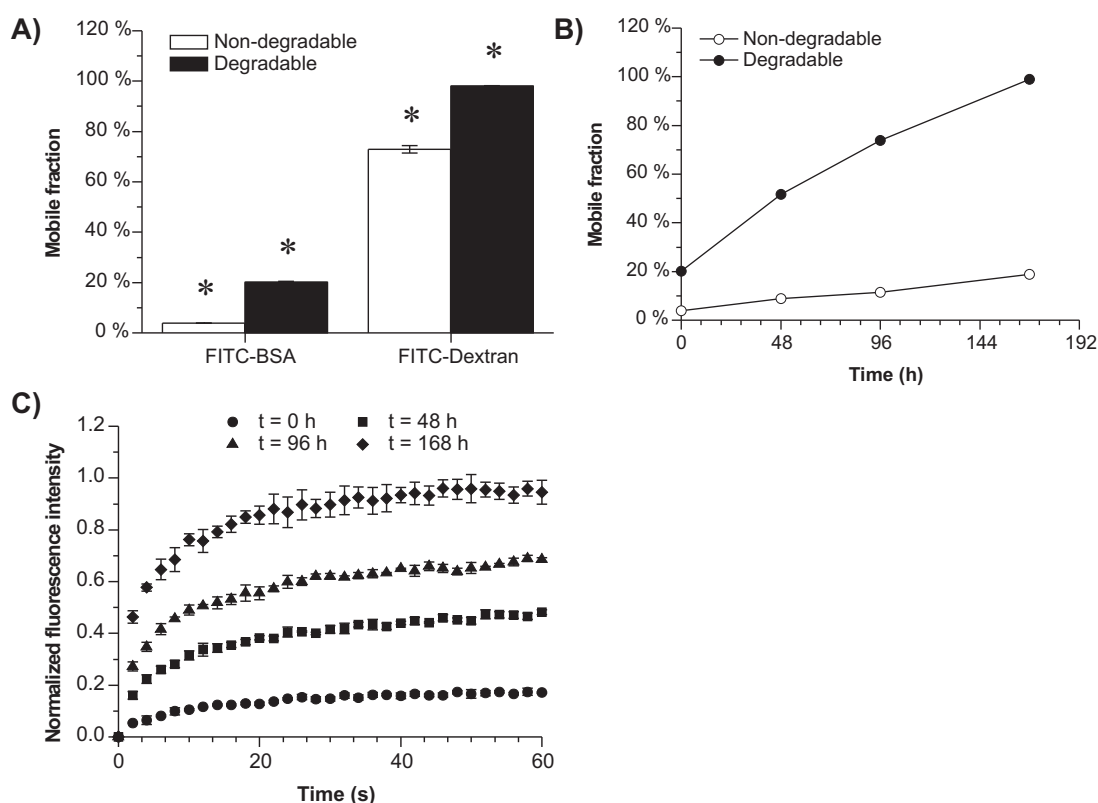


Figure 5.5: Mobile fractions of FITC-dextran and FITC-BSA in non-degradable (\square) and degradable (\blacksquare) hydrogels directly after cross-linking (A). * indicates statistical significance ($p < 0.05$). Mobile fractions of FITC-BSA in non-degradable (\circ) and degradable (\bullet) hydrogels over time (B). Mobility of FITC-BSA in degradable hydrogels (C). The recovery profiles were acquired 0 h (\bullet), 48 h (\blacksquare), 96 h (\blacktriangle), and 168 h (\blacklozenge) after cross-linking.

Directly after cross-linking, 73 % of the FITC-dextran molecules incorporated into non-degradable hydrogels were mobile. In case of degradable gels, even 98 % of the incorporated FITC-dextran were mobile (Figure 5.5A). Due to the lack of

amino groups, FITC-dextran cannot be bound to the gel network by reaction with PEG-succinimidyl carbonates. The obtained results further indicate that incorporated macromolecules will not be immobilized within the gel network by physical entrapment. In FITC-BSA loaded hydrogels, however, the situation was different. Directly after hydrogel preparation, most of the incorporated protein molecules were immobilized within the gel network. The mobile fractions were 4 % in non-degradable gels, and 20 % in degradable hydrogels (Figure 5.5A). Since the hydrodynamic diameter of FITC-BSA was well below the average network mesh size of the prepared gels, it was concluded that the protein molecules were successfully immobilized by covalent attachment to the hydrogel backbone. This demonstrates the general potential for tethering therapeutic peptides or proteins to the gel backbone by simply dissolving them together with the gel-forming polymers. Hydrogel cross-linking and drug loading can be performed simultaneously without the need for additional synthetic steps.

To follow the mobility of FITC-BSA over time, the gel samples were covered with PBS. In non-degradable hydrogels, protein mobility did not change substantially during the observation period. After 168 h of incubation, approx. 20 % of the incorporated protein molecules seemed to be mobile (Figure 5.5B). This increase can be attributed to hydrolysis of aliphatic carbamate groups, slow degradation of the protein, or release of the fluorescence label. In degradable hydrogels, however, FITC-BSA mobility gradually increased (Figure 5.5B and C). After 168 h, when the hydrogel was completely degraded, all protein molecules were mobile. The lower degradation rate most likely results from differences in the experimental setup (see Figure 5.4 for comparison). The FRAP experiments indicate that the developed hydrogels would allow for the time-controlled release of therapeutic peptides or proteins. As a result of the degradation mechanism, encapsulated peptides or proteins were expected to be released in the unaltered state, which preserves bioactivity and lowers the risk of unwanted immune reactions [169, 170].

5.3.4 Release of FITC-BSA and lysozyme

In the last experiment, the release of FITC-BSA and lysozyme was quantified. As expected from degradation studies and FRAP experiments, almost no FITC-BSA was released during the first 24 h (Figure 5.6). With the onset of gel degradation, however,

more and more protein was released into solution. The obtained release profile had a sigmoidal shape and matched the degradation profile very well. After 96 h, the release of FITC-BSA was completed. In FRAP experiments, only 75 % of the incorporated protein molecules were mobile after the same time period. These differences are most likely due to the different amounts of PBS used for FRAP and release experiments (500 μ L vs. 10 mL of PBS). Compared to FITC-dextran, which were released from similar gels almost completely within 24 h [139], the covalent attachment considerably prolonged the release of incorporated protein molecules. In addition to FITC-BSA, the hydrogels were also loaded with lysozyme. In general, the resulting release profile was similar to that of FITC-BSA (Figure 5.6). During the initial phase, however, the release of lysozyme was significantly higher. After 54 h, approx. 30 % of the total amount of lysozyme was released into solution. In the case of FITC-BSA, however, only 15 % of the incorporated protein molecules were released at the same time point. Furthermore, the release profile of lysozyme was almost linear during the first 54 h.

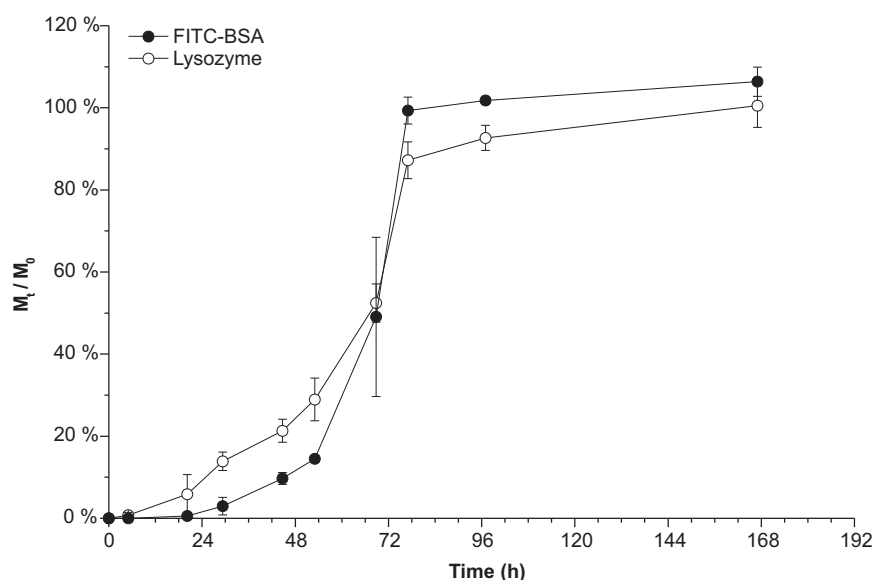


Figure 5.6: Release of FITC-BSA (●) and lysozyme (○) from biodegradable hydrogels. Data are presented as means \pm standard deviations ($n = 3$).

These variations are explained by the different characteristics of the encapsulated proteins. In the case of lysozyme, one protein molecule can be bound to the gel network by a maximum of 7 amino groups (amino terminus and ϵ -amino groups

of lysine residues). Bovine serum albumin, in contrast, is bearing 60 amino group (amino terminus and ϵ -amino groups of lysine residues) that can theoretically react with the hydrogel backbone. The probability that one protein molecule is detached from the polymer network is therefore much higher for lysozyme than for FITC-BSA. Furthermore, the lower mass of lysozyme (14 kDa vs. 66 kDa) results in an increased diffusivity within the hydrogel network. This effect will be particularly pronounced during the initial phase of protein release since the average network mesh size increases during hydrogel degradation.

Altogether, the prepared hydrogels proved to be suitable for the time-controlled release of incorporated peptides or proteins. The obtained release profiles will depend on both the encapsulated macromolecules and the polymers used for gel formation. In future experiments, different polymers (e.g. fast and slow degrading macromers) could be combined to adjust the resultant release profiles. In the end, this might allow for a constant release of therapeutic peptides or proteins over a time period of several days.

5.4 Conclusion

We successfully synthesized different derivatives of poly(ethylene glycol) that allow for the preparation of *in situ* forming hydrogels. Gel strength and degradability could be tailored by altering the polymer end-groups. Since cross-linking is performed *in situ*, the developed hydrogels could be easily delivered by injection. During the gelation process, dissolved proteins were covalently bound to the polymer backbone, as shown by FRAP experiments. In the same way, therapeutic peptides or proteins could be tethered to the hydrogel network without the need for chemical modifications of these molecules. The non-radical cross-linking approach is, thereby, favorable to the stability of these fragile molecules. During hydrogel degradation, the incorporated proteins were released into solution. Release kinetics will depend on both the incorporated proteins and the polymers used for gel formation. It is expected that the chosen linker group disintegrates without leaving any residues attached to the protein; this would preserve bioactivity and lower the risk of unwanted immune reactions. Altogether,

the developed hydrogels proved to be suitable for the time-controlled release of incorporated molecules. Further modifications of the described polymers might result in long-lasting hydrogels that would allow for the sustained release of therapeutic peptides or proteins over a time period of several days up to a few weeks.

Chapter 6

Biointeractive hydrogels for adipose tissue engineering

Ferdinand Brandl¹, Annina Seitz¹, Jörg Teßmar¹, Torsten Blunk¹,
Achim Göpferich¹

¹ *Department of Pharmaceutical Technology, University of Regensburg, 93040 Regensburg*

Submitted to *Biomaterials*.

Abstract

Adipose tissue engineering requires biomaterials that promote the differentiation of seeded adipocytes. Here, we report on the development and characterization of *in situ* forming, poly(ethylene glycol) (PEG) based hydrogels for soft tissue augmentation. Branched PEG-amines were modified with collagenase-sensitive peptides and cross-linked with branched PEG-succinimidyl propionates without the use of free-radical initiators (enzymatically degradable hydrogels). Alanine-modified PEG-amines were used for the preparation of non-degradable gels. Depending on the used polymer concentration, the strength of degradable gels ranged from 1708 to 7412 Pa; the strength of non-degradable hydrogels varied between 1496 and 7686 Pa. Enzyme mediated gel degradation occurred within 10, 16, and 19 days (5 %, 10 %, and 15 % initial polymer content). To evaluate their suitability as scaffold materials for adipose tissue engineering, the hydrogels were functionalized with the laminin-derived adhesion peptide YIGSR, and seeded with 3T3-L1 preadipocytes. Compared to a standard two-dimensional cell culture model, the developed hydrogels significantly enhanced the intracellular triglyceride accumulation of encapsulated adipocytes. Functionalization with YIGSR further enhanced lipid synthesis within differentiating adipocytes. Long-term studies suggested that enzymatically degradable hydrogels furthermore promote the formation of coherent adipose tissue-like structures featuring many mature unilocular fat cells.

6.1 Introduction

In reconstructive surgery, there is a tremendous need for suitable grafts to repair soft tissue defects following tumor resections, for example. However, none of the currently used strategies has proven to be ideal for permanent soft tissue augmentation. Adipose tissue engineering has been proposed as an alternative approach to generate functional tissue substitutes [171–174]. This will require biomaterials with mechanical properties close to those of natural adipose tissue; very rigid scaffolds will certainly not be appropriate to augment soft tissue defects. With regard to the desired substrate mechanics, poly(ethylene glycol) (PEG) based hydrogels would be qualified as three-dimensional (3-D) scaffolds for adipose tissue engineering [171, 172, 175–178]. These hydrophilic polymer networks absorb large amounts of water, allow for the unrestricted diffusion of low molecular weight nutrients and metabolites [179], and show an excellent biocompatibility because of their physicochemical similarity to the native extracellular matrix (ECM) [10]. In addition to the initial mechanical properties, the degradability of the supportive matrix must be considered as well. Current tissue engineering strategies favor biodegradable scaffolds that provide only transient stability; the newly developed tissue and the formed ECM will be responsible for the long-term maintenance of the tissue engineered construct. Therefore, it will be necessary to adapt the degradation rate to the rate of tissue formation [8, 10]. Since most synthetic hydrogels are biologically inert due to their limited interactions with ECM proteins, the gel-forming polymers may additionally be functionalized with cell adhesion ligands or growth factors in order to promote cell migration, proliferation, and differentiation [8, 10, 15].

For the preparation of such ‘biomimetic’ hydrogels, Lutolf et al. cross-linked vinylsulfone terminated PEG macromers with cysteine containing, matrix metalloproteinase (MMP) sensitive peptides [74, 90, 180]. In contrast to biomaterials with hydrolytically labile bonds, such as poly(lactic acid) blocks for example, these cell-responsive hydrogels are degraded by cell-secreted and cell-activated proteases. The gels formed *in situ*, allowed for the invasion of cells, and proved to be suitable for the regeneration of bone [100] and cartilage defects [82]. In another approach, collagenase-sensitive peptides (Gly–Gly–Leu↓Gly–Pro–Ala–Gly–Gly–Lys) and integrin-binding domains (Tyr–Ile–Gly–Ser–Arg) were coupled with amine-reactive PEG-monoacrylates. The

resulting triblock copolymers were terminated by acrylate groups and allowed for the preparation of photopolymerizable hydrogels that supported viability, adhesion, and proliferation of preadipocytes [176].

But despite these promising results, non-radical cross-linking schemes will be favored for the encapsulation of cells [181]. Furthermore, cytotoxic byproducts (such as unreacted macromers or degradation products of the polymers) may be leached out of radically cross-linked hydrogels, which have to be removed prior to their implantation into the patient [182]. Therefore, we aimed for developing injectable, biointeractive hydrogels that are cross-linked without the use of free-radical initiators (Figure 6.1). For this purpose, branched PEG-amines were functionalized with the collagenase-sensitive amino acid sequence Ala-Pro-Gly↓Leu (cleavage site between glycine and leucine) by means of classical liquid phase peptide synthesis. For the formation of hydrogels, these polymers were cross-linked with branched, amine-reactive PEG-succinimidyl propionates. In contrast to previously reported approaches, the described hydrogels can be functionalized with adhesion peptides or growth factors without requiring additional chemical modifications of these molecules (e.g. introduction of acrylate groups or cysteine residues). The prepared hydrogels were characterized for their mechanical properties, swelling behavior, and degradability. To evaluate their potential as scaffold materials for soft tissue engineering, these gels were seeded with 3T3-L1 preadipocytes, a commercially available cell line that has been extensively used to study adipocyte differentiation *in vitro* [174, 183]. By quantifying the intracellular triglyceride accumulation, we studied the effects of substrate stiffness and adhesiveness on adipocyte differentiation, and compared these results to the outcome of conventional two-dimensional (2-D) cell culture. Finally, we showed the advantage of enzymatically degradable hydrogels for the *in vitro* generation of adipose tissue-like constructs.

6.2 Materials and methods

6.2.1 Materials

Hexane, methylene chloride (DCM), and phthalimide was purchased from Acros Organics (Geel, Belgium). Murine 3T3-L1 preadipocytes were obtained from ATCC

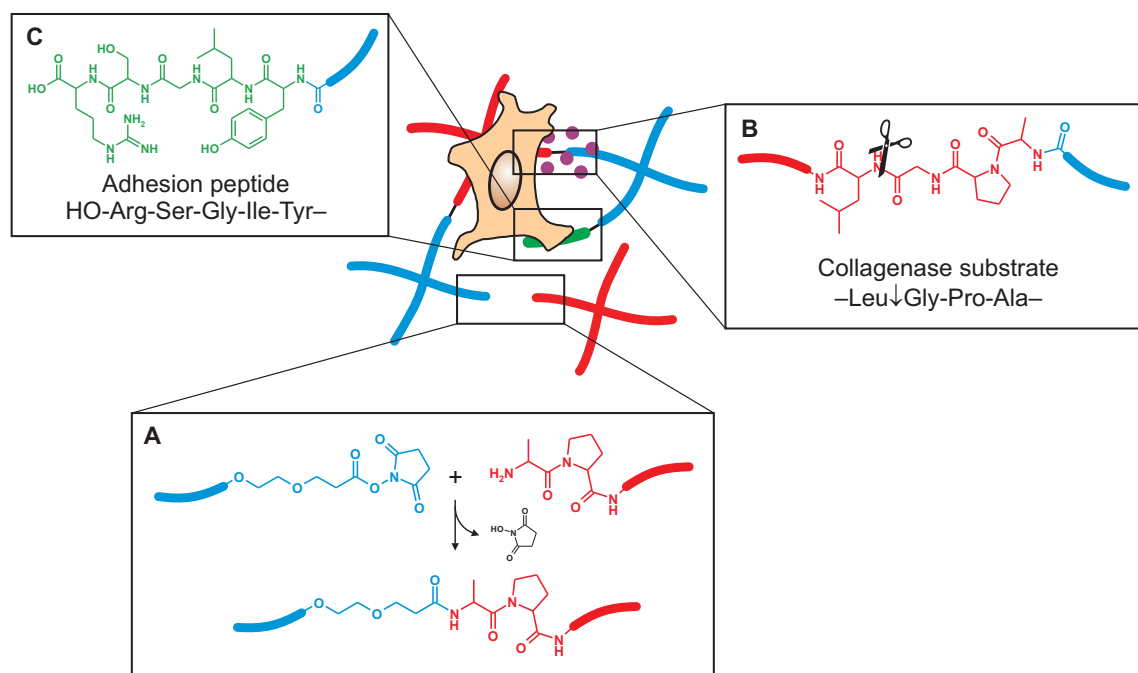


Figure 6.1: Schematic illustration of injectable, biointeractive hydrogels for soft tissue engineering applications. For gel formation, branched PEG-succinimidyl propionates are cross-linked with branched, amino acid-modified PEG-amines (A). The collagenase-sensitive peptide sequence Ala-Pro-Gly↓Leu allows for enzymatic gel degradation (B). To mediate cell-adhesion, the integrin-binding motif Tyr-Ile-Gly-Ser-Arg is reacted with branched PEG-succinimidyl propionates (C).

(Manassas, VA). Boc-protected alanine (Boc-Ala-OH), Boc-protected glycine (Boc-Gly-OH), and Boc-protected proline (Boc-Pro-OH) were bought from Bachem GmbH (Weil am Rhein, Germany). Dulbecco's modified Eagle's medium (DMEM) and trypsin (1 : 250) were purchased from Biochrom (Berlin, Germany). Deuterated chloroform (CDCl_3) was obtained from Deutero GmbH (Kastellaun, Germany). Fetal bovine serum (FBS, Lot. No. 40A0044K), penicillin-streptomycin solution, and phosphate buffered saline (PBS) were from Invitrogen GmbH (Karlsruhe, Germany). Four-armed poly(ethylene glycol) (molecular weight 10 kDa, 4armPEG10k-OH) was purchased from Nektar Therapeutics (Huntsville, AL). Hoechst 33258 dye was obtained from Polysciences (Warrington, PA); calcium chloride (CaCl_2) was from Carl Roth GmbH (Karlsruhe, Germany). Bovine insulin was kindly provided by Sanofi-Aventis (Frankfurt am Main, Germany). 3-Isobutyl-methylxanthine (IBMX) was bought from Serva Electrophoresis (Heidelberg, Germany). Acrylonitrile, Boc-protected leucine (Boc-Leu-OH), collagenase from *Clostridium histolyticum* (Type I), corticos-

terone, cysteine, *N,N'*-dicyclohexylcarbodiimide (DCC), diisopropyl azodicarboxylate, *N,N'*-diisopropylethylamine (DIPEA), DNA from calf thymus, fluorescamine, *N*-hydroxysuccinimide (HOSu), indomethacin, the laminin fragment Cys–Asp–Pro–Gly–Tyr–Ile–Gly–Ser–Arg (YIGSR), Minimum Essential Medium alpha modification (α -MEM), oil red O, and Sigmacote[®] were purchased from Sigma-Aldrich (Taufkirchen, Germany). Papainase was bought from Worthington (Lakewood, NJ). Diethyl ether was of technical grade and used without further purification. All other chemicals were of analytical grade and obtained from Merck KGaA (Darmstadt, Germany). Deionized water was obtained using a Milli-Q water purification system from Millipore (Schwalbach, Germany).

6.2.2 Synthesis of amine-reactive polymers (4armPEG10k-SPA)

Branched PEG-succinimidyl propionates (4armPEG10k-SPA) were synthesized as previously described [139]. In brief, PEG-propionic acid was obtained through Michael-type addition reaction of 4armPEG10k-OH onto acrylonitrile and subsequent hydrolysis under alkaline conditions. The obtained carboxylic acid groups were then converted into amine-reactive succinimidyl ester groups using HOSu and DCC.

6.2.3 Synthesis of collagenase-sensitive polymers (4armPEG10k-LGPA)

The synthesis of collagenase-sensitive polymers started from branched PEG-amines (4armPEG10k-NH₂), which were obtained as previously described [139]. In the first step, phthalimido-PEGs were synthesized by reaction of 4armPEG10k-OH, phthalimide, triphenylphosphine, and diisopropyl azodicarboxylate. The phthalimido groups were then converted into primary amines by hydrazinolysis. In the next step, the collagenase-sensitive tetrapeptide Ala–Pro–Gly↓Leu was synthesized using 4armPEG10k-NH₂ as polymeric support [184]. For the coupling reaction, 5.55 g of Boc-Leu-OH (24.0 mmol) and 2.48 g of DCC (12.0 mmol) were dissolved in 50 mL of dried DCM. After stirring for 30 min at room temperature, the solution was passed through a glass filter funnel to remove precipitated *N,N'*-dicyclohexylurea (DCU), and

combined with a solution of 4armPEG10k-NH₂ (15.0 g, 1.5 mmol) in DCM (150 mL). Then, 2000 μ L of DIPEA (12.0 mmol) were added, and the mixture was stirred for 1.5 h at room temperature. The solution was concentrated under reduced pressure and placed into an ice bath. The intermediate (4armPEG10k-Leu-Boc) was crystallized at 0 °C under vigorous stirring by drop-wise addition of cold diethyl ether. The precipitate was collected by filtration, washed with cold diethyl ether, and dried under vacuum to yield 16.0 g (98 %). Thin layer chromatography (3 : 1 : 1 glacial acetic acid/1-butanol/water) indicated the absence of free Boc-Leu-OH.

¹H-NMR (4armPEG10k-Leu-Boc, CDCl₃, 300 MHz): δ 0.94 ppm (d, 24H, -CH₂CH-(CH₃)₂), 1.40 – 1.50 ppm (m, 4H, -CH₂CH(CH₃)₂), 1.44 ppm (s, 36H, -OtBu), 1.60 – 1.70 ppm (m, 8H, -CH₂CH(CH₃)₂), 3.41 ppm (s, 8H, R₃CCH₂O-), 3.65 ppm (s, -OCH₂CH₂O-), 4.11 ppm (4H, -CH(NHBoc)R'), 5.02 ppm (4H, -CH(NHBoc)R'), 6.63 ppm (4H, -NHC(O)-)

The successful coupling of the amino acid was confirmed using a modified fluorescamine assay [185]. In brief, 5.0 μ mol of 4armPEG10k-Leu-Boc were dissolved in 500 μ L of 50 mM borate buffer, pH 8.5 ($c = 10 \mu\text{mol/mL}$). As reference, 5.0 μ mol of 4armPEG10k-NH₂ were dissolved in 500 μ L of the same buffer and diluted to a final concentration of 0.1 $\mu\text{mol/mL}$. Then, 50 μ L of each sample were diluted with 1350 μ L of 50 mM borate buffer, pH 8.5, and mixed with 600 μ L of a fluorescamine solution (15 mg in 50 mL of acetone). After vigorous stirring, the fluorescence intensities ($\lambda_{ex} = 390 \text{ nm}$, $\lambda_{em} = 480 \text{ nm}$) were measured on a PerkinElmer LS 55 Fluorescence spectrometer (Perkin-Elmer, Wiesbaden, Germany). The degree of end-group conversion was determined to be 99.7 %.

To deprotect the amino acid moiety, 16.0 g of 4armPEG10k-Leu-Boc (1.5 mmol) were dissolved in 176 mL of methanolic HCl (prepared by dropping 16 mL of acetyl chloride into 160 mL of ice-cooled methanol). After stirring for 30 min at room temperature, the solvent was evaporated, and the residue was dissolved in 80 mL of water. The pH of the aqueous solution was adjusted with sodium hydroxide (3 M) to 9 – 10. The raw product was subsequently extracted with DCM. The combined organic phases were dried over anhydrous Na₂SO₄, and the solution was concentrated under reduced pressure. The product was crystallized at 0 °C under vigorous stirring by drop-wise addition of diethyl ether. The precipitate was collected, washed with cold diethyl ether, and dried under vacuum to yield 14.9 g (97 %) of 4armPEG10k-Leu.

$^1\text{H-NMR}$ (4armPEG10k-Leu, CDCl_3 , 300 MHz): δ 0.85 – 1.10 ppm (m, 24H, $-\text{CH}_2\text{CH}(\text{CH}_3)_2$), 1.55 – 1.75 ppm (m, 8H, $-\text{CH}_2\text{CH}(\text{CH}_3)_2$), 1.75 – 1.95 ppm (m, 4H, $-\text{CH}_2\text{CH}(\text{CH}_3)_2$), 3.41 ppm (s, 8H, $\text{R}_3\text{CCH}_2\text{O}-$), 3.65 ppm (s, $-\text{OCH}_2\text{CH}_2\text{O}-$), 8.45 ppm (t, 4H, $-\text{NHC}(\text{O})-$)

The described steps were repeated for the subsequent addition of Boc-Gly-OH, Boc-Pro-OH, and Boc-Ala-OH. At each step, $^1\text{H-NMR}$ spectra were recorded, and the successful coupling of the amino acids was confirmed as described above. The degree of end-group conversion was almost quantitative. The resulting material is denoted 4armPEG10k-LGPA. The C-termini of the peptide (leucine residues) are conjugated to the PEG chain, and the N-termini (alanine residues) are free.

$^1\text{H-NMR}$ (4armPEG10k-LGPA, CDCl_3 , 600 MHz): δ 0.85 – 1.00 ppm (m, 24H, $-\text{CH}_2\text{CH}(\text{CH}_3)_2$), 1.34 ppm (d, 12H, $-\text{CH}_3$), 1.50 – 1.74 ppm (m, 12H, $-\text{CH}_2\text{CH}(\text{CH}_3)_2$), 1.90 – 2.25 ppm (m, 16H, $-\text{C}(\text{O})\text{CH}(\text{R}')\text{CH}_2\text{CH}_2-$), 3.41 ppm (s, 8H, $\text{R}_3\text{CCH}_2\text{O}-$), 3.65 ppm (s, $-\text{OCH}_2\text{CH}_2\text{O}-$), 3.83 ppm (4H, $-\text{C}(\text{O})\text{CH}(\text{R}')-$), 4.28 ppm (4H, $-\text{C}(\text{O})\text{CH}(\text{R}')-$), 4.42 ppm (4H, $-\text{C}(\text{O})\text{CH}(\text{R}')-$), 4.48 ppm (4H, $-\text{C}(\text{O})\text{CH}(\text{R}')-$)

6.2.4 Synthesis of non-degradable polymers (4armPEG10k-Ala)

4armPEG10k-Ala was synthesized from 4armPEG10k- NH_2 and Boc-Ala-OH in 91 % yield as described for 4armPEG10k-LGPA. Non-degradable and degradable polymers are both terminated by alanine residues; consequently, their reactivity towards PEG-succinimidyl propionates will be comparable.

$^1\text{H-NMR}$ (4armPEG10k-Ala, CDCl_3 , 600 MHz): δ 1.34 ppm (d, 12H, $-\text{CH}(\text{NH}_2)-\text{CH}_3$), 3.41 ppm (s, 8H, $\text{R}_3\text{CCH}_2\text{O}-$), 3.64 ppm (s, $-\text{OCH}_2\text{CH}_2\text{O}-$), 7.55 ppm (t, 4H, $-\text{NHC}(\text{O})-$)

6.2.5 Rheological characterization of hydrogels

Gelation kinetics and gel strength were studied by performing oscillatory shear experiments on a TA Instruments AR 2000 rheometer (TA Instruments, Eschborn, Germany) with parallel plate geometry at 37 °C. For the preparation of hydrogels, accurately weighed amounts of 4armPEG10k-LGPA (degradable gels) or 4armPEG10k-

Ala (non-degradable gels) were dissolved in 1000 μL of 25 mM phosphate buffer, pH 7.4, and cooled to 5 $^{\circ}\text{C}$. Immediately before starting the experiment, the polymer solutions were added to accurately weighed amounts of 4armPEG10k-SPA. The stoichiometric ratio between succinimidyl propionate and amino groups was balanced, and the overall polymer concentrations were 5 %, 10 %, and 15 % (w/v). After vortexing, the precursor solutions were poured onto the bottom plate of the rheometer. The upper plate (20 mm in diameter) was lowered to a gap size of 1000 μm , and the measurement was started. The evolution of storage (G') and loss moduli (G'') was recorded as a function of time at 1 Hz oscillatory frequency and a constant strain of 0.05. A solvent trap was used to prevent the evaporation of water. The cross-over of G' and G'' was regarded as the gel point. After 60 min, the absolute value of the complex shear modulus (G^*) was determined as a measure for the obtained gel strength. The gel disks were then removed from the rheometer, immersed in 10 mL of PBS, and incubated at 37 $^{\circ}\text{C}$ for 24 h. After swelling, the samples were again placed on the lower plate, and the measuring gap was slowly closed until a normal force of approx. 750 mN was reached. The resulting compression of the gels was sufficient to prevent slippage. The following frequency sweep was conducted at constant strain (0.01) as a function of frequency (from 0.1 to 10 Hz). Finally, an amplitude sweep (from 0.1 to 10,000 Pa oscillatory stress) was performed in order to confirm that all previous measurements were conducted within the linear viscoelastic region of the sample. All experiments were carried out in triplicate and the presented results are expressed as means \pm standard deviation.

6.2.6 Equilibrium swelling of hydrogels

For the swelling studies, accurately weighed amounts of 4armPEG10k-LGPA (degradable gels) or 4armPEG10k-Ala (non-degradable gels) were dissolved in 1000 μL of 25 mM phosphate buffer, pH 7.4, cooled to 5 $^{\circ}\text{C}$, and added to accurately weighed amounts of 4armPEG10k-SPA. The stoichiometric ratio between succinimidyl propionate and amino groups was balanced, and the overall polymer concentrations were 5 %, 10 %, and 15 % (w/v). After vortexing, 250 μL of the precursor solutions were cast into cylindrical glass molds (7 mm inner diameter) and allowed to gel for 2 h

at room temperature. The gel samples were then weighed in air and hexane after swelling for 24 h in 10 mL of PBS using a density determination kit (Mettler-Toledo, Gießen, Germany). Based on Archimedes' principle, the gel volume after swelling (V_{gs}) was determined. The volume of the dry polymer (V_p) was calculated from the mass of the freeze-dried hydrogel and the density of the polymer in the dry state (taken as the density of PEG, $1.12 \text{ g} \cdot \text{cm}^{-3}$). With these parameters, the volumetric swelling ratio, $Q = V_{gs}/V_p$, was calculated.

6.2.7 Degradation of hydrogels

The gel samples were prepared as described in section 6.2.6. Directly after gelation, the initial weight of the hydrogels was determined. The gel cylinders were then placed into 5 mL of 10 mM HEPES buffer, pH 7.4, which also contained 1 mM CaCl_2 and 0.025 % sodium azide. The samples were incubated for 24 h at 37 °C to allow them to reach their equilibrium swelling levels. Afterwards, their wet weight was determined (day 0). To study gel degradation, the samples were immersed in 5 mL of HEPES buffer and incubated at 37 °C in a shaking water bath (approx. 50 rpm), either without enzyme, or with 0.01 mg/mL collagenase (collagen digestion activity: 196 U/mg solid). At predetermined time points, the samples were poured out over 24 mm NetwellTM Inserts (Corning GmbH, Kaiserslautern, Germany) with a 500 μm mesh size polyester membrane. The wet weight of the gel cylinders was determined, and the buffer or enzyme solution was replaced. Degradation was assumed to be complete when the sample passed through the NetwellTM Insert and no remaining material could be detected.

6.2.8 Cell seeding and cell culture

3T3-L1 preadipocytes were plated in T150 culture flasks (Corning, Bodenheim, Germany) and expanded in DMEM supplemented with 10 % fetal bovine serum (FBS), penicillin (100 U/mL), and streptomycin (100 $\mu\text{g}/\text{mL}$). Cell cultures were incubated in a humidified atmosphere at 37 °C and 5 % CO_2 . The culture medium

was exchanged every two days. At confluency, the 3T3-L1 cells were harvested using trypsin-EDTA, centrifuged to a pellet (1200 rpm, 5 min) and washed with PBS.

For the preparation of hydrogels, accurately weight amounts of 4armPEG10k-LGPA (degradable gels) or 4armPEG10k-Ala (non-degradable gels) were dissolved in phosphate buffer (50 mM, pH 7.4) at 125 mg/mL. A solution of Cys-Asp-Pro-Gly-Tyr-Ile-Gly-Ser-Arg (YIGSR, $c = 10 \mu\text{mol/mL}$) or phosphate buffer was added, so that the final polymer concentrations were 100 mg/mL. In a similar manner, accurately weight amounts of 4armPEG10k-SPA were dissolved in water at 100 mg/mL. All polymer solutions were kept on ice until use. For cell seeding, the prepared 3T3-L1 preadipocytes were suspended in the amino component (4armPEG10k-LGPA or 4armPEG10k-Ala). Subsequently, an equal volume of 4armPEG10k-SPA was added. After vortexing, 50 μL of the polymer-cell solution were cast into cylindrical glass molds (5 mm inner diameter) that had been treated with Sigmacote[®]. The final polymer concentration was 10 % (w/v) and the cell number 100,000 cells per hydrogel construct. For long-term cell culture 5,000,000 cells were used. After 30 min of gelation at 37 °C, the glass rings were removed. Each gel sample was transferred into one well of 24-well plates and covered with 2 mL of basal medium (α -MEM supplemented with 10 % FBS, 100 U/mL penicillin, and 100 $\mu\text{g/mL}$ streptomycin). For standard 2-D cell culture, 100,000 3T3-L1 cells were seeded in 24-well plates and covered with 2 mL of basal medium.

Two days after cell seeding, adipogenesis was induced by applying induction medium (basal medium supplemented with 1 μM insulin, 0.1 μM corticosterone, 0.5 mM IBMX, and 60 μM indomethacin). The time point of induction was referred to as day 0. At day 2, the induction medium was replaced by differentiation medium (basal medium supplemented with 1 μM insulin). The hydrogel constructs were dynamically cultured (approx. 60 rpm) on an orbital shaker (Heidolph Instruments, Schwabach, Germany) in a humidified atmosphere at 37 °C and 5 % CO_2 . The culture medium was exchanged every two days.

6.2.9 Quantitative analysis of intracellular triglyceride accumulation

Nine days after induction, the intracellular triglyceride content was quantified using a serum triglyceride determination kit (Sigma-Aldrich, Taufkirchen, Germany). After washing with PBS, the hydrogel constructs were harvested in 0.5 % thesitol solution, disintegrated using a micropistill (Hartenstein Laborbedarf, Würzburg, Germany), and sonicated (Branson Ultrasonic Corporation, Danbury, CT). The spectroscopic quantification of triglycerides was performed according to the manufacturer's instructions. All measurements were done in three biological replicates. The amount of triglycerides per hydrogel construct was calculated and normalized to the cell number of the respective sample as determined by the DNA assay.

6.2.10 DNA assay

Aliquots of disintegrated and sonicated hydrogel constructs were completely digested with papainase (3.2 U/mL in 0.1 M Na_2HPO_4 buffer, pH 6.5 containing 10 mM Na_2EDTA and 2.5 mM cysteine) for 16 h at 60 °C, and the DNA content was determined using the intercalating Hoechst 33258 dye (0.1 $\mu\text{g}/\text{mL}$ in 0.1 M NaCl containing 1 mM Na_2EDTA and 10 mM Tris, pH 7.4) [186]. Fluorescence intensities were determined at 365 nm excitation wavelength and 458 nm emission wavelength on a LS 55 Fluorescence spectrometer (PerkinElmer, Wiesbaden, Germany) and correlated to DNA contents using standard dilutions of double-stranded DNA (from calf thymus). Cell numbers were calculated with a conversion factor of 26.1 pg of DNA per cell, which was determined previously.

6.2.11 Oil red O staining

In order to visualize cytoplasmic lipid droplets, the hydrogel constructs were washed with PBS, fixed in formalin (10 % in PBS) overnight, and stained with oil red O (3 mg/mL in 60 % isopropanol) for 12 h [187]. Excessive dye was removed by washing three times with PBS. Microscopical brightfield pictures were acquired at 20 \times magni-

fication using a Zeiss Axiovert 200 M microscope equipped with a Zeiss AxioCam HRc camera and the software ZEN 2008 (Carl Zeiss MicroImaging GmbH, Jena, Germany).

6.2.12 Statistics

All quantitative results are presented as mean values \pm standard deviation. The results of the triglyceride and DNA assay were compared using the unpaired Student's t-test. $p < 0.05$ was regarded as statistically significant. Statistical analysis was performed using PASW Statistics 17.0 software (SPSS Inc., Chicago, IL).

6.3 Results and discussion

6.3.1 Physicochemical characterization of hydrogels

For the preparation of biodegradable hydrogels, branched PEG-amines were functionalized with the synthetic tetrapeptide Ala-Pro-Gly↓Leu (4armPEG10k-LGPA). For non-degradable hydrogels, alanine-modified PEG-amines (4armPEG10k-Ala) were used instead of 4armPEG10k-LGPA. Gels were formed by step-growth polymerization of these macromers with branched PEG-succinimidyl propionates (4armPEG10k-SPA). At the beginning of the experiments, all samples behaved like free-flowing liquids ($G'' > G'$). In this state, the gels could be cast into molds and would easily pass through small-gauge needles in order to be injected into soft tissue defects. Furthermore, cells could be suspended in the liquid precursor solutions, which ensured their homogeneous distribution throughout the gel network. Although PEG-succinimidyl esters may also react with amino groups of cell surface proteins, these polymers were shown to be non-toxic and rapidly excluded from the cell surface without being taken up [188]. Gelation generally occurred within minutes with only minor differences between the tested experimental groups (Table 6.1). During the course of the experiment, cross-linking further proceeded as indicated by the steadily increasing value of G' . After approx. 60 min, the value of G' reached a plateau and exceeded that of G'' by several orders of magnitude ($G' \gg G''$). The gel strength ($|G^*|$) of the biodegrad-

able hydrogels ranged between 2230 ± 108 Pa (5 % polymer) and 9625 ± 407 Pa (15 % polymer, Table 6.1). Comparable values were obtained for the non-degradable hydrogels. In this group, the absolute value of G^* ranged between 1849 ± 26 Pa (5 % polymer) and 10150 ± 87 Pa (15 % polymer, Table 6.1). These data agreed well with those reported previously for gels prepared from 4armPEG10k-SPA and 4armPEG10k-NH₂ [139].

After swelling in PBS, G' and G'' were measured at constant strain as a function of frequency. The prepared hydrogels showed an elastic response ($G' > G''$) within the studied frequency range. Furthermore, both moduli were almost insensitive to the oscillatory frequency, which is typical for covalently cross-linked networks [149]. In the swollen state, the gel strength (determined at a frequency of 1 Hz) was generally lower than in the non-swollen state, which can be attributed to the uptake of a large amount of water (Table 6.1). Again, comparable values were obtained for degradable and non-degradable hydrogels. Amplitude sweep experiments indicated that all previous measurements were run well within the linear viscoelastic region of the samples.

When compared to each other, the gels prepared from 5 % polymer had the lowest cross-linking density (estimated by G^*), whereas those made from 15 % polymer showed the highest value. This corresponded well with the results of equilibrium swelling studies. The volumetric swelling ratio (Q) showed the opposite trend than G^* and was highest for hydrogels prepared from 5 % polymer and lowest for those prepared from 15 % polymer (Table 6.1). For that reasons, network defects seem to play a significant role in the structure of the prepared hydrogels [74]. At low precursor concentrations (5 % polymer), the concentration of elastically active chains is probably decreased by non-reacted groups and loops. At high precursor concentrations (above 10 % polymer), these effects are less pronounced and Q decreased only slightly when increasing the initial polymer concentration from 10 % to 15 % (Table 6.1).

With regard to their physicochemical characteristics, the prepared hydrogels meet the basic requirements for a successful application in adipose tissue engineering. They will be capable of being gelled in the presence of cells, allow for the unrestricted diffusion of nutrients and metabolites, and provide sufficient mechanical stability to withstand the occurring mechanical loads. The obtained gel strength, thereby, mainly depends on the initial polymer concentration; the different polymers (4armPEG10k-LGPA or 4armPEG10k-Ala) only have a minor influence on the result-

Table 6.1: Mechanical properties and swelling behavior of the prepared hydrogels. Data are presented as means \pm standard deviation ($n = 3$).

	Degradable (4armPEG10k-LGPA)			Non-degradable (4armPEG10k-Ala)		
	5 %	10 %	15 %	5 %	10 %	15 %
Polymer concentration						
Gelation time (min)	1.8 \pm 0.2	1.6 \pm 0.1	1.4 \pm 0.1	2.9 \pm 0.0	1.5 \pm 0.2	1.2 \pm 0.1
Gel strength $ G^* $ after cross-linking (Pa)	2230 \pm 108	6805 \pm 123	9625 \pm 407	1849 \pm 26	6375 \pm 487	10150 \pm 87
Gel strength $ G^* $ after swelling (Pa)	1708 \pm 307	5567 \pm 461	7412 \pm 263	1496 \pm 110	5097 \pm 137	7686 \pm 216
Volume increase (%)	73 \pm 1	141 \pm 1	194 \pm 1	71 \pm 0	132 \pm 1	176 \pm 2
Volumetric swelling ratio Q	29.7 \pm 0.2	20.9 \pm 0.3	18.2 \pm 0.2	31.1 \pm 0.1	22.0 \pm 0.2	18.5 \pm 0.2

ing gel. Therefore, biodegradable and non-degradable gels will have almost the same initial mechanical properties, which is relevant for the subsequent cell culture studies. On the other hand, the specific characteristics of adipocytes must be considered as well. These cells enlarge to over 100 μm in diameter during maturation and constantly change their size because of their lipid storage function [172]. For these reasons, hydrogels of intermediate stiffness (above 10 % polymer content) may be especially promising. These gels are mechanically stable to withstand the manipulations during cell culture and expected to enable the full differentiation of preadipocytes. In addition, their mechanical properties resemble those of human adipose tissue [176].

6.3.2 Degradation of hydrogels

Mechanical strength and degradability of the supportive matrix have been recognized to have a strong influence on cell migration, proliferation, and differentiation [102]. In most tissue engineering strategies, the scaffold materials are designed to provide only transient stability; the developing tissue will be responsible for the long-term maintenance of the construct. Therefore, it is necessary to adjust the degradation kinetics to the rate of tissue formation [172]. For this purpose, the gel-forming polymers were functionalized with the synthetic tetrapeptide Ala-Pro-Gly↓Leu to make them susceptible to proteolytic breakdown. To study gel degradation *in vitro*, the hydrogel samples were swollen to equilibrium and incubated in PBS containing 0.01 mg/mL collagenase. Although the enzymatic activity should be preserved in the presence of Ca^{2+} -ions [189], the collagenase solution was replaced every day.

After the non-degradable hydrogels had reached their equilibrium swelling levels (day 0), their wet weight remained almost constant (Figure 6.2A). This effect was independent of the absence or presence of collagenase, which illustrates the requirement of the Ala-Pro-Gly↓Leu sequence for gel degradation. Conversely, these experiments also showed the necessity of collagenase for the degradation of hydrogels. Without enzyme, the wet weight of enzymatically degradable gel samples did not change significantly during the course of the experiment. However, in the presence of 0.01 mg/mL collagenase, their wet weight considerably increased during the first 4 to 5 days. In the following days, gel decomposition further proceeded; after approx.

10 days, the degradation process was completed (Figure 6.2A). It can be concluded from these experiments that hydrogel degradation was due to the proteolytic activity of collagenase; non-enzymatic hydrolysis of amide bonds did not significantly contribute to gel degradation.

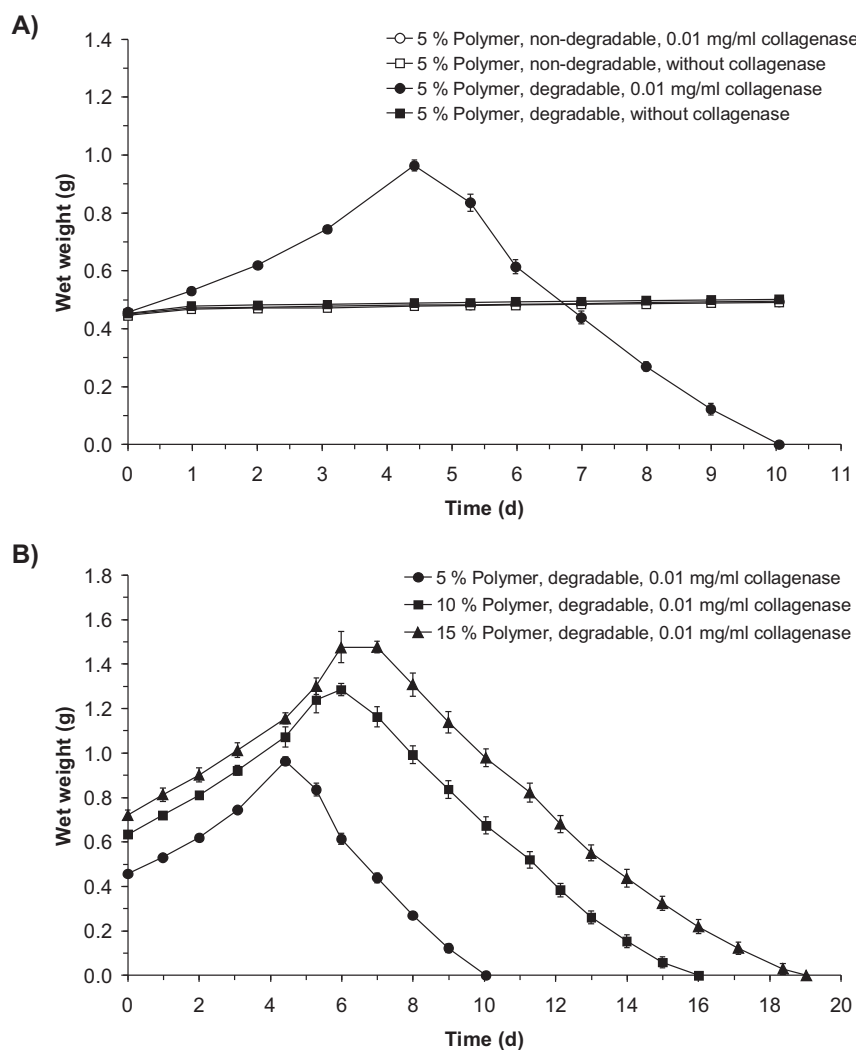


Figure 6.2: Wet weight of non-degradable (○/□) and degradable (●/■) hydrogels in the presence (○/●) and absence (□/■) of collagenase (A). Degradation of hydrogels containing 5% (●), 10% (■), and 15% (▲) polymer in the presence of 0.01 mg/mL collagenase (B).

Comparable results were obtained for all tested polymer concentrations (5 %, 10 %, and 15 % initial polymer content). During the initial phase of degradation, the gel samples considerably swelled as some of the Ala-Pro-Gly↓Leu sequences were cleaved by the action of collagenase (Figure 6.2B). This, in turn, enlarged the average network mesh size of hydrogels and increased their water absorption capacity. After a critical amount of peptide sequences had been degraded, the ongoing polymer loss was no longer overcompensated by swelling, and the wet weight reached a plateau. This effect was particularly pronounced in gels prepared from 10 % and 15 % polymer. After the maximum weight had been exceeded, the mass of the samples linearly decreased by ongoing release of polymer chains or gel fragments (Figure 6.2B). This indicates that both, surface and bulk erosion contribute to gel degradation. Gel degradation was completed after 10, 16, and 19 days (5 %, 10 %, and 15 % initial solid content). These findings correlated well with the results of equilibrium swelling studies. As expected, the gels with the lowest cross-linking density (5 % initial polymer content, $Q = 29.7$) showed the lowest resistance in the presence of collagenase (10 days degradation time). In contrast to that, the gels prepared from 10 % and 15 % polymer had comparatively high cross-linking densities ($Q = 20.9$ and 18.2 , respectively). Consequently, these hydrogels showed an increased stability towards proteolytic degradation with only moderate differences between the two polymer concentrations (16 and 19 days degradation time).

These results clearly demonstrate the enzyme dependent degradability of the synthesized polymers. Transferring these data to the situation in cell culture will be difficult, however. Here, the observed degradation rate will strongly depend on the local concentration of proteolytic enzymes, which may vary over time [180, 190, 191]. The expression pattern of cellular proteases will also depend on whether the cells are proliferating or differentiating, and their ability to migrate within the hydrogel network [192]. Although the exact degradation rate can hardly be predicted, this degradation mechanism is still favored over spontaneous hydrolytic degradation since material resorption is caused and affected by cellular activity. As a result, the degradation rate of the scaffold will be more closely related to the rate of tissue formation.

6.3.3 Adipogenic differentiation of 3T3-L1 preadipocytes

To evaluate their potential for soft tissue engineering, biodegradable hydrogels (10 % initial polymer content) were seeded with 3T3-L1 preadipocytes (3-D culture, 100,000 cells per hydrogel). Two days after cell seeding, adipogenic differentiation was induced by applying a hormonal cocktail containing insulin, corticosterone, IBMX, and indomethacin. At day 9 after induction, the hydrogel constructs were analyzed for their DNA content and intracellular triglyceride accumulation. For comparison, 100,000 3T3-L1 cells were seeded in 24-well plates and induced to undergo adipogenic differentiation (conventional 2-D culture).

In 2-D culture, the seeded 3T3-L1 cells proliferated during the initial culture period. At day 9 after induction, approx. 260,000 cells per well were found as determined by the DNA assay (Figure 6.3C). In contrast to that, cell proliferation seemed to be suppressed when 3T3-L1 cells were cultured within hydrogels. After the same time period, only 82,000 cells per hydrogel were detected (Figure 6.3C). This was consistent with the initial cell number, as determined in separate experiments in which gel samples were seeded with 3T3-L1 cells and immediately analyzed for their DNA content (data not shown). When regarding the intracellular triglyceride accumulation, the opposite trend was observed (Figure 6.3D). Compared to conventional 2-D culture, the amount of triglycerides accumulated per 100,000 cells increased approx. threefold when 3T3-L1 adipocytes were cultured in hydrogels. These findings were also illustrated by phase contrast images. Under 2-D culture conditions, the cells were well spread and showed a large number of small lipid droplets (Figure 6.3A). Within hydrogels, in contrast, 3T3-L1 adipocytes had a rounded morphology and contained comparatively large vacuoles that occupied most of the cytoplasm (Figure 6.3B).

Altogether, the developed hydrogels seemed to provide a suitable environment for 3T3-L1 preadipocytes to differentiate into mature adipocytes. Compared to standard 2-D cell culture, the adipogenic differentiation of 3T3-L1 cells was obviously enhanced under 3-D culture conditions. Adipogenesis has been reported to be inhibited when preadipocytes were cultured on strongly adhesive, fibronectin coated substrates [193, 194]. Under these culture conditions, morphological changes were prevented and the induction of lipogenic enzymes (such as fatty acid synthetase) was sharply reduced. However, the inhibitory effects of fibronectin on preadipocyte

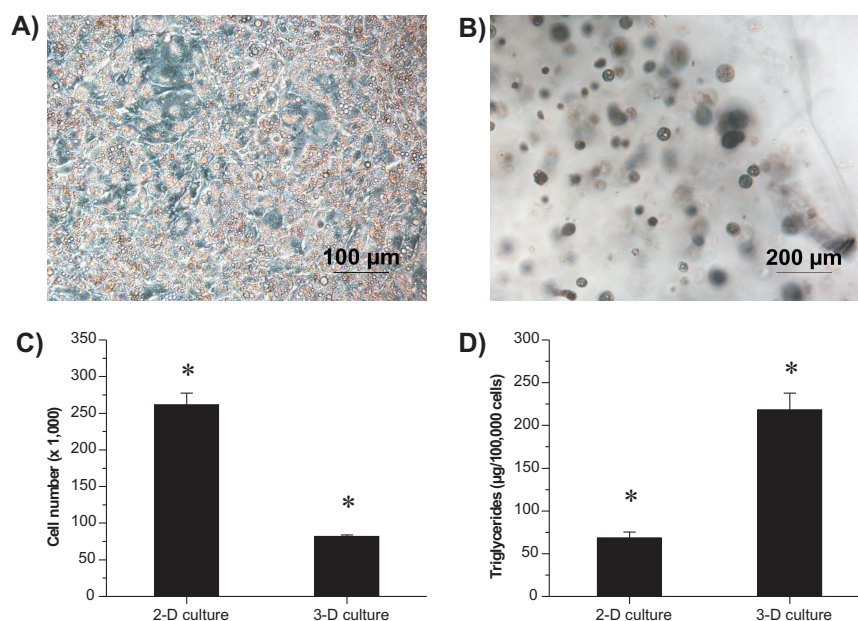


Figure 6.3: Microscopical images of 3T3-L1 cells at day 9 after induction. Adipocytes were cultured in 2-D cell culture (A) and within biodegradable hydrogels (B). Cell number determined at day 9 after induction (C). Triglyceride accumulation of 3T3-L1 adipocytes cultivated under 2-D and 3-D conditions (D). Data represent means \pm standard deviation of three biological replicates; * indicates statistically significant differences between the tested groups ($p < 0.05$).

differentiation could be reversed by keeping the cells in a rounded configuration e.g. by disrupting the cytoskeleton [193, 194]. A similar effect may explain the differences between the tested culture conditions. In 2-D cell culture, the 3T3-L1 adipocytes strongly adhered to the polystyrene substrate and spread over a large surface area. In contrast to the very adhesive polystyrene, PEG-based hydrogels effectively prevent the adsorption of ECM proteins such as fibronectin, laminin, and vitronectin [10]. Consequently, attached or embedded cells will exhibit only loose interactions with the gel network and assume a more rounded morphology. These loose interactions are thought to be necessary to allow the morphological changes that accompany adipogenic differentiation [195].

On the other hand, ECM components and in particular laminin have been shown to play a pivotal role in preadipocyte differentiation [196]. Furthermore, cell adhesion is known to be critical for the viability of anchorage-dependent cells [177]. Designing

suitable scaffolds for adipose tissue engineering will, therefore, require a balance between cell attachment, spreading, and differentiation [194]. Entrapping preadipocytes into weakly adhesive hydrogel matrices may satisfy these criteria. For this purpose, non-adhesive PEG hydrogels (degradable and non-degradable) were functionalized with the synthetic nonapeptide Cys–Asp–Pro–Gly–Tyr–Ile–Gly–Ser–Arg (YIGSR), which has been identified as the major cell-binding site in the B1 chain of laminin [197].

With regard to the detected cell numbers (determined at day 9 after induction), no significant differences were detected between hydrogels containing no YIGSR and those containing 1 $\mu\text{mol/mL}$ YIGSR (Figure 6.4E). The DNA content of degradable and non-degradable hydrogels was also comparable. Similar results have been reported by Patel et al. for preadipocytes cultivated in photopolymerizable PEG hydrogels. Cell proliferation was observed in biodegradable gels only after four days of cultivation [177]. In the present study, however, 3T3-L1 preadipocytes were induced to undergo adipogenic differentiation before significant cell proliferation had occurred (induction two days after cell seeding). When comparing the intracellular triglyceride accumulation, significant differences were observed depending on the addition of YIGSR (Figure 6.4F). In degradable hydrogels, the modification with YIGSR increased the intracellular triglyceride accumulation from approx. 260 μg per 100,000 cells to approx. 400 μg per 100,000 cells. A similar trend was observed in non-degradable hydrogels. These findings were also reflected in microscopical bright field images. Compared to hydrogels without YIGSR (Figure 6.4A and C), 3T3-L1 preadipocytes cultured in gels containing 1 $\mu\text{mol/mL}$ YIGSR seemed to be considerably enlarged with vacuoles that occupied most of the cytoplasm (Figure 6.4B and D). Together with the outcome of 2-D cell culture experiments, these results clearly demonstrate the effects of substrate stiffness and adhesiveness on adipocyte differentiation. Hydrogels functionalized with integrin-binding motifs obviously provide the right balance between cell attachment and differentiation, and promote the intracellular lipid accumulation of differentiated adipocytes.

To study the effects of substrate degradability on tissue development, non-degradable and degradable hydrogels were seeded with 3T3-L1 preadipocytes (5,000,000 cells per hydrogel construct) and cultured over 6 weeks. At day 42 after induction, microscopical bright field images revealed clear differences between the tested hydrogels. Within non-degradable gels, cells were not able to form coherent tissue structures and only

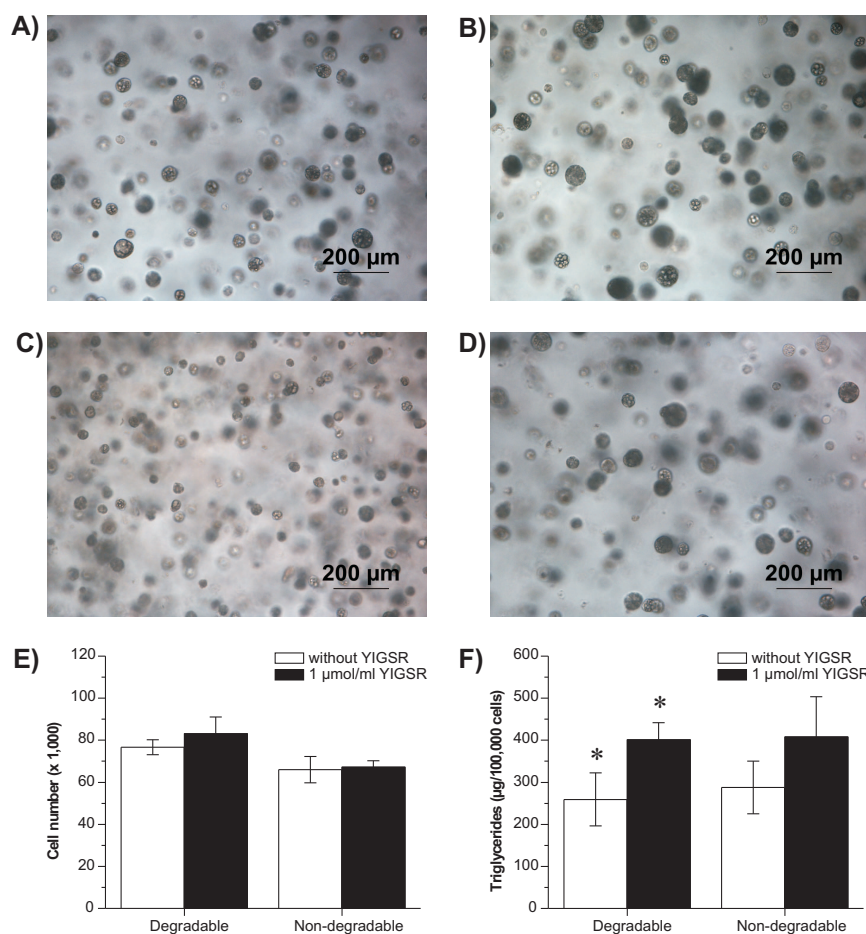


Figure 6.4: 3T3-L1 adipocytes cultured in degradable gels without YIGSR (A), degradable gels with 1 $\mu\text{mol/mL}$ YIGSR (B), non-degradable gels without YIGSR (C), and non-degradable gels with 1 $\mu\text{mol/mL}$ YIGSR (D). Cell number (E) and triglyceride accumulation (F) of 3T3-L1 cells determined at day 9 after induction. Data represent means \pm standard deviation of three biological replicates; * indicates statistically significant differences between the tested groups ($p < 0.05$).

isolated adipocytes were found. The individual cells contained multiple lipid droplets, however no unilocular fat cells were detected (Figure 6.5A and C). In contrast to that, adipose tissue-like structures were formed when 3T3-L1 adipocytes were cultured in enzymatically degradable gels; single cells were not detectable (Figure 6.5B and D). Compared to non-degradable hydrogels, the intracellular lipid droplets were considerably enlarged, resulting in many unilocular cells, a typical feature of mature adipocytes. Altogether, these first experiments clearly indicate the advantage of

enzymatically degradable hydrogels for adipose tissue engineering. The developed gels were sufficiently stable to withstand the manipulations associated with cell culture and provided a suitable microenvironment for the differentiation of adipocytes. In case of degradable hydrogels, the polymer network can be disintegrated by cell-secreted and cell-activated proteases (such as MMPs), which obviously promotes the development of coherent adipose tissue-like structures.

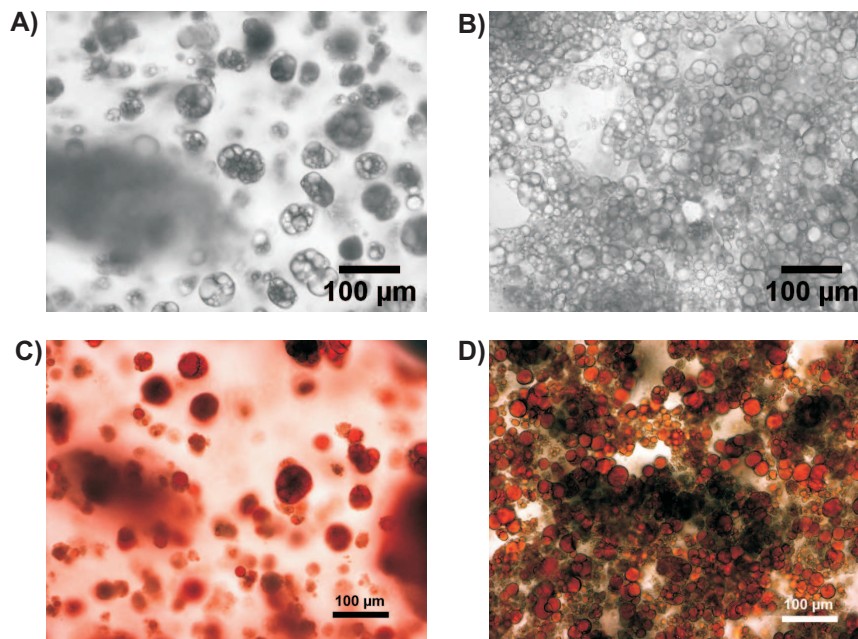


Figure 6.5: Phase contrast images of 3T3-L1 cells at day 42 after induction (A and B). The hydrogel constructs were stained with oil red O to visualize the size and amount of cytoplasmic lipid vesicles (C and D). 3T3-L1 adipocytes were cultured within non-degradable (A and C) and degradable hydrogels (B and D).

6.4 Conclusion

In summary, we successfully prepared PEG-based hydrogels that proved to be suitable as 3-D scaffolds for soft tissue engineering applications. The gels were cross-linked in the presence of cells without the use of free-radical initiators, showed mechanical properties close to those of adipose tissue, and were susceptible to proteolytic break-

down. In contrast to previously described approaches, the developed hydrogels could be easily functionalized with adhesion peptides without requiring chemical modifications of these molecules. Cell culture experiments indicated that these biointeractive hydrogels provide a suitable 3-D environment for 3T3-L1 cells to differentiate into adipocytes. Long-term studies suggested that enzymatically degradable hydrogels promote the formation of coherent tissue-like structures. In future experiments, cell seeding and culture conditions have to be further optimized in order to generate mature fat pads. Similar to the introduction of adhesion peptides, the hydrogels could also be functionalized with hormones or growth factors (such as insulin, basic fibroblast growth factor, or vascular endothelial growth factor). Since these molecules will be covalently attached to the gel network, hormones or growth factors are expected to interact only with encapsulated or invading cells and not with the surrounding tissue. In future applications, the polymer-cell mixture could be supplemented with biologically active molecules, directly injected into soft tissue defects, and cross-linked *in vivo* to generate functional tissue substitutes.

Chapter 7

Summary and conclusions

Summary

This thesis was focused on the development and characterization of PEG-based hydrogels for controlling drug delivery and promoting tissue regeneration. While various gelation methods (i.e. ionic, hydrophobic, or covalent interactions) can be used for the formation of injectable hydrogels [73], chemical or covalent cross-linking is favored because it results in stable gel structures with tunable physicochemical properties. Furthermore, physically cross-linked hydrogels (e.g. gels prepared from PEG-*b*-PLGA-*b*-PEG triblock copolymers) often become turbid during gelation [73, 198], which excludes them from applications in ophthalmology. For these reasons, hydrogels were synthesized by step-growth polymerization of amino-functionalized PEG macromers with branched, amine-reactive derivatives of PEG (Figure 7.1). This reaction could be performed under ambient conditions (pH 7.4, 37 °C) without the use of free-radical initiators and allowed for the incorporation of fragile biomolecules (e.g. proteins or nucleic acids) or living cells. The developed hydrogels can serve as inert space-filling agents, as carrier systems for the controlled release of drug molecules, or as three-dimensional scaffolds in tissue engineering approaches.

In first experiments, non-degradable hydrogels were synthesized that may act as injectable, biologically inert substitutes for the vitreous body (**Chapter 3**). Transparent hydrogels were formed by reaction between branched PEG-succinimidyl propionates and two different types of PEG-amines (Figure 7.1 and 7.2). The gels were characterized by oscillatory rheometry and ¹H-NMR experiments. The liquid precursor solutions easily passed through small-gauge needles but solidified within 5 to 10 min, which would be appropriate for intraocular injections. By varying the concentration of macromers, the functionality of the PEG-amine, and the conditions during cross-linking, gels with mechanical properties similar to those of the natural vitreous body were obtained. The cross-linked hydrogels showed no cytotoxic effects and may be used as vitreous substitutes or as intraocular drug delivery systems.

As shown in **Chapter 3**, the developed hydrogels have great promise as matrices for the controlled release of macromolecules. To enable the efficient characterization of hydrogel-based drug delivery systems, mechanical testing, fluorescence recovery after photobleaching (FRAP), and pulsed field gradient NMR spectroscopy were investigated as alternatives to release experiments (**Chapter 4**). The developed hydrogels were

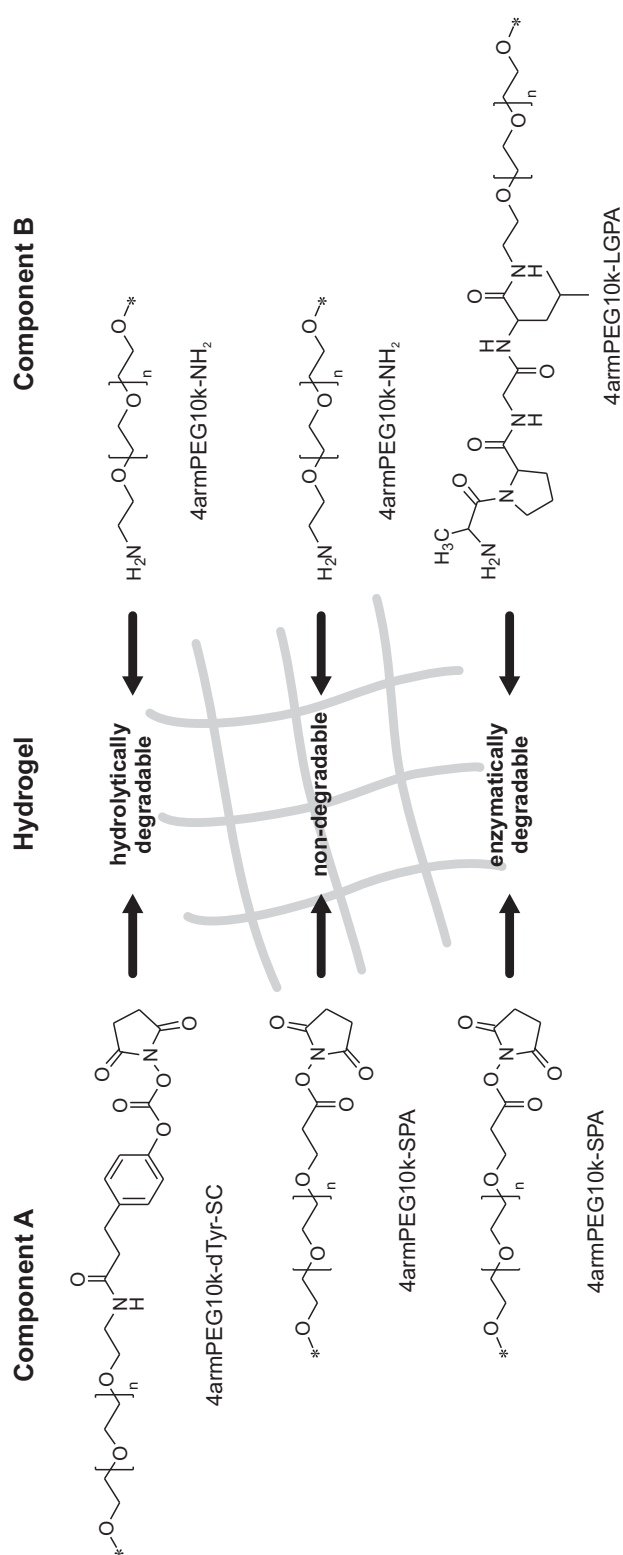


Figure 7.1: Polymers derived from four-armed poly(ethylene glycol) (molecular weight 10 kDa, 4armPEG10k-OH). Non-degradable hydrogels were prepared by step-growth polymerization of branched PEG-succinimidyl propionates (4armPEG10k-SPA) and branched PEG-amines (4armPEG10k-NH₂). Reaction of aromatic PEG-succinimidyl carbonates (4armPEG10k-dTyr-SC) with 4armPEG10k-NH₂ resulted in hydrolytically degradable gels. For the preparation of enzymatically degradable hydrogels, branched PEG-amines were functionalized with the collagenase-sensitive peptide Ala-Pro-Gly↓Leu (4armPEG10k-LGPA) and cross-linked with 4armPEG10k-SPA. Structural changes of the PEG macromers (e.g. variations in the molecular weight and/or number of branches) would additionally alter the gel properties.



Figure 7.2: PEG hydrogel formed by reaction between branched PEG-succinimidyl propionates and branched PEG-amines. The gels have a high water content (up to 97 % in the swollen state) and are optically transparent.

loaded with FITC-dextran and characterized for their mechanical properties and swelling characteristics. Subsequently, the translational diffusion coefficients (D) of the incorporated FITC-dextran were measured. Since the determined values of D agreed very well with those obtained from release studies, mechanical testing, FRAP, and pulsed field gradient NMR spectroscopy can be used to rapidly evaluate the potential of newly developed drug delivery systems.

One drawback of hydrogel-based drug delivery systems is their limited capacity to restrict the mobility of encapsulated molecules, which usually results in relatively rapid drug release (**Chapter 3 and 4**). To prolong the release rates of hydrogels, drug molecules were covalently tethered to the gel network via hydrolytically degradable anchor groups. For this purpose, branched PEG was functionalized with aromatic succinimidyl carbonate groups (Figure 7.1) that readily react with amino groups of other polymers, peptides, or proteins under formation of biodegradable carbamate bonds (**Chapter 5**). The strength of the prepared hydrogels ranged from 1075 to 2435 Pa; the degradation time varied between 24 and 120 h. FRAP experiments showed that FITC-BSA was successfully bound to the gel network. During polymer degradation, the mobility of the tethered molecules gradually increased. Using FITC-BSA and lysozyme as model proteins, the suitability of the developed hydrogels for the time-controlled release of proteins was shown. The obtained release profiles had a sigmoidal shape; protein release and gel degradation occurred simultaneously.

In the last study, the virtually inert PEG hydrogels were modified to become biointeractive and used as three-dimensional scaffolds for adipose tissue engineering. Since substrate mechanics and degradability were recognized to have a strong influence on cell differentiation and tissue morphogenesis (**Chapter 2**), branched PEG-amines were modified with the collagenase-sensitive peptide sequence Ala-Pro-Gly↓Leu. To

form hydrogels, these peptide-modified PEG-amines were cross-linked with branched PEG-succinimidyl propionates (Figure 7.1). The gel strength ranged from 1708 to 7412 Pa, depending on the initial polymer concentration. To mediate cell adhesion, the gels were functionalized with the integrin-binding motif Tyr-Ile-Gly-Ser-Arg (YIGSR). These hydrogels mimic the cellular recognition of the natural extracellular matrix (ECM) and were degraded by cell-secreted proteases. Cell culture experiments clearly demonstrated the suitability of these biointeractive hydrogels for soft tissue regeneration (**Chapter 6**). Compared to standard two-dimensional cell culture, the developed hydrogels significantly enhanced the intracellular triglyceride accumulation of encapsulated 3T3-L1 adipocytes. Functionalization with YIGSR further enhanced lipid synthesis of differentiating adipocytes. Long-term studies suggested that enzymatically degradable hydrogels furthermore promote the formation of coherent adipose tissue-like structures.

Conclusions and outlook

In conclusion, branched PEG proved to be the ideal starting material for the synthesis of hydrogels for regenerative medicine. Using a combinatorial approach, a variety of hydrogels could be prepared from comparatively few building blocks. The synthesized macromers allowed for the preparation of non-degradable, hydrolytically degradable, and enzymatically degradable hydrogels (Figure 7.1). Cross-linking could be performed in the presence of cells without the use of free-radical initiators. In a recent study beyond this thesis, non-degradable hydrogels were injected into enucleated porcine eyes [199]. These gels solidified approx. 5 min after injection and remained optically transparent. The tissue compatibility of the developed hydrogels was evaluated *in vitro* using a perfusion organ culture model of full-thickness porcine retina (Figure 7.3) [200, 201]. Altogether, these non-degradable hydrogels have great promise as long-term substitutes for the natural vitreous body [199, 200].

Because of their amine-reactive character, the gel-forming polymers can also be functionalized with biologically active peptides or proteins (e.g. adhesion peptides, growth factors, or antibodies) without requiring chemical modifications of these molecules. In future applications, therapeutic peptides or proteins could be dissolved



Figure 7.3: PEG hydrogels in perfusion organ culture of adult porcine retina (A) and after four days of perfusion (B). Light micrograph of porcine retina stained with haematoxylin and eosin (C). Histologically, the retinal structure remained well preserved [200]. Scale bar represents 100 μm .

together with the gel-forming polymers and injected into the patient in a minimally invasive manner (e.g. into the vitreous cavity). During gelation, these molecules are covalently tethered to the gel network, which effectively prevents their immediate release. If hydrolytically degradable polymers are used for gel preparation, this will allow for the time-controlled release of therapeutic peptide or proteins. Potential candidates for pharmacologically active proteins include antibodies against vascular endothelial growth factor (VEGF), a growth factor that is involved in the pathogenesis of proliferative diabetic retinopathy (PDR).

For applications in soft tissue engineering, enzymatically degradable hydrogels seem to be especially promising. These gels are sufficiently stable to withstand the manipulations associated with implantation and provide a suitable microenvironment that directs cell proliferation and differentiation. Once placed at the application site, the gels are degraded by cell-secreted proteases; matrix degradation is expected to occur in spatial and temporal synchrony with the deposition of ECM. As described above, the hydrogels can be easily functionalized with integrin-binding peptides or growth factors. This creates biointeractive hydrogels that mimic the complexity of the natural ECM. Structural changes of the PEG macromers (e.g. variations in the molecular weight and/or number of branches) would provide additional control over the mechanical properties, swelling behavior, and degradation rate of the formed hydrogels. Although further experiments will have to be carried out in the future, these first studies demonstrate that the developed hydrogels have great promise for a number of applications in regenerative medicine.

Bibliography

- [1] R. Langer and J. P. Vacanti. Tissue engineering. *Science*, 260(5110):920–926, 1993.
- [2] S. Petit-Zeman. Regenerative medicine. *Nat. Biotechnol.*, 19(3):201–206, 2001.
- [3] K. Ghosh and D. E. Ingber. Micromechanical control of cell and tissue development: Implications for tissue engineering. *Adv. Drug Deliv. Rev.*, 59(13):1306–1318, 2007.
- [4] A. Oosterlee and A. Rahmel, editors. *Annual Report 2008*. Eurotransplant International Foundation, Leiden, 2008.
- [5] R. R. Chen and D. J. Mooney. Polymeric growth factor delivery strategies for tissue engineering. *Pharm. Res.*, 20(8):1103–1112, 2003.
- [6] L. Cao and D. J. Mooney. Spatiotemporal control over growth factor signaling for therapeutic neovascularization. *Adv. Drug Deliv. Rev.*, 59(13):1340–1350, 2007.
- [7] J. K. Teßmar and A. M. Göpferich. Matrices and scaffolds for protein delivery in tissue engineering. *Adv. Drug Deliv. Rev.*, 59(4-5):274–291, 2007.
- [8] M. P. Lutolf and J. A. Hubbell. Synthetic biomaterials as instructive extracellular microenvironments for morphogenesis in tissue engineering. *Nat. Biotechnol.*, 23(1):47–55, 2005.

- [9] A. S. Hoffman. Hydrogels for biomedical applications. *Adv. Drug Deliv. Rev.*, 54(1):3–12, 2002.
- [10] J. L. Drury and D. J. Mooney. Hydrogels for tissue engineering: scaffold design variables and applications. *Biomaterials*, 24(24):4337–4351, 2003.
- [11] C.-C. Lin and K. Anseth. PEG hydrogels for the controlled release of biomolecules in regenerative medicine. *Pharm. Res.*, 26(3):631–643, 2009.
- [12] T. R. Hoare and D. S. Kohane. Hydrogels in drug delivery: Progress and challenges. *Polymer*, 49(8):1993–2007, 2008.
- [13] J. Teßmar, F. Brandl, and A. Göpferich. *Fundamentals of tissue engineering and regenerative medicine*, chapter Hydrogels for tissue engineering, pages 495–518. Springer, Berlin, 2009.
- [14] J. Harris. *Poly(ethylene glycol) chemistry: biotechnical and biomedical applications*. Plenum Press, New York, 1992.
- [15] H. Shin, S. Jo, and A. G. Mikos. Biomimetic materials for tissue engineering. *Biomaterials*, 24(24):4353–4364, 2003.
- [16] J. A. Hubbell. Materials as morphogenetic guides in tissue engineering. *Curr. Opin. Biotechnol.*, 14(5):551–558, 2003.
- [17] E. A. Silva and D. J. Mooney. Synthetic extracellular matrices for tissue engineering and regeneration. *Curr. Top. Dev. Biol.*, 64:181–205, 2004.
- [18] I. Kocur and S. Resnikoff. Visual impairment and blindness in Europe and their prevention. *Br. J. Ophthalmol.*, 86(7):716–722, 2002.
- [19] U. S. Schwarz and I. B. Bischofs. Physical determinants of cell organization in soft media. *Med. Eng. Phys.*, 27(9):763–772, 2005.
- [20] J. Y. Wong, J. B. Leach, and X. Q. Brown. Balance of chemistry, topography, and mechanics at the cell-biomaterial interface: Issues and challenges for assessing the role of substrate mechanics on cell response. *Surf. Sci.*, 570(1-2):119–133, 2004.

- [21] D. E. Discher, P. Janmey, and Y.-l. Wang. Tissue cells feel and respond to the stiffness of their substrate. *Science*, 310(5751):1139–1143, 2005.
- [22] A. Curtis and M. Riehle. Tissue engineering: the biophysical background. *Phys. Med. Biol.*, 46(4):R47–R65, 2001.
- [23] L. G. Griffith. Emerging design principles in biomaterials and scaffolds for tissue engineering. *Ann. N. Y. Acad. Sci.*, 961(1):83–95, 2002.
- [24] W. F. Liu and C. S. Chen. Engineering biomaterials to control cell function. *Mater. Today*, 8(12):28–35, 2005.
- [25] K. Y. Lee and D. J. Mooney. Hydrogels for tissue engineering. *Chem. Rev.*, 101(7):1869–1880, 2001.
- [26] J. Vitte, A. M. Benoliel, A. Pierres, and P. Bongrand. Is there a predictable relationship between surface physical-chemical properties and cell behaviour at the interface? *Eur. Cell Mater.*, 7:52–63, 2004.
- [27] Y. Tabata. Tissue regeneration based on growth factor release. *Tissue Eng.*, 9(Suppl. 1):S5–S15, 2003.
- [28] C. Sfeir, J. Jadlowiec, H. Koch, and P. Campbell. Signaling molecules for tissue engineering. In J. Hollinger, T. Einhorn, B. Doll, and C. Sfeir, editors, *Bone Tissue Engineering*, pages 125–147. CRC Press, Boca Raton, 2005.
- [29] R. Vasita and D. S. Katti. Growth factor-delivery systems for tissue engineering: a materials perspective. *Expert Rev. Med. Devices*, 3(1):29–47, 2006.
- [30] S. B. Carter. Principles of cell motility: the direction of cell movement and cancer invasion. *Nature*, 208(16):1183–1187, 1965.
- [31] S. B. Carter. Haptotaxis and the mechanism of cell motility. *Nature*, 213(73):256–260, 1967.
- [32] B. K. Brandley and R. L. Schnaar. Tumor cell haptotaxis on covalently immobilized linear and exponential gradients of a cell adhesion peptide. *Dev. Biol.*, 135(1):74–86, 1989.

- [33] M. E. Chicurel, C. S. Chen, and D. E. Ingber. Cellular control lies in the balance of forces. *Curr. Opin. Cell Biol.*, 10(2):232–239, 1998.
- [34] D. E. Ingber. Tensegrity I. Cell structure and hierarchical systems biology. *J. Cell Sci.*, 116(7):1157–1173, 2003.
- [35] D. E. Ingber. Tensegrity II. How structural networks influence cellular information processing networks. *J. Cell Sci.*, 116(8):1397–1408, 2003.
- [36] A. J. Garcia. Get a grip: integrins in cell-biomaterial interactions. *Biomaterials*, 26(36):7525–7529, 2005.
- [37] B. Geiger, A. Bershadsky, R. Pankov, and K. M. Yamada. Transmembrane crosstalk between the extracellular matrix and the cytoskeleton. *Nat. Rev. Mol. Cell Biol.*, 2(11):793–805, 2001.
- [38] B. Geiger and A. Bershadsky. Exploring the neighborhood: adhesion-coupled cell mechanosensors. *Cell*, 110(2):139–142, 2002.
- [39] E. Cukierman, R. Pankov, D. R. Stevens, and K. M. Yamada. Taking cell-matrix adhesions to the third dimension. *Science*, 294(5547):1708–1712, 2001.
- [40] E. Cukierman, R. Pankov, and K. M. Yamada. Cell interactions with three-dimensional matrices. *Curr. Opin. Cell Biol.*, 14(5):633–640, 2002.
- [41] D. Choquet, D. P. Felsenfeld, and M. P. Sheetz. Extracellular matrix rigidity causes strengthening of integrin-cytoskeleton linkages. *Cell*, 88(1):39–48, 1997.
- [42] C. M. Lo, H. B. Wang, M. Dembo, and Y. L. Wang. Cell movement is guided by the rigidity of the substrate. *Biophys. J.*, 79(1):144–152, 2000.
- [43] D. S. Gray, J. Tien, and C. S. Chen. Repositioning of cells by mechanotaxis on surfaces with micropatterned Young’s modulus. *J. Biomed. Mater. Res. A*, 66A(3):605–614, 2003.
- [44] R. J. Pelham and Y.-l. Wang. Cell locomotion and focal adhesions are regulated by substrate flexibility. *Proc. Natl. Acad. Sci. U.S.A.*, 94(25):13661–13665, 1997.

- [45] H. B. Wang, M. Dembo, and Y.-l. Wang. Substrate flexibility regulates growth and apoptosis of normal but not transformed cells. *Am. J. Physiol. Cell Physiol.*, 279(5):C1345–C1350, 2000.
- [46] B. Vailhé, X. Ronot, P. Tracqui, Y. Usson, and L. Tranqui. In vitro angiogenesis is modulated by the mechanical properties of fibrin gels and is related to $\alpha_v\beta_3$ integrin localization. *In Vitro Cell. Dev. Biol. Anim.*, 33(10):763–773, 1997.
- [47] C. F. Deroanne, C. M. Lapierre, and B. V. Nusgens. In vitro tubulogenesis of endothelial cells by relaxation of the coupling extracellular matrix-cytoskeleton. *Cardiovasc. Res.*, 49(3):647–658, 2001.
- [48] L. A. Flanagan, Y. E. Ju, B. Marg, M. Osterfield, and P. A. Janmey. Neurite branching on deformable substrates. *Neuroreport*, 13(18):2411–2415, 2002.
- [49] A. D. Bershadsky, N. Q. Balaban, and B. Geiger. Adhesion-dependent cell mechanosensitivity. *Annu. Rev. Cell Dev. Biol.*, 19(1):677–695, 2003.
- [50] J. A. Rowley and D. J. Mooney. Alginate type and RGD density control myoblast phenotype. *J. Biomed. Mater. Res.*, 60(2):217–223, 2002.
- [51] A. Engler, L. Bacakova, C. Newman, A. Hategan, M. Griffin, and D. Discher. Substrate compliance versus ligand density in cell on gel responses. *Biophys. J.*, 86(1):617–628, 2004.
- [52] S. R. Peyton and A. J. Putnam. Extracellular matrix rigidity governs smooth muscle cell motility in a biphasic fashion. *J. Cell. Physiol.*, 204(1):198–209, 2005.
- [53] H. Abe, K. Hayashi, and M. Sato, editors. *Data Book on Mechanical Properties of Living Cells, Tissues, and Organs*. Springer-Verlag, Tokyo, 1996.
- [54] K. S. Anseth, C. N. Bowman, and L. Brannon-Peppas. Mechanical properties of hydrogels and their experimental determination. *Biomaterials*, 17(17):1647–1657, 1996.

- [55] R. K. Korhonen, M. S. Laasanen, J. Toyras, J. Rieppo, J. Hirvonen, H. J. Helminen, and J. S. Jurvelin. Comparison of the equilibrium response of articular cartilage in unconfined compression, confined compression and indentation. *J. Biomech.*, 35(7):903–909, 2002.
- [56] H. A. Barnes, J. F. Hutton, and K. Walters, editors. *An introduction to rheology*. Elsevier Science Publishers B.V., Amsterdam, 1989.
- [57] K. Ichihara, T. Taguchi, I. Sakuramoto, S. Kawano, and S. Kawai. Mechanism of the spinal cord injury and the cervical spondylotic myelopathy: new approach based on the mechanical features of the spinal cord white and gray matter. *J. Neurosurg.*, 99(3 Suppl):278–285, 2003.
- [58] K. A. Athanasiou, A. Agarwal, and F. J. Dzida. Comparative study of the intrinsic mechanical properties of the human acetabular and femoral head cartilage. *J. Orthop. Res.*, 12(3):340–349, 1994.
- [59] D. Raftopoulos, E. Katsamanis, F. Saul, W. Liu, and S. Saddemi. An intermediate loading rate technique for the determination of mechanical properties of human femoral cortical bone. *J. Biomed. Eng.*, 15(1):60–66, 1993.
- [60] J. Domke and M. Radmacher. Measuring the elastic properties of thin polymer films with the atomic force microscope. *Langmuir*, 14(12):3320–3325, 1998.
- [61] W. R. Bowen, R. W. Lovitt, and C. J. Wright. Application of atomic force microscopy to the study of micromechanical properties of biological materials. *Biotechnol. Lett.*, 22(11):893–903, 2000.
- [62] A. J. Engler, L. Richert, J. Y. Wong, C. Picart, and D. E. Discher. Surface probe measurements of the elasticity of sectioned tissue, thin gels and polyelectrolyte multilayer films: correlations between substrate stiffness and cell adhesion. *Surf. Sci.*, 570(1-2):142–154, 2004.
- [63] A. Manduca, T. E. Oliphant, M. A. Dresner, J. L. Mahowald, S. A. Kruse, E. Amromin, J. P. Felmlee, J. F. Greenleaf, and R. L. Ehman. Magnetic resonance elastography: non-invasive mapping of tissue elasticity. *Med. Image Anal.*, 5(4):237–254, 2001.

- [64] G. Madelin, N. Baril, J. D. De Certaines, J.-M. Franconi, and E. Thiaudière. NMR characterization of mechanical waves. In G. Webb, editor, *Annual Reports on NMR Spectroscopy*, volume Volume 53, pages 203–244. Academic Press, 2004.
- [65] S. I. Ringleb, Q. Chen, D. S. Lake, A. Manduca, R. L. Ehman, and K. N. An. Quantitative shear wave magnetic resonance elastography: comparison to a dynamic shear material test. *Magn. Reson. Med.*, 53(5):1197–1201, 2005.
- [66] S. F. Othman, H. Xu, T. J. Royston, and R. L. Magin. Microscopic magnetic resonance elastography (μ MRE). *Magn. Reson. Med.*, 54(3):605–615, 2005.
- [67] H. J. Kong, T. R. Polte, E. Alsberg, and D. J. Mooney. FRET measurements of cell-traction forces and nano-scale clustering of adhesion ligands varied by substrate stiffness. *Proc. Natl. Acad. Sci. U.S.A.*, 102(12):4300–4305, 2005.
- [68] J. Szöllosi, S. Damjanovich, and L. Mátyus. Application of fluorescence resonance energy transfer in the clinical laboratory: routine and research. *Cytometry*, 34(4):159–179, 1998.
- [69] E. A. Jares-Erijman and T. M. Jovin. FRET imaging. *Nat. Biotechnol.*, 21(11):1387–1395, 2003.
- [70] A. Baruch, D. A. Jeffery, and M. Bogyo. Enzyme activity – it’s all about image. *Trends Cell Biol.*, 14(1):29–35, 2004.
- [71] O. Smidsrød and G. Skjåk-Bræk. Alginate as immobilization matrix for cells. *Trends Biotechnol.*, 8:71–78, 1990.
- [72] A. S. Sawhney, C. P. Pathak, and J. A. Hubbell. Bioerodible hydrogels based on photopolymerized poly(ethylene glycol)-co-poly(α -hydroxy acid) diacrylate macromers. *Macromolecules*, 26(4):581–587, 1993.
- [73] W. E. Hennink and C. F. van Nostrum. Novel crosslinking methods to design hydrogels. *Adv. Drug Deliv. Rev.*, 54(1):13–36, 2002.

- [74] M. P. Lutolf and J. A. Hubbell. Synthesis and physicochemical characterization of end-linked poly(ethylene glycol)-co-peptide hydrogels formed by Michael-type addition. *Biomacromolecules*, 4(3):713–722, 2003.
- [75] E. Ruel-Gariépy and J. C. Leroux. In situ-forming hydrogels—review of temperature-sensitive systems. *Eur. J. Pharm. Biopharm.*, 58(2):409–426, 2004.
- [76] S. Zhang. Fabrication of novel biomaterials through molecular self-assembly. *Nat. Biotechnol.*, 21(10):1171–1178, 2003.
- [77] K. Y. Lee, J. A. Rowley, P. Eiselt, E. M. Moy, K. H. Bouhadir, and D. J. Mooney. Controlling mechanical and swelling properties of alginate hydrogels independently by cross-linker type and cross-linking density. *Macromolecules*, 33(11):4291–4294, 2000.
- [78] M. A. LeRoux, F. Guilak, and L. A. Setton. Compressive and shear properties of alginate gel: effects of sodium ions and alginate concentration. *J. Biomed. Mater. Res.*, 47(1):46–53, 1999.
- [79] J. W. Gunn, S. D. Turner, and B. K. Mann. Adhesive and mechanical properties of hydrogels influence neurite extension. *J. Biomed. Mater. Res. A*, 72A(1):91–97, 2005.
- [80] S. J. Bryant and K. S. Anseth. Hydrogel properties influence ECM production by chondrocytes photoencapsulated in poly(ethylene glycol) hydrogels. *J. Biomed. Mater. Res.*, 59(1):63–72, 2002.
- [81] G. M. Cruise, D. S. Scharp, and J. A. Hubbell. Characterization of permeability and network structure of interfacially photopolymerized poly(ethylene glycol) diacrylate hydrogels. *Biomaterials*, 19(14):1287–1294, 1998.
- [82] Y. Park, M. P. Lutolf, J. A. Hubbell, E. B. Hunziker, and M. Wong. Bovine primary chondrocyte culture in synthetic matrix metalloproteinase-sensitive poly(ethylene glycol)-based hydrogels as a scaffold for cartilage repair. *Tissue Eng.*, 10(3-4):515–522, 2004.

-
- [83] R. H. Li, D. H. Altreuter, and F. T. Gentile. Transport characterization of hydrogel matrices for cell encapsulation. *Biotechnol. Bioeng.*, 50(4):365–373, 1996.
- [84] H. A. Leddy, H. A. Awad, and F. Guilak. Molecular diffusion in tissue-engineered cartilage constructs: effects of scaffold material, time, and culture conditions. *J. Biomed. Mater. Res. B Appl. Biomater.*, 70(2):397–406, 2004.
- [85] S. P. Baldwin and M. W. Saltzman. Materials for protein delivery in tissue engineering. *Adv Drug Deliver Rev*, 33(1-2):71–86, 1998.
- [86] K. Kellner, G. Liebsch, I. Klimant, O. S. Wolfbeis, T. Blunk, M. B. Schulz, and A. Göpferich. Determination of oxygen gradients in engineered tissue using a fluorescent sensor. *Biotechnol. Bioeng.*, 80(1):73–83, 2002.
- [87] E. Alsberg, H. Kong, Y. Hirano, M. K. Smith, A. Albeiruti, and D. J. Mooney. Regulating bone formation via controlled scaffold degradation. *J. Dent. Res.*, 82(11):903–908, 2003.
- [88] H. J. Kong, D. Kaigler, K. Kim, and D. J. Mooney. Controlling rigidity and degradation of alginate hydrogels via molecular weight distribution. *Biomacromolecules*, 5(5):1720–1727, 2004.
- [89] T. Boontheekul, H.-J. Kong, and D. J. Mooney. Controlling alginate gel degradation utilizing partial oxidation and bimodal molecular weight distribution. *Biomaterials*, 26(15):2455–2465, 2005.
- [90] M. P. Lutolf, J. L. Lauer-Fields, H. G. Schmoekel, A. T. Metters, F. E. Weber, G. B. Fields, and J. A. Hubbell. Synthetic matrix metalloproteinase-sensitive hydrogels for the conduction of tissue regeneration: engineering cell-invasion characteristics. *Proc. Natl. Acad. Sci. U.S.A.*, 100(9):5413–5418, 2003.
- [91] K. J. Gooch and C. J. Tennant, editors. *Mechanical forces: their effects on cells and tissues*. Springer-Verlag, Berlin, 1997.
- [92] A. Katsumi, A. W. Orr, E. Tzima, and M. A. Schwartz. Integrins in mechanotransduction. *J. Biol. Chem.*, 279(13):12001–12004, 2004.

- [93] G. P. Dillon, X. Yu, A. Sridharan, J. P. Ranieri, and R. V. Bellamkonda. The influence of physical structure and charge on neurite extension in a 3D hydrogel scaffold. *J. Biomater. Sci. Polym. Ed.*, 9(10):1049–1069, 1998.
- [94] A. P. Balgude, X. Yu, A. Szymanski, and R. V. Bellamkonda. Agarose gel stiffness determines rate of DRG neurite extension in 3D cultures. *Biomaterials*, 22(10):1077–1084, 2001.
- [95] M. Wong, M. Siegrist, X. Wang, and E. Hunziker. Development of mechanically stable alginate/chondrocyte constructs: effects of guluronic acid content and matrix synthesis. *J. Orthop. Res.*, 19(3):493–499, 2001.
- [96] A. L. Sieminski, R. P. Hebbel, and K. J. Gooch. The relative magnitudes of endothelial force generation and matrix stiffness modulate capillary morphogenesis in vitro. *Exp. Cell Res.*, 297(2):574–584, 2004.
- [97] S. J. Bryant and K. S. Anseth. Controlling the spatial distribution of ECM components in degradable PEG hydrogels for tissue engineering cartilage. *J. Biomed. Mater. Res. A*, 64(1):70–79, 2003.
- [98] M. J. Mahoney and K. S. Anseth. Three-dimensional growth and function of neural tissue in degradable polyethylene glycol hydrogels. *Biomaterials*, 27(10):2265–2274, 2006.
- [99] L. Meinel, S. Hofmann, V. Karageorgiou, L. Zichner, R. Langer, D. Kaplan, and G. Vunjak-Novakovic. Engineering cartilage-like tissue using human mesenchymal stem cells and silk protein scaffolds. *Biotechnol. Bioeng.*, 88(3):379–391, 2004.
- [100] M. P. Lutolf, F. E. Weber, H. G. Schmoekel, J. C. Schense, T. Kohler, R. Muller, and J. A. Hubbell. Repair of bone defects using synthetic mimetics of collagenous extracellular matrices. *Nat. Biotechnol.*, 21(5):513–518, 2003.
- [101] M. H. Zaman, R. D. Kamm, P. Matsudaira, and D. A. Lauffenburger. Computational model for cell migration in three-dimensional matrices. *Biophys. J.*, 89(2):1389–1397, 2005.

- [102] F. Brandl, F. Sommer, and A. Göpferich. Rational design of hydrogels for tissue engineering: Impact of physical factors on cell behavior. *Biomaterials*, 28(2):134–146, 2007.
- [103] M. C. Cushing and K. S. Anseth. Hydrogel cell cultures. *Science*, 316(5828):1133–1134, 2007.
- [104] P. N. Bishop. Structural macromolecules and supramolecular organisation of the vitreous gel. *Prog. Ret. Eye Res.*, 19(3):323–344, 2000.
- [105] N. Soman and R. Banerjee. Artificial vitreous replacements. *Biomed. Mater. Eng.*, 13(1):59–74, 2003.
- [106] M. J. Colthurst, R. L. Williams, P. S. Hiscott, and I. Grierson. Biomaterials used in the posterior segment of the eye. *Biomaterials*, 21(7):649–665, 2000.
- [107] T. V. Chirila, Y. Hong, P. D. Dalton, I. J. Constable, and M. F. Refojo. The use of hydrophilic polymers as artificial vitreous. *Prog. Polym. Sci.*, 23(3):475–508, 1998.
- [108] P. Gargiulo, C. Giusti, D. Pietrobono, D. La Torre, D. Diacono, and G. Tamburano. Diabetes mellitus and retinopathy. *Dig. Liver Dis.*, 36(Supplement 1):S101–S105, 2004.
- [109] P. D. Dalton, T. V. Chirila, Y. Hong, and A. Jefferson. Oscillatory shear experiments as criteria for potential vitreous substitutes. *Polym. Gels Netw.*, 3(4):429–444, 1995.
- [110] T. Yasukawa, Y. Ogura, Y. Tabata, H. Kimura, P. Wiedemann, and Y. Honda. Drug delivery systems for vitreoretinal diseases. *Prog. Ret. Eye Res.*, 23(3):253–281, 2004.
- [111] W. Eichler, Y. Yafai, P. Wiedemann, and D. Fengler. Antineovascular agents in the treatment of eye diseases. *Curr. Pharm. Des.*, 12(21):2645–2660, 2006.
- [112] C. A. P. Quinn, R. E. Connor, and A. Heller. Biocompatible, glucose-permeable hydrogel for in situ coating of implantable biosensors. *Biomaterials*, 18(24):1665–1670, 1997.

- [113] G. M. C. Wallace. A tissue sealant based on reactive multifunctional polyethylene glycol. *J. Biomed. Mater. Res.*, 58(5):545–555, 2001.
- [114] M. Wathier, M. S. Johnson, M. A. Carnahan, C. Baer, B. W. McCuen, and M. W. Kim, T.; Grinstaff. In situ polymerized hydrogels for repairing scleral incisions used in pars plana vitrectomy procedures. *ChemMedChem*, 1(8):821–825, 2006.
- [115] P. Mongondry, C. Bonnans-Plaisance, M. Jean, and J.-F. Tassin. Mild synthesis of amino-poly(ethylene glycol)s. Application to steric stabilization of clays. *Macromol. Rapid Commun.*, 24(11):681–685, 2003.
- [116] M. Sedaghat-Herati, P. Miller, A. Kozlowski, and J. M. Harris. Synthesis of methoxypoly(oxyethylene)propionic acid. *Polym. Bull.*, 43(1):35–41, 1999.
- [117] A. Metters and J. Hubbell. Network formation and degradation behavior of hydrogels formed by Michael-type addition reactions. *Biomacromolecules*, 6(1):290–301, 2005.
- [118] M. Mensitieri, L. Ambrosio, L. Nicolais, L. Balzano, and D. Lepore. The rheological behaviour of animal vitreous and its comparison with vitreal substitutes. *J. Mater. Sci. Mater. Med.*, 5(9 - 10):743–747, 1994.
- [119] C. S. Nickerson, H. L. Karageozian, J. Park, and J. A. Kornfield. Internal tension: a novel hypothesis concerning the mechanical properties of the vitreous humor. *Macromol. Symp.*, 227(1):183–189, 2005.
- [120] A. Pizzoferrato, G. Ciapetti, S. Stea, E. Cenni, C. Arciola, D. Granchi, and L. Savarino. Cell culture methods for testing biocompatibility. *Clin. Mater.*, 15(3):173–190, 1994.
- [121] W. W. Minuth, S. Kloth, J. Aigner, M. Sittlinger, and W. Rockl. Organo-typical environment for cultured cells and tissues. *Bioforum*, 17:412–416, 1994.
- [122] W. A. Herrmann, K. Kobuch, S. Kloth, C. Framme, and J. Roeder. Full-thickness adult retina in perfusion culture. A new organotypical model for toxicity tests. *Invest. Ophthalmol. Vis. Sci.*, 40 (Supl.):S989–, 1999.

- [123] A. A. Moshfeghi and G. A. Peyman. Micro- and nanoparticulates. *Adv. Drug Deliv. Rev.*, 57(14):2047–2052, 2005.
- [124] S. Drotleff, U. Lungwitz, M. Breunig, A. Dennis, T. Blunk, J. Teßmar, and A. Göpferich. Biomimetic polymers in pharmaceutical and biomedical sciences. *Eur. J. Pharm. Biopharm.*, 58(2):385–407, 2004.
- [125] F. Sommer, K. Kobuch, F. Brandl, B. Wild, C. Framme, B. Weiser, J. Teßmar, V. P. Gabel, T. Blunk, and A. Göpferich. Ascorbic acid modulates proliferation and extracellular matrix accumulation of hyalocytes. *Tissue Eng.*, 13(6):1281–1289, 2007.
- [126] C.-C. Lin and A. T. Metters. Hydrogels in controlled release formulations: network design and mathematical modeling. *Adv. Drug Deliv. Rev.*, 58(12-13):1379–1408, 2006.
- [127] J. Siepmann and A. Göpferich. Mathematical modeling of bioerodible, polymeric drug delivery systems. *Adv. Drug Deliv. Rev.*, 48(2-3):229–247, 2001.
- [128] J. Siepmann and F. Siepmann. Mathematical modeling of drug delivery. *Int. J. Pharm.*, 364(2):328–343, 2008.
- [129] D. Axelrod, D. E. Koppel, J. Schlessinger, E. Elson, and W. W. Webb. Mobility measurement by analysis of fluorescence photobleaching recovery kinetics. *Biophys. J.*, 16(9):1055–1069, 1976.
- [130] K. Braeckmans, L. Peeters, N. N. Sanders, S. C. De Smedt, and J. Demeester. Three-dimensional fluorescence recovery after photobleaching with the confocal scanning laser microscope. *Biophys. J.*, 85(4):2240–2252, 2003.
- [131] T. K. Meyvis, S. C. De Smedt, P. Van Oostveldt, and J. Demeester. Fluorescence recovery after photobleaching: a versatile tool for mobility and interaction measurements in pharmaceutical research. *Pharm. Res.*, 16(8):1153–1162, 1999.
- [132] M. C. Branco, D. J. Pochan, N. J. Wagner, and J. P. Schneider. Macromolecular diffusion and release from self-assembled β -hairpin peptide hydrogels. *Biomaterials*, 30(7):1339–1347, 2009.

- [133] M. D. Burke, J. O. Park, M. Srinivasarao, and S. A. Khan. A novel enzymatic technique for limiting drug mobility in a hydrogel matrix. *J. Controlled Release*, 104(1):141–153, 2005.
- [134] A. J. Kuijpers, G. H. M. Engbers, T. K. L. Meyvis, S. S. C. De Smedt, J. De-meester, J. Krijgsveld, S. A. J. Zaat, J. Dankert, and J. Feijen. Combined gelatin-chondroitin sulfate hydrogels for controlled release of cationic antibacterial proteins. *Macromolecules*, 33(10):3705–3713, 2000.
- [135] S. R. Van Tomme, B. G. De Geest, K. Braeckmans, S. C. De Smedt, F. Siepman, J. Siepman, C. F. Van Nostrum, and W. E. Hennink. Mobility of model proteins in hydrogels composed of oppositely charged dextran microspheres studied by protein release and fluorescence recovery after photobleaching. *J. Controlled Release*, 110(1):67–78, 2005.
- [136] F. Weinbreck, H. S. Rollema, R. H. Tromp, and C. G. De Kruif. Diffusivity of whey protein and gum Arabic in their coacervates. *Langmuir*, 20(15):6389–6395, 2004.
- [137] W. S. Price. Pulsed-field gradient nuclear magnetic resonance as a tool for studying translational diffusion: Part I. Basic theory. *Concepts Magn. Reson.*, 9(5):299–336, 1997.
- [138] W. S. Price. Pulsed-field gradient nuclear magnetic resonance as a tool for studying translational diffusion: Part II. Experimental aspects. *Concepts Magn. Reson.*, 10(4):197–237, 1998.
- [139] F. Brandl, M. Henke, S. Rothschenk, R. Gschwind, M. Breunig, T. Blunk, J. Teßmar, and A. Göpferich. Poly(ethylene glycol) based hydrogels for intraocular applications. *Adv. Eng. Mater.*, 9(12):1141–1149, 2007.
- [140] P. J. Flory. *Principles of polymer chemistry*. Cornell University Press, Ithaca, 1953.
- [141] J. C. Bray and E. W. Merrill. Poly(vinyl alcohol) hydrogels. Formation by electron beam irradiation of aqueous solutions and subsequent crystallization. *J. Appl. Polym. Sci.*, 17(12):3779–3794, 1973.

- [142] D. L. Elbert, A. B. Pratt, M. P. Lutolf, S. Halstenberg, and J. A. Hubbell. Protein delivery from materials formed by self-selective conjugate addition reactions. *J. Controlled Release*, 76(1-2):11–25, 2001.
- [143] T. Canal and N. A. Peppas. Correlation between mesh size and equilibrium degree of swelling of polymeric networks. *J. Biomed. Mater. Res.*, 23(10):1183–1193, 1989.
- [144] G. P. Raeber, M. P. Lutolf, and J. A. Hubbell. Molecularly engineered PEG hydrogels: a novel model system for proteolytically mediated cell migration. *Biophys. J.*, 89(2):1374–1388, 2005.
- [145] L. G. Cima and S. T. Lopina. Network structures of radiation-crosslinked star polymer gels. *Macromolecules*, 28(20):6787–6794, 1995.
- [146] Y. Gnanou, G. Hild, and P. Rempp. Molecular structure and elastic behavior of poly(ethylene oxide) networks swollen to equilibrium. *Macromolecules*, 20(7):1662–1671, 1987.
- [147] D. M. Soumpasis. Theoretical analysis of fluorescence photobleaching recovery experiments. *Biophys. J.*, 41(1):95–97, 1983.
- [148] C. Guse, S. Könnings, F. Kreye, F. Siepmann, A. Göpferich, and J. Siepmann. Drug release from lipid-based implants: elucidation of the underlying mass transport mechanisms. *Int. J. Pharm.*, 314(2):137–144, 2006.
- [149] G. M. Kavanagh and S. B. Ross-Murphy. Rheological characterisation of polymer gels. *Prog. Polym. Sci.*, 23(3):533–562, 1998.
- [150] E. W. Merrill, K. A. Dennison, and C. Sung. Partitioning and diffusion of solutes in hydrogels of poly(ethylene oxide). *Biomaterials*, 14(15):1117–1126, 1993.
- [151] V. S. Sukumar and S. T. Lopina. Network model for the swelling properties of end-linked linear and star poly(ethylene oxide) hydrogels. *Macromolecules*, 35(27):10189–10192, 2002.

- [152] S. R. Lustig and N. A. Peppas. Solute diffusion in swollen membranes. IX. Scaling laws for solute diffusion in gels. *J. Appl. Polym. Sci.*, 36(4):735–747, 1988.
- [153] M. Henke, F. Brandl, A. M. Göpferich, and J. K. Teßmar. Size dependent release of fluorescent macromolecules and nanoparticles from radically cross-linked hydrogels. *Eur. J. Pharm. Biopharm.*, in press, 2009.
- [154] N. A. Peppas, P. Bures, W. Leobandung, and H. Ichikawa. Hydrogels in pharmaceutical formulations. *Eur. J. Pharm. Biopharm.*, 50(1):27–46, 2000.
- [155] J. W. DuBose, C. Cutshall, and A. T. Metters. Controlled release of tethered molecules via engineered hydrogel degradation: Model development and validation. *J. Biomed. Mater. Res. A*, 74A(1):104–116, 2005.
- [156] H. Soye, E. Schacht, M. Jelinkova, and B. Rihova. Biological evaluation of mitomycin C bound to a biodegradable polymeric carrier. *J. Controlled Release*, 47(1):71–80, 1997.
- [157] D. Seliktar, A. H. Zisch, M. P. Lutolf, J. L. Wrana, and J. A. Hubbell. MMP-2 sensitive, VEGF-bearing bioactive hydrogels for promotion of vascular healing. *J. Biomed. Mater. Res. A*, 68A(4):704–716, 2004.
- [158] R. G. Schoenmakers, P. van de Wetering, D. L. Elbert, and J. A. Hubbell. The effect of the linker on the hydrolysis rate of drug-linked ester bonds. *J. Controlled Release*, 95(2):291–300, 2004.
- [159] S. Lee, R. B. Greenwald, J. McGuire, K. Yang, and C. Shi. Drug delivery systems employing 1,6-elimination: Releasable poly(ethylene glycol) conjugates of proteins. *Bioconjug. Chem.*, 12(2):163–169, 2001.
- [160] M. J. Roberts, M. D. Bentley, and J. M. Harris. Chemistry for peptide and protein PEGylation. *Adv. Drug Deliv. Rev.*, 54(4):459–476, 2002.
- [161] R. B. Greenwald, K. Yang, H. Zhao, C. D. Conover, S. Lee, and D. Filpula. Controlled release of proteins from their poly(ethylene glycol) conjugates: drug

- delivery systems employing 1,6-elimination. *Bioconjug. Chem.*, 14(2):395–403, 2003.
- [162] D. Filpula and H. Zhao. Releasable PEGylation of proteins with customized linkers. *Adv. Drug Deliv. Rev.*, 60(1):29–49, 2008.
- [163] M. M. Bradford. A rapid and sensitive method for the quantitation of microgram quantities of protein utilizing the principle of protein-dye binding. *Anal. Biochem.*, 72(1-2):248–254, 1976.
- [164] G. T. Hermanson. *Bioconjugate Techniques*. Academic Press, Amsterdam, The Netherlands, 2nd edition, 2008.
- [165] L. W. Dittert and T. Higuchi. Rates of hydrolysis of carbamate and carbonate esters in alkaline solution. *J. Pharm. Sci.*, 52:852–857, 1963.
- [166] J. Hansen, N. Mrk, and H. Bundgaard. Phenyl carbamates of amino acids as prodrug forms for protecting phenols against first-pass metabolism. *Int. J. Pharm.*, 81(2-3):253–261, 1992.
- [167] E. Johnson, D. A. Berk, R. K. Jain, and W. M. Deen. Hindered diffusion in agarose gels: test of effective medium model. *Biophys. J.*, 70(2):1017–1023, 1996.
- [168] S. C. De Smedt, A. Lauwers, J. Demeester, Y. Engelborghs, G. De Mey, and M. Du. Structural information on hyaluronic acid solutions as studied by probe diffusion experiments. *Macromolecules*, 27(1):141–146, 1994.
- [169] A. Lucke, E. Fustella, J. Temar, A. Gazzaniga, and A. Gpferich. The effect of poly(ethylene glycol)-poly(D,L-lactic acid) diblock copolymers on peptide acylation. *J. Controlled Release*, 80(1-3):157–168, 2002.
- [170] A. Lucke, J. Kiermaier, and A. Gpferich. Peptide acylation by poly(alpha-hydroxy esters). *Pharm. Res.*, 19(2):175–181, 2002.
- [171] C. W. Patrick. Tissue engineering strategies for adipose tissue repair. *Anat. Rec.*, 263(4):361–366, 2001.

- [172] B. Weiser, M. Neubauer, A. Göpferich, and T. Blunk. *Encyclopedia of Biomaterials and Biomedical Engineering*, volume 4, chapter Tissue Engineering, Fat, pages 2725–2736. Marcel Dekker Inc., New York, 2 edition, 2005.
- [173] B. Weiser, L. Prantl, T. E. O. Schubert, J. Zellner, C. Fischbach-Teschl, T. Spruß, A. K. Seitz, J. Teßmar, A. Göpferich, and T. Blunk. In vivo development and long-term survival of engineered adipose tissue depend on in vitro precultivation strategy. *Tissue Eng. Part A*, 14(2):275–284, 2008.
- [174] C. Fischbach, T. Spruß, B. Weiser, M. Neubauer, C. Becker, M. Hacker, A. Göpferich, and T. Blunk. Generation of mature fat pads in vitro and in vivo utilizing 3-D long-term culture of 3T3-L1 preadipocytes. *Exp. Cell Res.*, 300(1):54–64, 2004.
- [175] A. Alhadlaq, M. Tang, and J. J. Mao. Engineered adipose tissue from human mesenchymal stem cells maintains predefined shape and dimension: implications in soft tissue augmentation and reconstruction. *Tissue Eng.*, 11(3-4):556–566, 2005.
- [176] P. N. Patel, C. K. Smith, and C. W. Patrick. Rheological and recovery properties of poly(ethylene glycol) diacrylate hydrogels and human adipose tissue. *J. Biomed. Mater. Res. A*, 73A(3):313–319, 2005.
- [177] P. N. Patel, A. S. Gobin, J. L. West, and C. W. Patrick. Poly(ethylene glycol) hydrogel system supports preadipocyte viability, adhesion, and proliferation. *Tissue Eng.*, 11(9-10):1498–1505, 2005.
- [178] A. V. Vashi, E. Keramidaris, K. M. Abberton, W. A. Morrison, J. L. Wilson, A. J. O’Connor, J. J. Cooper-White, and E. W. Thompson. Adipose differentiation of bone marrow-derived mesenchymal stem cells using Pluronic F-127 hydrogel in vitro. *Biomaterials*, 29(5):573–579, 2008.
- [179] F. Brandl, F. Kastner, R. Gschwind, T. Blunk, J. Teßmar, and A. Göpferich. Hydrogel-based drug delivery systems: Comparison of drug diffusivity and release kinetics. *J. Controlled Release*, in press, 2009.

- [180] M. P. Lutolf, G. P. Raeber, A. H. Zisch, N. Tirelli, and J. A. Hubbell. Cell-Responsive Synthetic Hydrogels. *Advanced Materials*, 15(11):888–892, 2003.
- [181] S. J. Bryant, C. R. Nuttelman, and K. S. Anseth. Cytocompatibility of UV and visible light photoinitiating systems on cultured NIH/3T3 fibroblasts in vitro. *J. Biomater. Sci. Polym. Ed.*, 11(5):439–457, 2000.
- [182] M. D. Timmer, H. Shin, R. A. Horch, C. G. Ambrose, and A. G. Mikos. In vitro cytotoxicity of injectable and biodegradable poly(propylene fumarate)-based networks: unreacted macromers, cross-linked networks, and degradation products. *Biomacromolecules*, 4(4):1026–1033, 2003.
- [183] C. Fischbach, J. Seufert, H. Staiger, M. Hacker, M. Neubauer, A. Göpferich, and T. Blunk. Three-dimensional in vitro model of adipogenesis: comparison of culture conditions. *Tissue Eng.*, 10(1-2):215–229, 2004.
- [184] M. Mutter, R. Uhlmann, and E. Bayer. Die Liquid-Phase-Methode zur Peptidsynthese; Strategie und experimentelle Grundlagen. *Justus Liebig's Ann. Chem.*, 1975(5):901–915, 1975.
- [185] S. Udenfriend, S. Stein, P. Bohlen, W. Dairman, W. Leimgruber, and M. Weigle. Fluorescamine: A reagent for assay of amino acids, peptides, proteins, and primary amines in the picomole range. *Science*, 178(4063):871–872, 1972.
- [186] Y.-J. Kim, R. L. Y. Sah, J.-Y. H. Doong, and A. J. Grodzinsky. Fluorometric assay of DNA in cartilage explants using Hoechst 33258. *Anal. Biochem.*, 174(1):168–176, 1988.
- [187] J. L. Ramírez-Zacarias, F. Castro-Muñozledo, and W. Kuri-Harcuch. Quantitation of adipose conversion and triglycerides by staining intracytoplasmic lipids with Oil red O. *Histochem. Cell Biol.*, 97(6):493–497, 1992.
- [188] Y. Teramura, Y. Kaneda, T. Totani, and H. Iwata. Behavior of synthetic polymers immobilized on a cell membrane. *Biomaterials*, 29(10):1345–1355, 2008.

- [189] A. Nordwig and L. Strauch. Stabilitätsverhalten der Kollagenase aus *Clostridium histolyticum*. *Hoppe-Seyler's Z. Physiol. Chem.*, 330:153–160, 1963.
- [190] J. L. West and J. A. Hubbell. Polymeric biomaterials with degradation sites for proteases involved in cell migration. *Macromolecules*, 32(1):241–244, 1999.
- [191] B. K. Mann, A. S. Gobin, A. T. Tsai, R. H. Schmedlen, and J. L. West. Smooth muscle cell growth in photopolymerized hydrogels with cell adhesive and proteolytically degradable domains: synthetic ECM analogs for tissue engineering. *Biomaterials*, 22(22):3045–3051, 2001.
- [192] M. D. Sternlicht and Z. Werb. How matrix metalloproteinases regulate cell behavior. *Annu. Rev. Cell Dev. Biol.*, 17:463–516, 2001.
- [193] B. M. Spiegelman and C. A. Ginty. Fibronectin modulation of cell shape and lipogenic gene expression in 3T3-adipocytes. *Cell*, 35(3, Part 2):657–666, 1983.
- [194] K. C. O'Connor, H. Song, N. Rosenzweig, and D. A. Jansen. Extracellular matrix substrata alter adipocyte yield and lipogenesis in primary cultures of stromal-vascular cells from human adipose. *Biotechnol. Lett.*, 25(23):1967–1972, 2003.
- [195] C. M. Smas and H. S. Sul. Control of adipocyte differentiation. *Biochem. J.*, 309(3):697–710, 1995.
- [196] G. J. Hausman, J. T. Wright, and R. L. Richardson. The influence of extracellular matrix substrata on preadipocyte development in serum-free cultures of stromal-vascular cells. *J. Anim. Sci.*, 74(9):2117–2128, 1996.
- [197] C. W. Patrick and X. Wu. Integrin-mediated preadipocyte adhesion and migration on laminin-1. *Ann. Biomed. Eng.*, 31(5):505–514, 2003.
- [198] B. Jeong, S. W. Kim, and Y. H. Bae. Thermosensitive sol-gel reversible hydrogels. *Adv. Drug Deliv. Rev.*, 54(1):37–51, 2002.
- [199] C. Framme, F. Brandl, S. Rothschenk, A. Göpferich, H. Helbig, and K. Kobuch. Development and evaluation of new hydrogels for vitreous substitution and intravitreal drug application. 106th DOG Congress, Berlin, Germany, 2008.

- [200] F. Brandl, K. Kobuch, S. Rothschenk, T. Blunk, J. Teßmar, and A. Göpferich. In situ-forming hydrogels for intraocular drug delivery. 8th World Biomaterials Congress, Amsterdam, The Netherlands, 2008.
- [201] K. Kobuch, W. A. Herrmann, C. Framme, H. G. Sachs, V.-P. Gabel, and J. Hillenkamp. Maintenance of adult porcine retina and retinal pigment epithelium in perfusion culture: Characterisation of an organotypic in vitro model. *Exp. Eye Res.*, 86(4):661–668, 2008.

List of Figures

1.1	Principle of <i>in situ</i> forming hydrogels	7
2.1	Repositioning of cells by mechanotaxis on surfaces with micropatterned Young's modulus	16
2.2	Schematic diagram of atomic force microscopy (AFM)	21
2.3	Schematic diagram of magnetic resonance elastography (MRE)	22
2.4	Principle of fluorescence resonance energy transfer (FRET)	24
2.5	Michael-type addition reaction between vinylsulfone-functionalized PEG macromers and cysteine containing peptides	26
2.6	Schematic illustration of cell-responsive hydrogels	33
3.1	Synthesis of PEG2k-NH ₂ and 4armPEG10k-SPA	43
3.2	Typical rheogram of a gel formed by polymerization of PEG2k-NH ₂ with 4armPEG10k-SPA	48
3.3	Dependence of gelation time and gel strength on the stoichiometric ratio, polymer concentration, pH, and temperature	49
3.4	¹ H-NMR spectra of a hydrogel formed by reaction of 4armPEG10k-SPA and PEG2k-NH ₂	53
3.5	Cell viability after exposure to hydrogel extracts	54
3.6	Release of FITC-dextran from non-degradable hydrogels	55
4.1	Image stack of a typical FRAP experiment	71
4.2	Diffusion coefficients of FITC-dextran determined by FRAP	73

4.3	Release of FITC-dextrans from non-degradable hydrogels	75
5.1	Schematic illustration of hydrolytically degradable hydrogels	80
5.2	Polymers derived from branched poly(ethylene glycol)	83
5.3	Typical rheograms of degradable and non-degradable hydrogels	92
5.4	Degradation of hydrogels	94
5.5	Mobile fractions of FITC-dextran and FITC-BSA	96
5.6	Release of FITC-BSA and lysozyme from biodegradable hydrogels . .	98
6.1	Schematic illustration of injectable, biointeractive hydrogels for soft tissue engineering applications	105
6.2	Degradation of hydrogels	117
6.3	Comparison of 2-D and 3-D cell culture	120
6.4	3T3-L1 adipocytes cultured in hydrogels without and with 1 $\mu\text{mol/mL}$ YIGSR	122
6.5	Long-term culture of 3T3-L1 adipocytes	123
7.1	Polymers derived from four-armed poly(ethylene glycol)	127
7.2	PEG hydrogel formed by reaction between branched PEG-succinimidyl propionates and branched PEG-amines.	128
7.3	PEG hydrogels in perfusion organ culture	130

List of Tables

2.1	Mechanical properties of different biological tissues	19
3.1	Composition of hydrogels and conditions of gel preparation	45
4.1	Physicochemical characteristics of the prepared hydrogels	68
4.2	Hydrodynamic radii and diffusion coefficients of FITC-dextran	70
4.3	Mobile fractions and diffusion coefficients of FITC-dextran	72
5.1	Composition of the prepared hydrogels	87
5.2	Physicochemical characteristics of the prepared hydrogels	93
6.1	Physicochemical characteristics of the prepared hydrogels	115

Appendix

Acronyms

2-D	two-dimensional
3-D	three-dimensional
AFM	atomic force microscopy
Ala	alanine
AMD	age-related macular degeneration
ANOVA	analysis of variance
Arg	arginine
Asp	aspartic acid
BMP-2	bone morphogenic protein-2
BMSC	bone marrow stromal cell
BSA	bovine serum albumin
¹³ C-NMR	carbon-13 nuclear magnetic resonance
Cys	cysteine
DCC	<i>N,N'</i> -dicyclohexylcarbodiimide
DCM	methylene chloride
DCU	<i>N,N'</i> -dicyclohexylurea
DIAD	diisopropyl azodicarboxylate
DIPEA	<i>N,N'</i> -diisopropylethylamine
DMA	dynamic mechanical analysis
DMEM	Dulbecco's modified Eagle's medium
DNA	desoxyribonucleic acid
DOSY	diffusion ordered NMR spectroscopy
DRG	dorsal root ganglion

DSC	<i>N,N'</i> -discuccinimidyl carbonate
ECM	extracellular matrix
EDTA	ethylenediaminetetraacetic acid
FBS	fetal bovine serum
FITC	fluoresceine isothiocyanate
FRAP	fluorescence recovery after photobleaching
FRET	fluorescence resonance energy transfer
G	guluronic acid
GAG	glycosaminoglycan
Gly	glycine
¹ H-NMR	proton nuclear magnetic resonance
HBOEC	human blood outgrowth endothelial cell
HEPES	4-(2-hydroxyethyl)-1-piperazineethanesulfonic acid
HMBC	heteronuclear multiple bond coherence
HOSu	N-hydroxysuccinimide
HUVEC	human umbilical vein endothelial cell
IBMX	3-isobutyl-methylxanthine
Ile	isoleucine
Leu	leucine
Lys	lysine
M	mannuronic acid
α-MEM	Minimum Essential Medium alpha modification
μCT	microcomputed tomography
μMRE	microscopic magnetic resonance elastography
MMP	matrix metalloproteinase
MR	magnetic resonance
MRE	magnetic resonance elastography
MRI	magnetic resonance imaging
MW	molecular weight
NHS	N-hydroxysuccinimide
NMR	nuclear magnetic resonance
PAA	poly(acrylic acid)

PAAM	polyacrylamide
PBS	phosphate buffered saline
PCR	polymerase chain reaction
PDMS	poly(dimethylsiloxane)
PDR	proliferative diabetic retinopathy
PEG	poly(ethylene glycol)
PEG2k-OH	poly(ethylene glycol), molecular weight 2 kDa
4armPEG10k-OH	four-armed poly(ethylene glycol), molecular weight 10 kDa
PGA	poly(glycolic acid)
PLA	poly(lactic acid)
PLGA	poly(lactide- <i>co</i> -glycolide)
PPh ₃	triphenylphosphine
Pro	proline
PSPD	position sensitive photodiode
PVA	poly(vinyl alcohol)
RF	radiofrequency
RGD	arginine–glycine–aspartic acid
RGDSP	arginine–glycine–aspartic acid–serine–proline
SDS	sodium dodecyl sulfate
Ser	serine
SMC	smooth muscle cell
TGF- β 3	transforming growth factor- β 3
THF	tetrahydrofuran
TLC	thin layer chromatography
Tris	tris(hydroxymethyl)aminomethane
Tyr	tyrosine
UV	ultraviolet
VEGF	vascular endothelial growth factor
YIGSR	tyrosine–isoleucine–glycine–serine–arginine

Symbols

c	concentration
χ_1	Flory-Huggins interaction parameter
C_n	Flory characteristic ratio
D	diffusion coefficient
D_0	theoretical diffusion coefficient in water
Δ	diffusion time
δ	chemical shift
δ	gradient pulse length
D_g	estimated diffusion coefficient in hydrogels
η	dynamic viscosity
f	functionality of the cross-link
$f(t)$	normalized fluorescence intensity
G^*	complex shear modulus
G'	storage modulus
G''	loss modulus
γ^*	oscillatory shear strain
G_e	equilibrium modulus
h	height of the gel cylinder
I_0	modified Bessel function of the first kind of zero order
I_1	modified Bessel function of the first kind of first order
k	mobile fraction
k	Boltzmann constant
l	bond length along the polymer backbone

λ_{em}	emission wavelength
λ_{ex}	excitation wavelength
\bar{M}_c	average molecular weight between cross-links
m_p	total mass of polymer in the hydrogel
M_r	molecular mass of the polymer repeating unit
M_t	absolute cumulative amount released at time point t
μ_e	number of moles of cross-links
M_∞	absolute cumulative amount released at infinity
ν_e	number of moles of elastically active chains
Q	volumetric swelling ratio
q_n	roots of the Bessel function of the first kind of zero order
R	molar gas constant
r	stoichiometric ratio
r	radius of the gel cylinder
r_H	hydrodynamic radius
σ^*	oscillatory shear stress
T	absolute temperature
t	time
τ_D	characteristic diffusion time
V_1	molar volume of the solvent
v_{2c}	polymer fraction of the gel after cross-linking
v_{2s}	polymer fraction of the gel in the swollen state
V_{gc}	gel volume after cross-linking
V_{gs}	gel volume after swelling
V_p	volume of the dry polymer
w	radius of the bleached spot
ξ	average network mesh size
Y	ratio of the critical volume

Curriculum vitae

Personal information

Name:	Ferdinand Paul Brandl
Date of birth:	02/17/1979
Place of birth:	Hirschau, Germany
Nationality:	German
Marital Status:	Single

Professional training

Since 12/2004	University of Regensburg PhD program at the Department of Pharmaceutical Technology (Prof. Dr. Achim Göpferich)
12/17/2004	Approbation zum Apotheker (Acquisition of the license to practice as pharmacist)
05/2004 – 10/2004	Dispensary of the University Hospital, Regensburg Practical training

11/2003 – 04/2004 Rosen Apotheke, Amberg
Practical training

11/1999 – 09/2003 University of Regensburg
Pharmaceutics course

Civilian service

07/1998 - 07/1999 Bund Naturschutz in Bayern e.V., Wiesenfelden
(Environmental association of Bavaria)

Education

06/26/1998 Allgemeine Hochschulreife
(General qualification for university entrance)

09/1989 - 06/1998 Erasmus-Gymnasium, Amberg
(Grammar School)

09/1985 - 07/1989 Albert-Schweitzer-Schule, Amberg
(Primary School)

List of publications

Publications in scientific journals

1. **Ferdinand Brandl**, A. Seitz, J. Teßmar, T. Blunk, and A. Göpferich. Biointeractive hydrogels for adipose tissue engineering. Submitted to *Biomaterials*. (**Chapter 6**)
2. **Ferdinand Brandl**, J. Teßmar, T. Blunk, and A. Göpferich. Biodegradable hydrogels for time-controlled release of tethered peptides or proteins. Submitted to *Biomacromolecules*. (**Chapter 5**)
3. **Ferdinand Brandl**, F. Kastner, R. Gschwind, T. Blunk, J. Teßmar, and A. Göpferich. Hydrogel-based drug delivery systems: Comparison of drug diffusivity and release kinetics. *J. Controlled Release*, in press. (**Chapter 4**)
4. M. Henke, **Ferdinand Brandl**, A. Göpferich, and J. Teßmar. Size dependent release of fluorescent macromolecules and nanoparticles from radically cross-linked hydrogels. *Eur. J. Pharm. Biopharm.*, in press.
5. F. Sommer, **Ferdinand Brandl**, B. Weiser, J. Teßmar, T. Blunk, and A. Göpferich. FACS as useful tool to study distinct hyalocyte populations. *Exp. Eye Res.* 88(5):995–999, 2009.
6. F. Sommer, K. Pollinger, **Ferdinand Brandl**, B. Weiser, J. Teßmar, T. Blunk, and A. Göpferich. Hyalocyte proliferation and ECM accumulation modulated by bFGF and TGF- β 1. *Graefes Arch. Clin. Exp. Ophthalmol.* 246(9):1275–1284, 2008.
7. **Ferdinand Brandl**, M. Henke, S. Rothschenk, R. Gschwind, M. Breunig, T. Blunk, J. Teßmar, and A. Göpferich. Poly(ethylene glycol) based hydrogels for intraocular applications. *Adv. Eng. Mater.* 9(12):1141–1149, 2007. (**Chapter 3**)

8. F. Sommer, K. Kobuch, **Ferdinand Brandl**, B. Wild, C. Framme, B. Weiser, J. Teßmar, V.-P. Gabel, T. Blunk, and A. Göpferich. Ascorbic acid modulates proliferation and extracellular matrix accumulation of hyalocytes. *Tissue Eng.* 13(6):1281–1289, 2007.
9. **Ferdinand Brandl**, F. Sommer, and A. Göpferich. Rational design of hydrogels for tissue engineering: Impact of physical factors on cell behaviour. *Biomaterials* 28(2):134–146, 2007. (Chapter 2)
10. D. Eyrich, **Ferdinand Brandl**, B. Appel, H. Wiese, G. Maier, M. Wenzel, R. Staudenmaier, A. Göpferich, and T. Blunk. Long-term stable fibrin gels for cartilage engineering. *Biomaterials* 28(1):55–65, 2007.

Book chapters

1. J. K. Teßmar, **Ferdinand Brandl**, and A. M. Göpferich. *Fundamentals of Tissue Engineering and Regenerative Medicine*, chapter Hydrogels for Tissue Engineering, pages 495–517. Springer, Berlin, 2009.
2. F. Sommer, **Ferdinand Brandl**, and A. Göpferich. *Advances in Experimental Medicine and Biology* Vol. 585, chapter Ocular Tissue Engineering, pages 413–429. Springer, Berlin, 2007.

Conference abstracts

1. **Ferdinand Brandl**, T. Blunk, J. Teßmar, and A. Göpferich. Novel biodegradable hydrogels for peptide and protein delivery. 2nd PharmSciFair, Nice, France (2009).
2. **Ferdinand Brandl**, K. Kobuch, S. Rothschenk, T. Blunk, J. Teßmar, and A. Göpferich. In situ-gelling hydrogels for intraocular drug delivery. 8th World Biomaterials Congress, Amsterdam, The Netherlands (2008).
3. A. Göpferich, **Ferdinand Brandl**, and R. Knerr. Tools for the characterization of biomimetic and interactive polymers. 8th World Biomaterials Congress, Amsterdam, Netherlands (2008).
4. **Ferdinand Brandl**, S. Rothschenk, A. Blaimer, T. Blunk, J. Teßmar, and A. Göpferich. In situ-forming hydrogels for intraocular drug delivery. 6th World Meeting on Pharmaceutics, Biopharmaceutics and Pharmaceutical Technology, Barcelona, Spain (2008).

-
5. S. Rothschenk, **Ferdinand Brandl**, J. Teßmar, T. Blunk, and A. Göpferich. Release of immunoglobulin G from in situ-forming hydrogels for intraocular drug delivery. 6th World Meeting on Pharmaceutics, Biopharmaceutics and Pharmaceutical Technology, Barcelona, Spain (2008).
 6. C. Framme, **Ferdinand Brandl**, S. Rothschenk, A. Göpferich, H. Helbig, and K. Kobuch. Development and evaluation of new hydrogels for vitreous substitution and intravitreal drug application. 106th DOG Congress, Berlin, Germany (2008).
 7. A. Göpferich, **Ferdinand Brandl**, J. Teßmar, and M. Breunig. Strategies for local protein and nucleic acid delivery. 3rd International Conference on Tissue Engineering, Rhode, Greece (2008).
 8. **Ferdinand Brandl**, S. Rothschenk, M. Breunig, J. Teßmar, T. Blunk, and A. Göpferich. Polyethylene glycol macromers as building blocks for versatile hydrogels. 1st International Congress on Biohydrogels, Viareggio, Italy (2007).
 9. **Ferdinand Brandl**, F. Launay, F. Sommer, T. Blunk, J. Teßmar, and A. Göpferich. In situ-gelling poly(ethylene glycol) based hydrogels for biomedical applications. PolyPharma, Halle (Saale), Germany (2006).
 10. **Ferdinand Brandl**, F. Sommer, U. Lungwitz, T. Blunk, J. Teßmar, and A. Göpferich. In situ-gelling hydrogels based on poly(ethylene glycol). 2nd International Symposium Interface Biology of Implants, Rostock, Germany (2006).
 11. F. Sommer, **Ferdinand Brandl**, B. Weiser, J. Teßmar, T. Blunk, and A. Göpferich. Hyalocytes within the vitreous body – a homogenous population? First evidence for two distinct populations. 2nd International Conference on Strategies in Tissue Engineering, Würzburg, Germany (2006).
 12. F. Sommer, K. Pollinger, **Ferdinand Brandl**, B. Weiser, J. Teßmar, T. Blunk, and A. Göpferich. Towards a cell-based vitreous substitute – The effect of bFGF and TGF- β 1 on hyalocytes. 33rd Annual Meeting & Exposition of the Controlled Release Society, Vienna, Austria (2006).
 13. F. Sommer, K. Kobuch, **Ferdinand Brandl**, B. Wild, B. Weiser, V.-P. Gabel, T. Blunk, and A. Göpferich. Ascorbic acid for in vitro hyalocyte culture – an important factor towards a cellular vitreous substitute. 2nd International Conference on Tissue Engineering, Crete, Greece (2005).
 14. F. Sommer, K. Kobuch, **Ferdinand Brandl**, B. Wild, B. Weiser, V.-P. Gabel, T. Blunk, and A. Göpferich. Ascorbic acid influences hyalocytes on the molecular level – increased

List of publications

expression of collagen type V/XI. 4th Annual Meeting of the European Tissue Engineering Society, Munich, Germany (2005).

Acknowledgments

An dieser Stelle möchte ich all jenen meinen herzlichen Dank aussprechen, die zum Gelingen dieser Arbeit und der unvergesslichen Zeit am Lehrstuhl beigetragen haben.

Mein ganz besonderer Dank gilt Herrn Prof. Dr. Achim Göpferich für die Überlassung des Themas, seine kontinuierliche Unterstützung bei dessen Bearbeitung, sein stetes Interesse am Fortgang der Experimente und für die Freiheit, eigene Ideen und Ansätze verwirklichen zu können. Die zahlreichen wissenschaftlichen Diskussion und Anregungen waren immer sehr hilfreich für mich. Ganz besonders möchte ich mich auch für die Möglichkeit bedanken, meine Arbeiten auf nationalen und internationalen Kongressen zu präsentieren.

Herrn Dr. Torsten Blunk und Herrn Dr. Jörg Teßmar danke ich sehr herzlich für unzählige konstruktive Ratschläge, zahlreiche wissenschaftliche Diskussionen und die freundschaftliche Zusammenarbeit. Insbesondere möchte ich ihnen für die Unterstützung bei der Niederschrift dieser Arbeit danken.

Mein Dank gilt auch Frau Dr. Karin Kobuch, Herrn PD Dr. Carsten Framme, Brigitte Wild und Petra Eberl für die gute Zusammenarbeit im Glaskörper-Projekt.

Für die finanzielle Unterstützung des Projektes möchte ich mich bei der Bayerischen Forschungstiftung bedanken (AZ 616/04).

Weiterhin danke ich allen derzeitigen und ehemaligen Kolleginnen und Kollegen am Lehrstuhl für das gute, oft freundschaftliche Arbeitsklima, die konstruktive Zusammenarbeit und die vielen außerfachlichen Gespräche und Aktivitäten.

Mein herzlicher Dank gilt insbesondere:

- Dr. Florian Sommer und Dr. Stefan Rothschenk für die gute und motivierte Zusammenarbeit im Glaskörper-Projekt – in guten wie in schlechten Zeiten
- Annina Seitz, Renate Liebl und Julia Baumer für die Durchführung von zahlreichen Zellkulturexperimenten
- Dr. Thomas Burgemeister, Fritz Kastner, Annette Schramm und Georgine Stühler für die Durchführung zahlloser NMR-Messungen
- Nadine Hammer und Alexandra Frimberger für die Unterstützung im Labor
- Andrea Blaimer für die Unterstützung am Rheometer
- Angelika Berié, Lydia Frommer, Stefan Kolb, Liane Öttl und Edith Schindler für vielerlei technische und organisatorische Hilfe
- Leon Bellan, Allison Dennis, Leda Klouda und Peter Yang für die schnelle und gewissenhafte Durchsicht zahlreicher Manuskripte einschließlich dieser Arbeit
- Dr. Bernhard Appel, Axel Ehmer, Matthias Henke, Constantin Hozsa und Dr. Florian Sommer für die engagierte Zusammenarbeit im **bitsandbytes**-Team
- Constantin Hozsa für die heitere Laborgemeinschaft und seine Freundschaft
- Dr. Bernhard Appel, Christian Becker, Dr. Uta Lungwitz, Dr. Angelika Maschke, Dr. Barbara Weiser und allen anderen Doktoranden der alten Riege für die freundliche Aufnahme und die vielen gemeinsamen Unternehmungen

Besonderer Dank gilt meinen Eltern, die mir diesen Weg ermöglicht haben und mich – wo immer sie nur konnten – bestärkt und unterstützt haben.

